INVESTIGATION OF PHYSICS OF SYNTHETIC APERTURE RADAR IN OCEAN REMOTE SENSING

TOWARD 84/86 FIELD EXPERIMENT

INTERIM REPORT
VOLUME I:
DATA SUMMARY AND EARLY RESULTS
MAY 1986

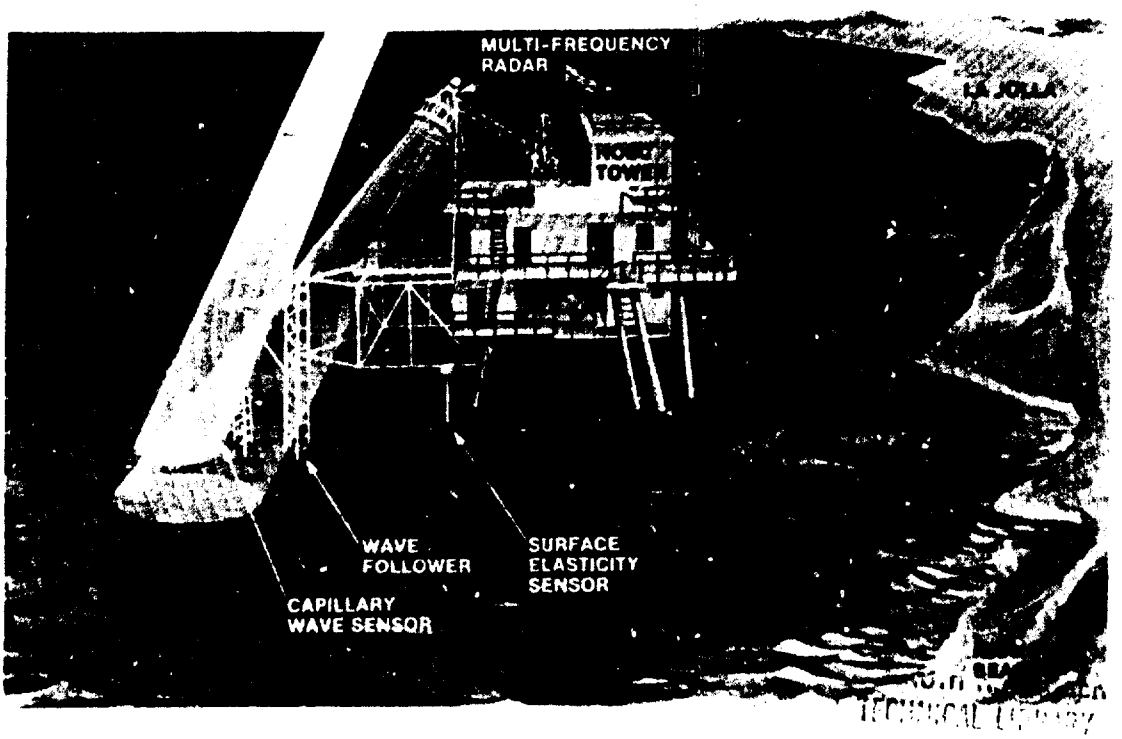

Approved for Public Release; Distribution Unlimited.

Unclassified

SECURITY CLASSIFICATION OF THIS

REPORT DOCU

READ INSTRUCTIONS FORE COMPLETING FORM

1. REPORT NUMBER

AD-A174 197

ENT'S CATALOG NUMBER

4. TITLE (and Subtitle)

TOWARD FIELD EXPERIMENT INTERIM REPORT - VOLUME I: DATA SUMMARY AND EARLY RESULTS VOLUME II: CONTRIBUTIONS OF INDIVIDUAL INVESTIGATORS

5. TYPE OF REPORT & PERIOD COVERED

Interim Technical Report September 1984 to May 1985

6. PERFORMING ORG. REPORT NUMBER

7. AUTHOR(s)

OMAR H. SHEMDIN WITH TOWARD EXPERIMENT TEAM

8. CONTRACT OR GRANT NUMBER(s)

N0001486WRM2412

9. PERFORMING ORGANIZATION NAME AND ADDRESS

Jet Propulsion Laboratory
4800 Oak Grove Drive
Pasadena, California 91109

10. PROGRAM ELEMENT, PROJECT, TASK AREA & WORK UNIT NUMBERS

0810-Physical Oceanography
0803-Dynamic Oceanography
1709-Radar Detection

11. CONTROLLING OFFICE NAME AND ADDRESS

Office of Naval Research
800 N. Quincy Street
Arlington, VA 22217

12. REPORT DATE

May 1986

13. NUMBER OF PAGES

14. MONITORING AGENCY NAME & ADDRESS(if different from Controlling Office)

15. SECURITY CLASS. (of this report)

Unclassfied

15a. DECLASSIFICATION/DOWNGRADING SCHEDULE

16. DISTRIBUTION STATEMENT (of this Report)

Approved for public release; distribution unlimited

17. DISTRIBUTION STATEMENT (of the abstract entered in Block 20, if different from Report)

18. SUPPLEMENTARY NOTES

19. KEY WORDS (Continue on reverse side if necessary and identify by block number)

Synthetic Aperture Radar, Surface Waves, Radar Backscatter, Capillary Waves.

20. ABSTRACT (Continue on reverse side if necessary and identify by block number)

The mechanisms responsible for SAR imaging of the ocean surface are not adequately understood at present. Conflicting hypotheses have been proposed that remain without valid proof, because of lack of adequate data sets to test these hypotheses. The influence of environmental parameters has prevented extending relationships that were demonstrated under one set of conditions to another beyond the range used in formulating the relationships.

DD FORM 1 JAN 73 1473 EDITION OF 1 NOV 65 IS OBSOLETE

S/N 0102-LF-014-6601

Unclassified

SECURITY CLASSIFICATION OF THIS PAGE (When Data Entered)

The TOWARD experiment was conceived to overcome these difficulties.

The experimental phase of TOWARD has been concluded successfully. It is estimated that 95% of all planned measurements were acquired. Other complementary data sets, not envisioned possible in the planning phase, were conveniently added later. The data analysis process and synthesis is in progress and continuing. Of the data sets collected, 80% of those acquired in Phase I and 50% in Phase II have been processed. Of the data sets processed, 90% obtained in Phase I and 80% obtained in Phase II are considered critical for meeting the primary objectives of TOWARD. Comparisons between the different data sets are pursued. Of these, 25% of all desirable intercomparisons have been achieved and are being used in formulating a synthesis for the entire experiment.

The single most significant achievement to date is the determination that none of the available theories on SAR imaging of long surface waves has been demonstrated to explain the SAR observations obtained in TOWARD. Work is presently in progress to amend existing models and to develop new ones. More specifically, the following results are reported:

1. The probability density functions of wave slopes indicate Gaussian distribution for wave frequencies less than 2.5 Hz and non-Gaussian distribution for wave frequencies greater than 7.5 Hz. These suggest that the longer ocean waves are weakly coupled, as expected, but that the very short surface waves are strongly coupled through strong non-linear interaction.

2. The measured wave slope spectra in TOWARD have significantly different intensity levels compared to predictions by Pierson and Stacy (1973) for equivalent wind speeds.

3. Radar backscatter results suggest that sea spikes do not contribute critically to the average backscattered power at L-Band, for the geometries implemented in TOWARD. Sea spikes occurence increases with frequency and wind speed.

4. Cross-wind radar backscatter results suggest that cross-wind or cross-wave modulation can occur, and may constitute the mechanism for SAR imaging of azimuthally traveling waves. We have also data indicating that the radar backscatter spectrum has a small peak near the dominant frequency of long waves. The resolution of this question is presently under debate.

5. SAR focusing results for azimuthally traveling waves indicate that waves are most detectable at a focus setting that is one order of magnitude greater than the wave orbital velocity.

6. Based on data analysis results to date, neither the "Velocity Bunching" model nor the "Distributed surface" model has been demonstrated to explain the TOWARD observations, but the data obtained in TOWARD will allow significant progress toward resolution of the differences.

"TOWARD 84/86"* FIELD EXPERIMENT
INVESTIGATION OF PHYSICS OF SYNTHETIC APERTURE RADAR IN OCEAN REMOTE SENSING

INTERIM REPORT

VOLUME I: DATA SUMMARY AND EARLY RESULTS

PREPARED BY

OMAR H. SHEMDIN,

PRINCIPAL INVESTIGATOR

LIST OF PARTICIPANTS:

ERIM:	D. Lyzenga	NRL:	W. Garrett
			W. Keller
JPL:	W. Brown		W. Plant
	D. Held		
	D. Hoff	ORE:	P. Hwang
	T. W. Thompson		E. Tajirian
			D. Thomas
NPGS:	K. Davidson		
	G. Geernaert	SIO:	R. Guza
NOSC:	P. Hanson	UKa:	H. Chaudry
	J. Wright		R. Moore
		UMd:	R. Harger

FOR

OCEAN SCIENCES DIVISION
OFFICE OF THE CHIEF OF NAVAL RESEARCH
ARLINGTON, VIRGINIA

(Technical Monitor: Hans Dolezalek)

MAY 1986

(TOWER OCEAN WAVE AND RADAR DEPENDENCE)

PREFACE

Divergent opinions prevail regarding the mechanisms involved in SAR imaging of the ocean surface. The TOWARD experiment represents a coordinated investigation, involving both field experimentation and theoretical simulation, of these mechanisms and related processes in an effort to understand them in sufficient detail to allow formulation of scientific consensus. The TOWARD investigators include representatives from all the divergent points of view, and three committees of distinguished experts are formed to advise on data analysis and to insure objective determination of the relevant processes.

This is an "Interim Report". The results discussed and the conclusions derived in Volume I are, by necessity, preliminary. They are based on those data sets whose evaluation has been completed, and on a limited number of intercomparisons between such results. Likewise, Volume II contains "Interim Reports" from only some of the individual investigators, including also a contribution from a committee member (M. S. Longuett-Higgins). The investigator reports are compiled in Volume II for the convenience of the reader. Whenever ready, individual investigator papers and interrelating synthesis papers will be submitted to refereed journals. The Interim Reports, consisting of Volumes I and II, are working documents for the TOWARD participants, Discipline Review Committees, and the Sponsor; they are distributed to the scientific community for comments, suggestions and possible additions.

Volume I is written by the Principal Investigator as a synthesis of the independent contributions provided by the individual investigators. The conclusions stated in Volume I have been discussed in detail by the three committees. Chapter VI, entitled: "SAR Imaging Arguments", is contributed by the Principal Investigator as a perspective on the state-of-the art, to guide the SAR data analysis effort. Taken as a whole, Volume I provides: (1) a basis for reviewing the different points of view on SAR imaging of the ocean surface, (2) a summary of the data sets acquired in TOWARD, (3) a review of the data analysis in progress, and (4) a discussion of the results that have emerged to date.

The data sets acquired in TOWARD form a unique data base that will be useful beyond the immediate objectives of TOWARD. The results to date provide valuable insights and promise to meet all the primary objectives of TOWARD. The results reported in the Interim Report constitute a back-drop against which a perspective on future SAR research is proposed.

Omar H. Shemdin*

*Jet Propulsion Laboratory
M/S 183-301
4800 Oak Grove Drive
Pasadena, CA 91109

DISCIPLINE REVIEW COMMITTEES

Hydrodynamics	Radar Backscatter	SAR Imaging
S.R. Borchardt, chairman	R.K. Moore, chairman	W.J. Plant, chairman
W.D. Garrett	W.E. Brown, Jr.	W. Alpers
G. Geernaert	K. Davidson	W.E. Brown, Jr.
R. Guza	G.P. deLoor	R.O. Harger
P. Hwang	A.K. Fung	K. Hasselmann
B.A. Hughes	B. Green	D. Held
M.S. Longuett-Higgins	W. Keller	D.R. Lyzenga
O.M. Phillips	D. Kwoh	
J. Wu	W.J. Pierson	
	M.G. Wurtele	
	S.P. Gogineni	

ACKNOWLEDGEMENT

The scientific success of the TOWARD experiment could not have been achieved without the operational support provided by a number of organizations, which is gratefully acknowledged here. The tower facility and support for operation were provided by Naval Ocean Systems Center (NOSC) through Dr. Jurgin H. Richter. Daily weather forecasts were provided by Mr. Collin Campbell of the Navy Oceanographic Command Facility (NOCFAC), San Diego. Mr. Robert Lawson of the Office of Naval Research - Pasadena, coordinated and controlled the TOWARD flights over the NOSC tower with the Radar Air Traffic Control Center (RATCC), located at Naval Air station, Miramar. The NASA: CV-990 aircraft was operated by Ames Research Center. The aircraft participation was arranged through Mr. John Reller; Mr. George Grant acted as Mission Director. The U.S. Marine Corps (VMFP-3) at El Toro, California provided RF-4B aircraft with X-Band Synthetic Aperture Radars. The U.S. Army (III Corps) at Fort Hood, Texas provided OV-1(D) aircraft with X-Band Real Aperture Radars. Water transportation between Mission Beach and the tower was provided by NOSC. The responsive support of EN-2 William Edward Ball and his crew aboard "Florida 33" contributed frequently to successful data sessions, especially in changing weather conditions. Logistical support and coordination were provided by Bobbie Videon, Test Director. Instrumentation support (two electromagnetic current meters) during "Mini-TOWARD" was provided by Dr. Ed Thornton of the Naval Post Graduate School, Monterey. The foresight and support of Dr. Robert Winokur in the planning and early execution stages are credited for the technical successes that followed. The Office of the Chief of Naval Operations provided support for the Principal Investigator in the planning and early execution stages of the experiment.

EXECUTIVE SUMMARY

SAR imaging of the ocean surface promises to be an important tool in ocean remote sensing. The long range goal of present research is to understand SAR imaging of the ocean surface so that airborne and/or spaceborne SAR's can become reliable tools for oceanic research, and for operational use.

The mechanisms responsible for SAR imaging of the ocean surface are not adequately understood at present. Conflicting hypotheses have been proposed that remain without valid proof, because of lack of adequate data sets to test these hypotheses. The influence of environmental parameters has prevented extending relationships that were demonstrated under one set of conditions to another beyond the range used in formulating the relationships. The TOWARD experiment was conceived to overcome these difficulties.

The experimental phase of TOWARD has been concluded successfully. It is estimated that 95% of all planned measurements were acquired. Other complementary data sets, not envisioned possible in the planning phase, were conveniently added later. The data analysis process and synthesis is in progress and continuing. Of the data sets collected 80% of those acquired in Phase I and 50% in Phase II have been processed. Of the data sets processed, 90% obtained in Phase I and 80% obtained in Phase II are considered critical for meeting the primary objectives of TOWARD. Comparisons between the different data sets are pursued. Of these, 25% of all desirable intercomparisons have been achieved and are being used in formulating a synthesis for the entire experiment.

The single most significant achievement to date is the determination that none of the available hypotheses on SAR imaging of long surface waves has been demonstrated to explain the SAR observations obtained in TOWARD. Work is presently in progress to amend existing models and to develop new ones. More specifically, the following results are reported:

1. The probability density functions of wave slopes indicate Gaussian distribution for wave frequencies less than 2.5 Hz and non-Gaussian distribution for wave frequencies greater than 7.5 Hz. These suggest that the longer ocean waves are weakly coupled, as expected, but that the very short surface waves are strongly coupled through possibly strong non-linear interaction.

2. The measured wave slope spectra in TOWARD have significantly different intensity levels compared to predictions by Pierson and Stacy (1973) for equivalent wind speeds.

3. Radar backscatter results suggest that sea spikes do not contribute significantly to the average backscattered power at L-Band, for the geometries implemented in TOWARD. Sea spike occurrence increases with radar frequency and wind speed.

4. Cross-Wind radar backscatter results suggest that cross-wind or cross-wave modulation can occur, and may constitute the mechanism for SAR imaging of azimuthally traveling waves. We have also data indicating

that the radar backscatter spectrum has a small peak near the dominant frequency of long waves. The resolution of this question is presently under debate.

5. SAR focusing results for azimuthally traveling waves indicate that waves are most detectable at a focus setting that is one order of magnitude greater than the wave orbital velocity.

6. Based on data analysis results to date, neither the "Velocity Bunching" model nor the "Distributed Surface" model has been demonstrated to explain the TOWARD observations, but the data obtained in TOWARD will allow significant progress toward resolution of the differences.

In conclusion, the available data sets and preliminary results strongly suggest that definitive conclusions, regarding the physics of SAR imaging of the ocean surface, will follow the data analysis effort that is in progress. Also, because the TOWARD data sets provide the most complete surface-truth measurements in support of SAR today, it is anticipated that these data sets will be used for a number of specific scientific investigations related to SAR in the future. It is noted, however, that the TOWARD data sets were directed at solving the L-Band SAR problem. A relatively small number of X-Band measurements were obtained at the same time to improve the basis for planning of future investigations on SAR imaging at C-, X- and K_u-Bands.

TABLE OF CONTENTS

FIGURES

TABLES

I. INTRODUCTION

The TOWARD experiment provides a comprehensive data set required for verification of theoretical concepts on SAR imaging of the ocean surface. The planning phase of the experiment was described in detail in the TOWARD Science Plan (Shemdin, 1984). In the formulation of the experiment it was recognized that three distinct disciplines were to be addressed: (a) hydrodynamics, (b) radar backscatter and (c) SAR image processing. The processes involved in each discipline and their interrelationships are depicted schematically in Figure 1. The definition and verification of these processes and their interactionships form the central objectives of TOWARD.

The formulation of the TOWARD experiment followed an intensive period of theoretical discussions where differing hypotheses were posed and defended based on available observations. Necessary proof, however, required additional or more complete observations which were unavailable. Periodically, an unsatisfactory situation would be dramatized when different hypotheses would predict conflicting results for a known ocean surface. Such inability to delineate correct hypotheses formed the need for acquiring the data sets specified in the TOWARD science plan.

A. State-of-the-Art

In assessing the state-of-the-art on SAR imaging of the ocean surface, the following is a concise summary of the outstanding issues:

1. Nonlinear SAR equation is not satisfactorily solved, nor simplified solutions tested in presence of surface waves. A detailed discussion relative to this point is given in Chapter VI.

2. Degradation of SAR resolution in presence of surface waves is figuratively equivalent to the opacity of a glass surface through which subsurface features are observed. In high sea states the surface is highly opaque.

3. SAR imaging of the ocean surface presupposes validity of radar backscatter models which appear to require additional testing.

4. Radar backscatter from the ocean surface is directly related to the hydrodynamics of short waves and their modulation by long waves. These processes are ill understood at present (except under a small subset of environmental conditions). Related to this subject, with specific interest to ship wakes, is the decay rate of short waves.

B. TOWARD Objectives

The TOWARD experiment was executed to address specific objectives related to SAR imaging of the ocean surface. These are:

1. Develop a verifiable theory for SAR imaging of the ocean surface.

2. Verify assumptions stipulated in radar backscatter theory that are used in SAR imaging of the ocean surface. More specifically, es-

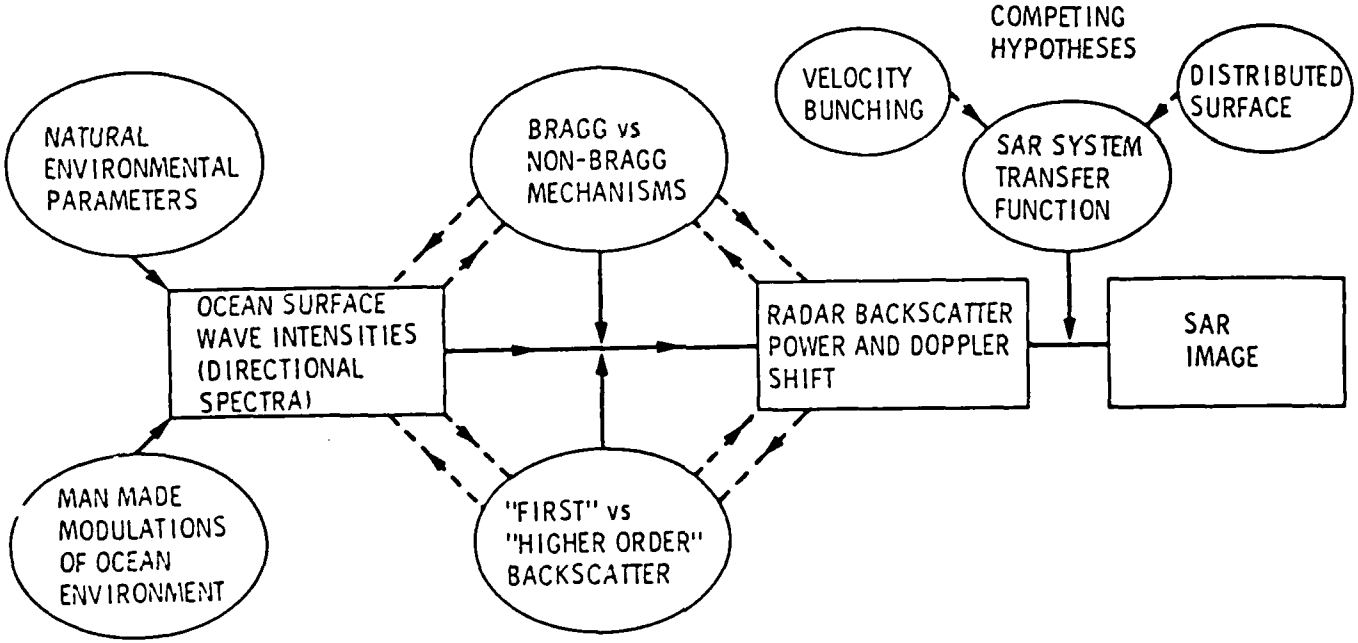

Figure 1. Schematic of Processes Involved in SAR Imaging of Ocean Surface.

tablish the importance of specular and wedge mechanisms in relation to Bragg, and the importance of cross-wind and/or cross-wave modulation in radar backscatter in relation to SAR imaging of the ocean surface.

3. Contribute to the much needed insight in hydrodynamics of short waves and their modulation by long waves.

4. Quantify the influence of the microlayer on dynamics of short waves, radar backscatter and SAR imaging of the ocean surface.

5. Investigate wherever possible the modulation of short waves by internal waves, and the related modulation in radar backscatter.

6. Measure decay rates of short waves in the ocean.

C. Experimental Approach

Having established that a complete data set is required to resolve the issues, including radar backscatter and surface slope measurements, the following guidelines were adopted for executing the experiment.

1. Use a stable platform so that measurements of short waves and radar backscatter can be free of platform motion.

2. Provide simultaneous measurements of short waves, long waves and relevant environmental parameters.

3. Obtain SAR images of the ocean surface at various azimuthal angles, height to velocity ratios and environmental conditions.

4. Provide SAR digital recording and processing to facilitate precise variation in SAR processing parameters.

5. Incorporate specialized systems for measuring surface tension, decay rate of short waves (Bobbing Buoy) and near surface wind speed (wave follower wind-shear system).

II. EXPERIMENT STRATEGY AND MEASUREMENTS

The Naval Oceans System Center (NOSC) tower is used as the stable platform for the TOWARD experiment. The tower is located at 32° 47' N and 117° 17' W, 1.4 km offshore of Mission Beach, San Diego, in 18 m water depth. A side view of the tower is given in Figure 2.

The NOSC tower is situated in the Southern California Bight, the western end of which is delineated by the Channel Islands of Southern California (see Figure 3). The North Pacific storms generate waves which propagate as swell to Southern California and enter the Southern California Bight through the windows between the Channel Islands. A typical storm is shown in Figure 4. Southern swell is also encountered at the tower from distant South Pacific storms. The latter is generally smaller in amplitude and longer in period compared to the North Pacific Swell.

The bathymetry surrounding the NOSC tower is shown in Figure 5. The water depth 10 km offshore of the tower exceeds 100m (50 fathoms). The water depth decreases gradually to 18m at the tower site. The window oriented at 290°T from the tower site is shown in Figure 5. This orientation also corresponds to Leg-1 of the flight pattern over the tower (to be discussed in more detail later in this chapter). Each segment along this line, shown in Figure 5, is 2.8 km long.

The TOWARD data sets were obtained during three phases of intensive measurements. Phase-I was executed during 2 October - 7 November 1984, and Phase-II was executed during 4 March - 1 April 1985. The wind speed and significant wave height occurrences in both Phases I and II are shown in Figure 6. As planned, Phase-I corresponded to less active environmental conditions and a well defined mixer layer. Phase-II corresponded to more intense wind and waves and no mixed layer. A third phase of measurements, denoted by "MINI-TOWARD", was executed during 15-20 December 1985 and 21-24 January 1986. This phase was added in order to secure a complementary set of wind measurements very close to the water surface, using the wave follower. Also, the spatial distribution of wave heights in the proximity of a newly developed circular wave generator could be measured under various wind conditions. The wave generator, denoted as "Bobbing Buoy", generates waves with lengths in the proximity of 30cm. The spatial distribution of wave heights was obtained with a pair of Hasselblad cameras configured for stereo-photographic analysis.

The experimental resources utilized in the TOWARD Experiment were described in the TOWARD Science Plan (Shemdin, 1984). They are briefly reviewed here for completeness.

A. In-Situ Measurements

The in-situ measurements included the following:

1. Directional Short Waves - The wave follower, shown in Figure 7, was used to measure two components of wave slope and the wave height of short waves. Optical sensors that were mounted on the wave follower were used. A laser and optical receiver system was mounted on a

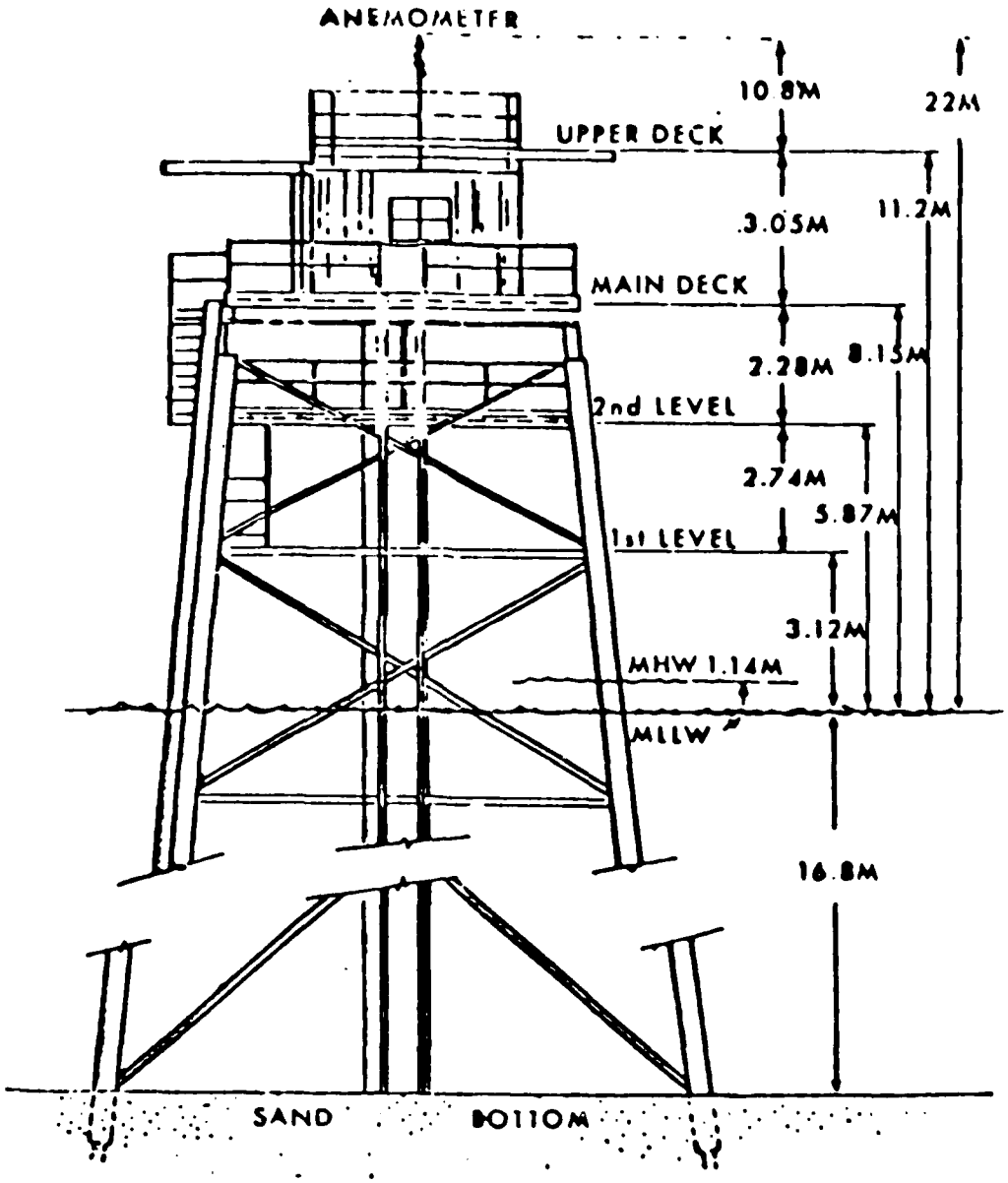

Figure 2 Side View of NOSC Tower Seen from the North, (the south extension does not appear).

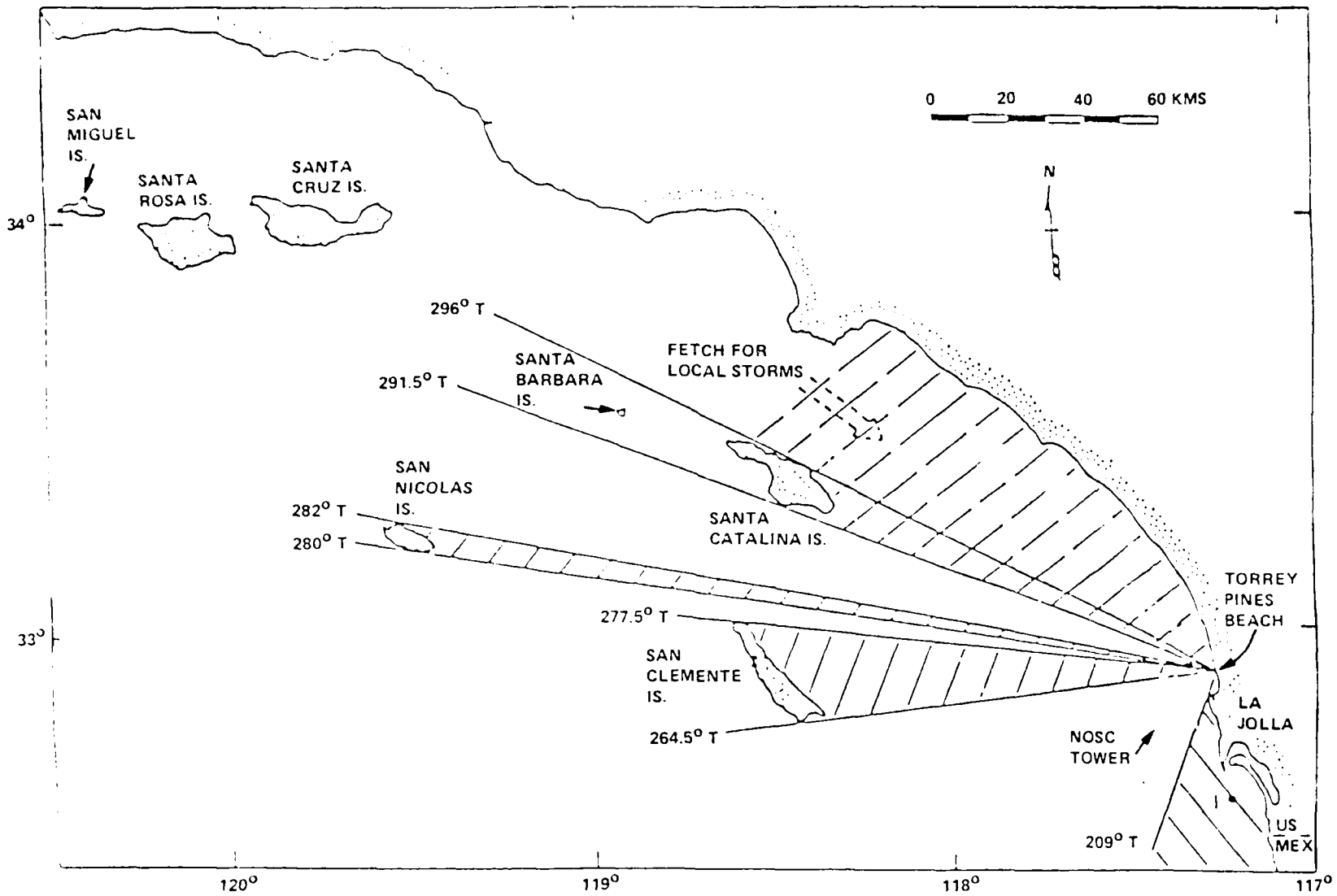

Figure 3. Southern California Bight, Showing Location of NOSC Tower and Windows of Wave Approach from the North Pacific to Torrey Pines Beach.

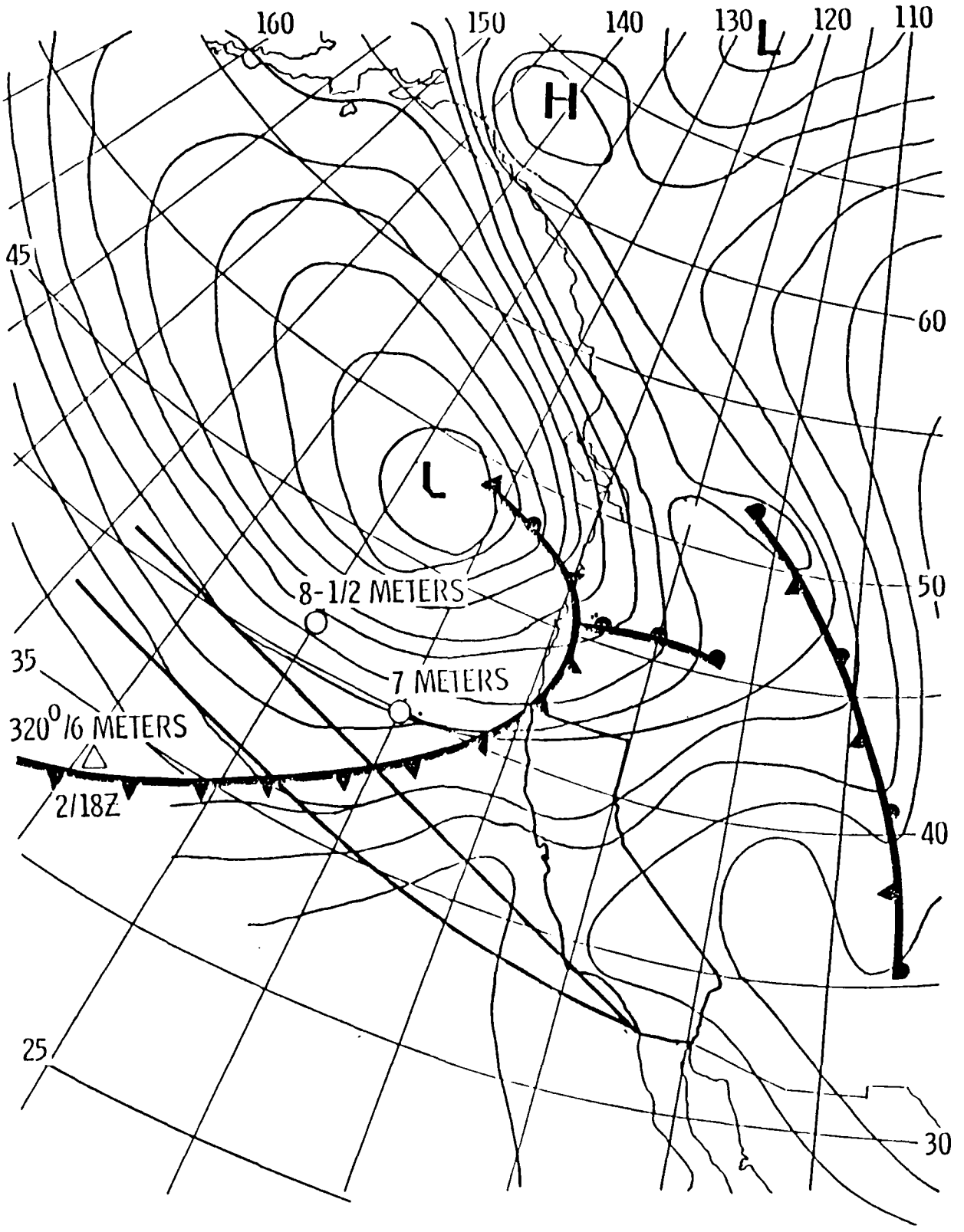

Figure 4 Typical Winter Storm in the North Pacific from Which Swell Propagates to and Penetrates the Southern California Bight. This Event Was Depicted at 12 Z on 2 November.

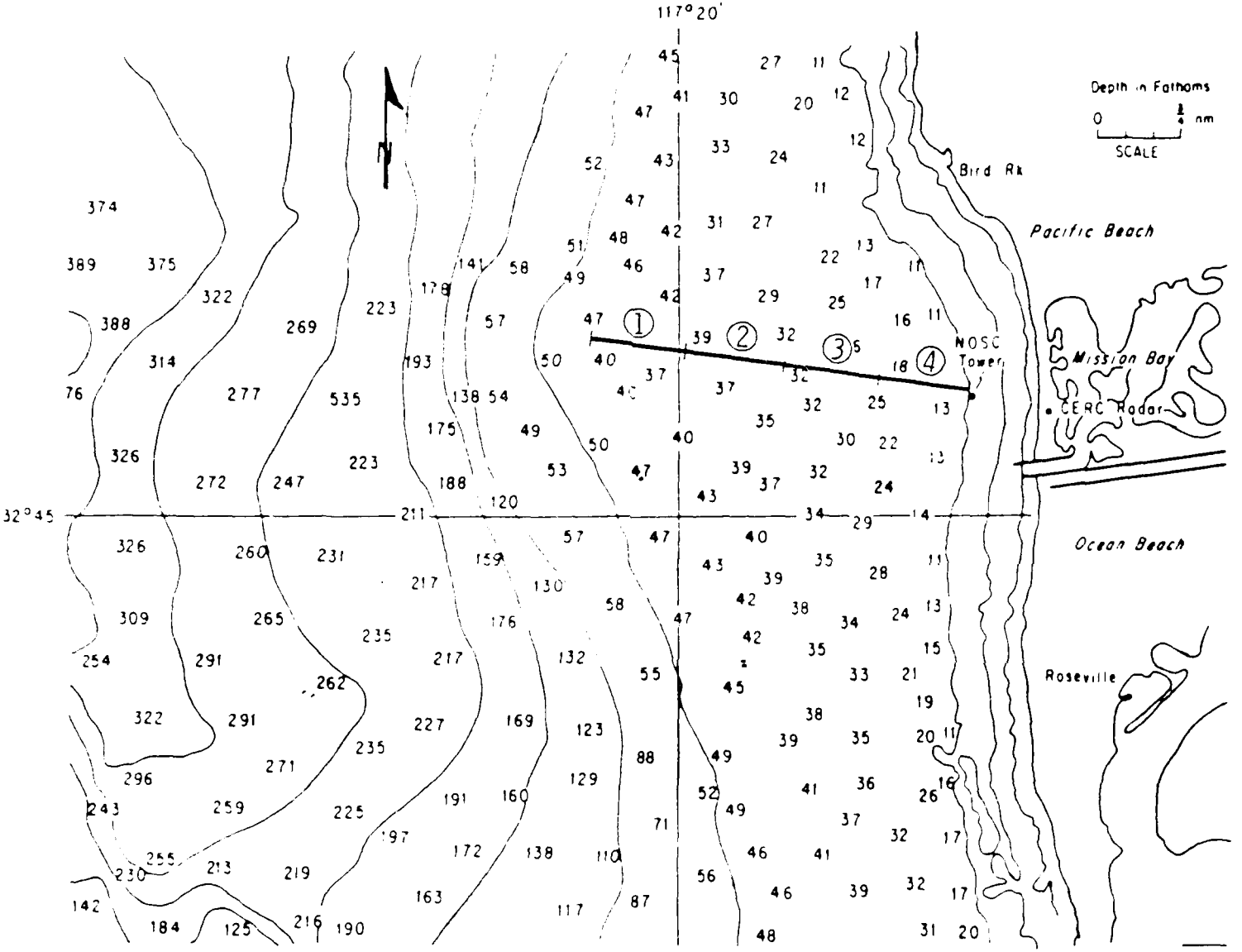

Figure 5. Map of Bathymetry Surrounding NOSC Tower (the depth contours are in fathoms).

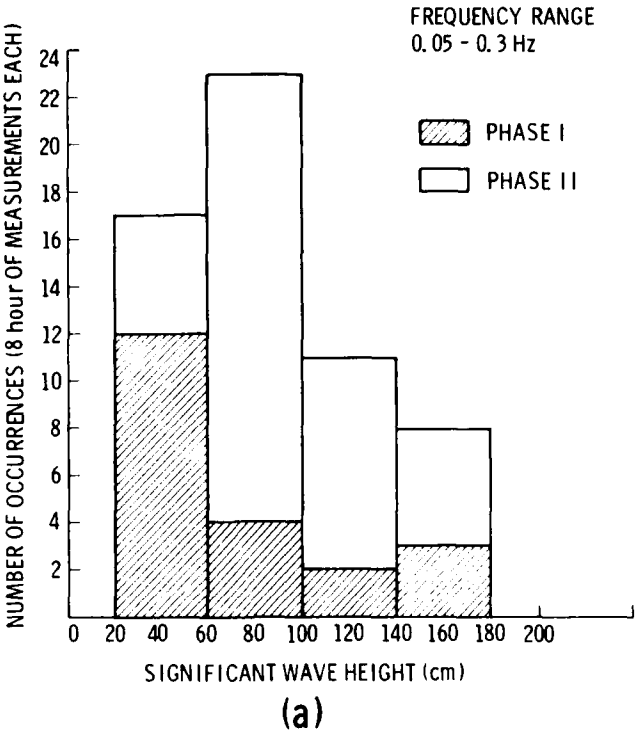

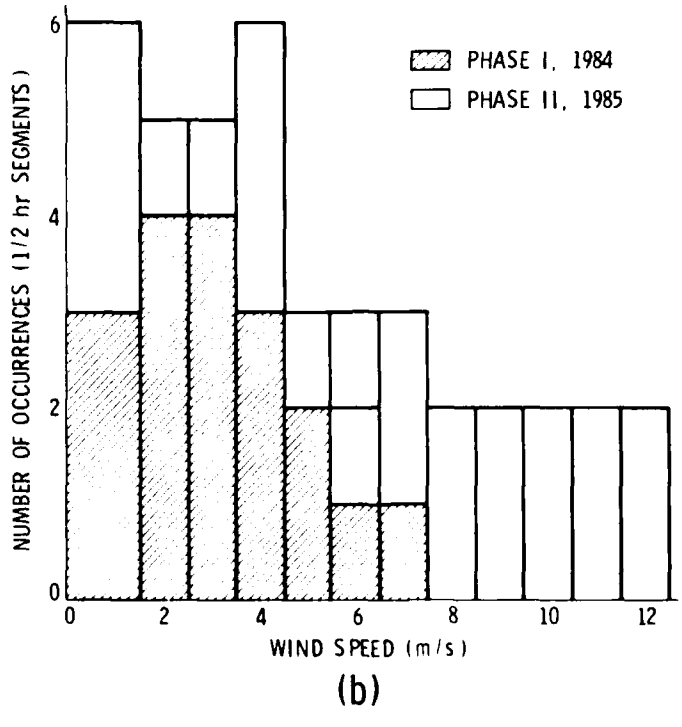

Figure 6. Experimental Conditions Encountered in Phases I and II of TOWARD 84/85.

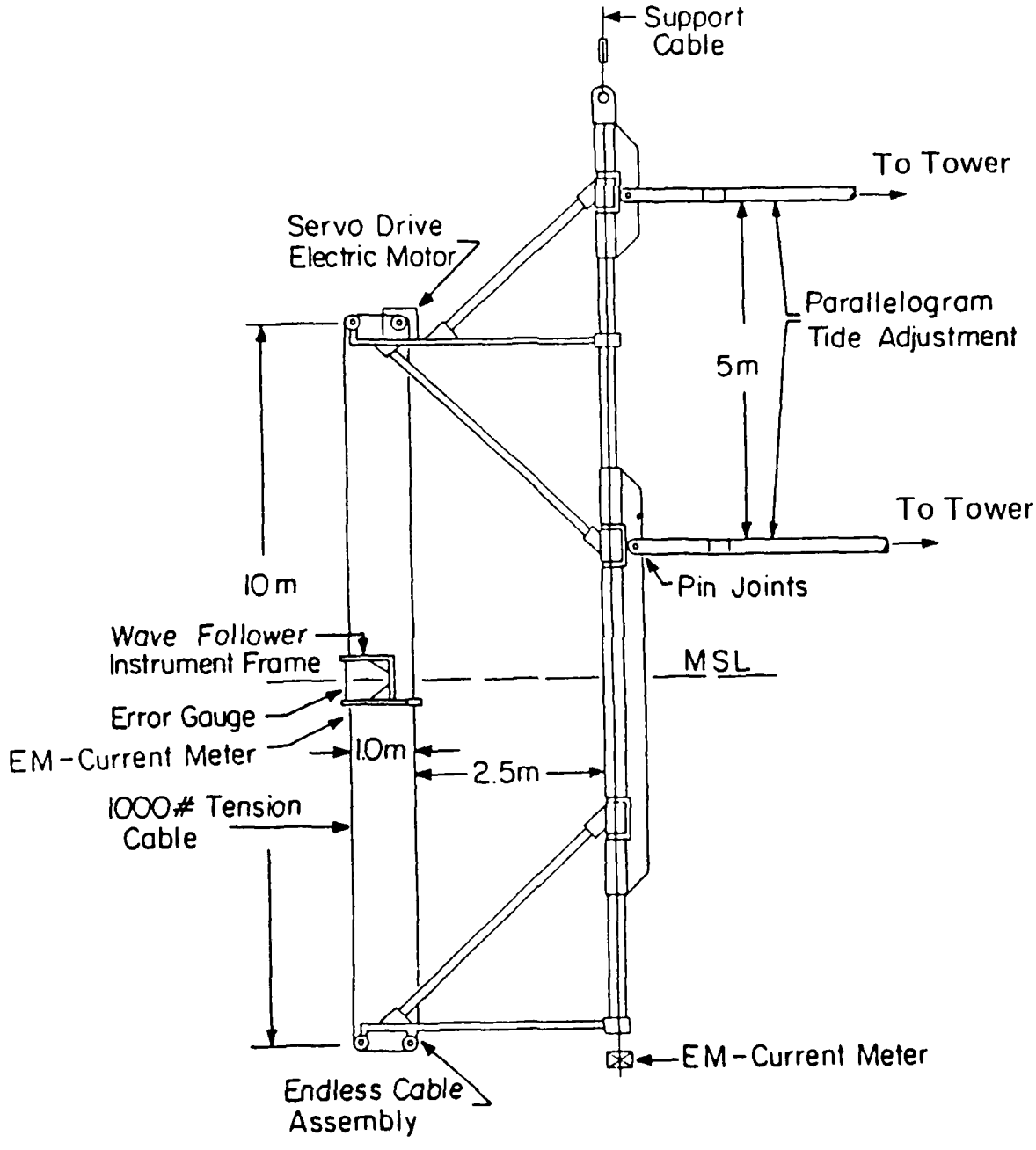

Figure 7. Wave Follower Structural Assembly .

C-Frame, forming an optical bench (see Figure 8) that followed the water surface displacement of long waves, while measuring slopes and height of short waves. The wave follower system is described by Shemdin and Hoff (1986). Samples of measurements and early results are given by Hwang (1986) which is also included in Volume II of this report. A similar laser-optical system was used by Hughes et al (1977) to measure short wave modulation by internal waves in enclosed bodies of water. The laser-optical sensor mounted on the wave-follower provides a unique system for measuring short wave modulation in the open ocean.

2. Directional Long Waves - A submerged pressure gage array, composed of 4 pressure sensors, was used at the NOSC site for this purpose. The system and early results are given by Guza in Volume II of this report. In addition, an electro-magnetic current meter and a pressure gage were placed on the fixed frame of the wave follower to provide directional properties of long waves at the wave follower position. Both systems provided directional properties of long waves to within a directional resolution of ±25°.

   A third system, composed of an electromagnetic current meter mounted on the C-Frame, provided two horizontal components of current in the wave-following frame (see Figure 8). The latter system was used primarily to provide near surface current measurements needed for removing the doppler contribution to frequency in the wave slope and height measurements.

   A C-Frame vertical displacement sensor was included to provide, in combination with the C-Frame error gage, the local vertical water surface displacement. This measurement is comparable to that provided by the pressure sensor that is mounted on the fixed frame. The pressure gage provided more accurate measurements at frequencies below the cut-off frequency (0.3 Hz) which is imposed by the depth position of the sensor. For frequencies higher than 0.3 Hz the C-Frame displacement sensor provided superior measurements. The latter were limited in accuracy because of non-linear properties of the C-frame error gage.

   It is important to note that a higher resolution array, composed of 11 pressure sensors, would have provided a directional resolution of ±10°. Such a system would have produced superior results compared to the 4 sensor array used in TOWARD. It was not incorporated because of cost limitations.

3. Surface Energy - A newly described system that utilizes the concept of surface adhesion between a plate and ocean water was used. The system and sample measurements are given by Garrett in Volume II.

4. Meteorological Measurements - A complete set of meteorological measurements, including wind stress, were obtained by a team from the Naval Post Graduate School. Their measurements and early results are given by Geernaert in Volume II.

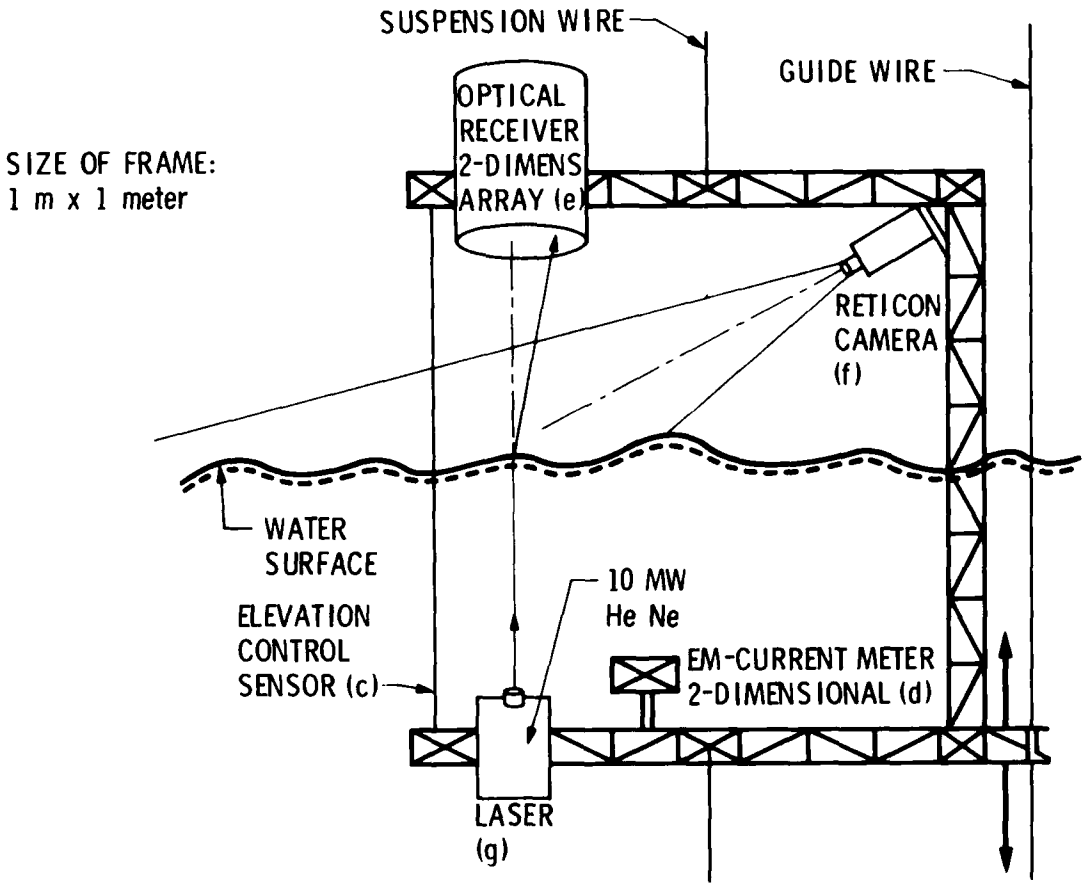

Figure 8. Wave Follower Instrument Frame. Capacitance Gage is Used as Elevation Control Sensor (c); Two-Dimensional Current Meter is Used for Measuring Two Horizontal Current Components Below Water Surface (d); Optical Receiver Records Two Slope Components of Surface Normal (e); Reticon Camera Records Vertical Displacement of Water Surface (f), Using He-Ne Laser (g).

A second set of measurements which included only wind speed and direction, air and water temperatures were acquired by NOSC. The latter measurements were also recorded independently by the Scripps recording system.

In Phase III, wind speed measurements in the proximity of the moving water surface were obtained with pitot-static sensors mounted at different levels on the wave follower. This system, denoted by "Wind Shear" system, is described in detail by Tang and Shemdin (1983).

5. Ambient Oceanographic Measurements - A thermistor chain, shown in Figure 9, was used to measure instantaneous temperatures at several elevations distributed over the entire water column. An electromagnetic current meter was deployed 5.0 m below the water surface to provide the two horizontal components of the ambient current. The thermistor chain and current meter were operated continuously throughout Phases I and II, but were removed in Phase III.

6. Bragg Wave Generator "Bobbing Buoy" - This devise is basically a free floating buoy that has within it a moving mass which is capable of oscillating the buoy vertically at a prescribed frequency, set by the frequency of the interior mass motion. The buoy design is shown schematically in Figure 10. The buoy was designed to generate waves in the frequency range 2.5 - 3.5 Hz, which correspond to circular waves with lengths in the L-Band range. A typical wave system generated by this buoy is shown in Figure 11. An extensive set of measurements were obtained in Phase III; the "Bobbing Buoy" was operated in the proximity of the wave follower and in the view of the stereo-cameras. The wind speed varied from calm to 6.0 m/s.

B. Tower-Based Radar Measurements

The tower-based remote measurement capabilities deployed at the site were described in detail in the TOWARD Science Plan. These are briefly reviewed here.

1. Multi-Frequency Radars - Two such systems were operated at the tower, in both Phases I and II of TOWARD. One was operated by JPL and the other by the University of Kansas. Both systems provided the frequency range 1-15 GHz. In addition, NRL operated an L-Band radar in Phase-I, and L- and K_u-Band radars in Phase-II of TOWARD.

2. Stereo Photography - An extensive set of wave height measurements using stereo-photographs was obtained during all three phases of TOWARD. All photography was conducted from the tower. The cameras were placed apart at an elevation above the mean water level such that a minimum base to height ratio of 0.4 could be maintained. A horizontal T-bar was placed approximately 3.0m above the mean water level to provide target calibration for the cameras. The lenses were set at different incidence angles to capture different scales of the sea surface. A subset of photographs was devoted to obtaining comparisons between wave heights measured with the stereo-cameras and

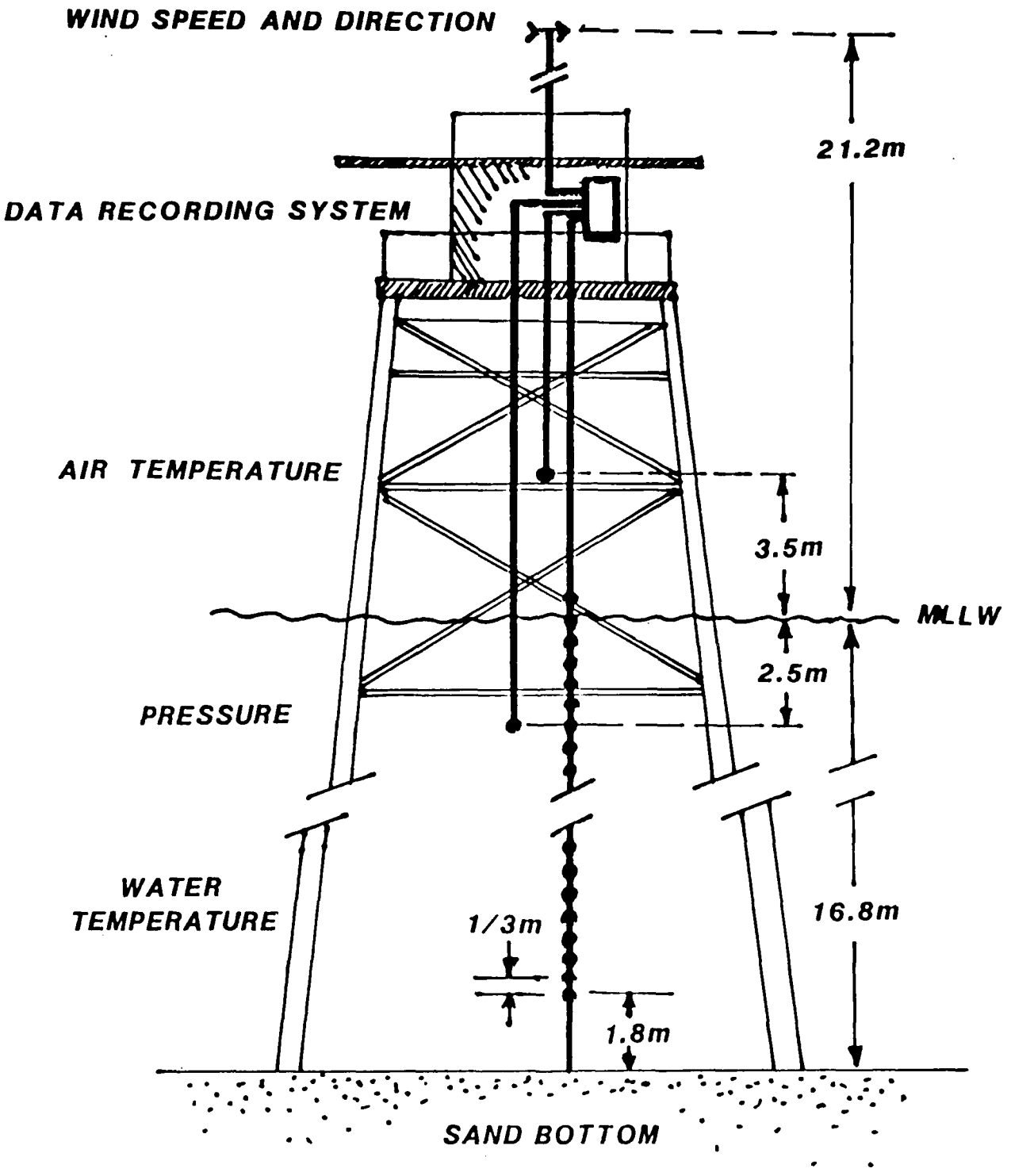

Figure 9. Subsurface Environmental Measurements Recorded by NOSC in Support of TOWARD.

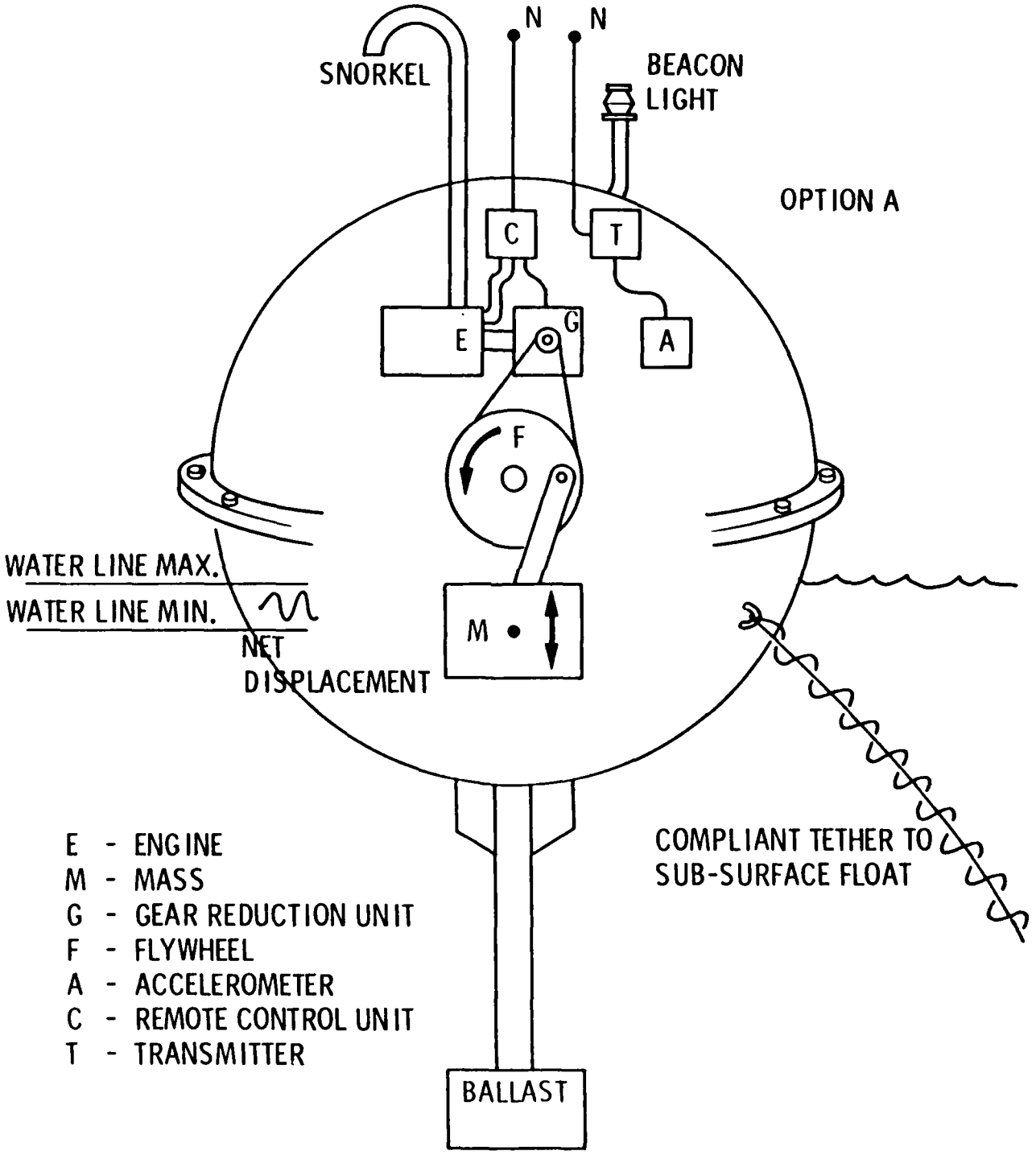

Figure 10. Schematic Design for L-Band Bragg Wave Generator, "Bobbing Buoy".

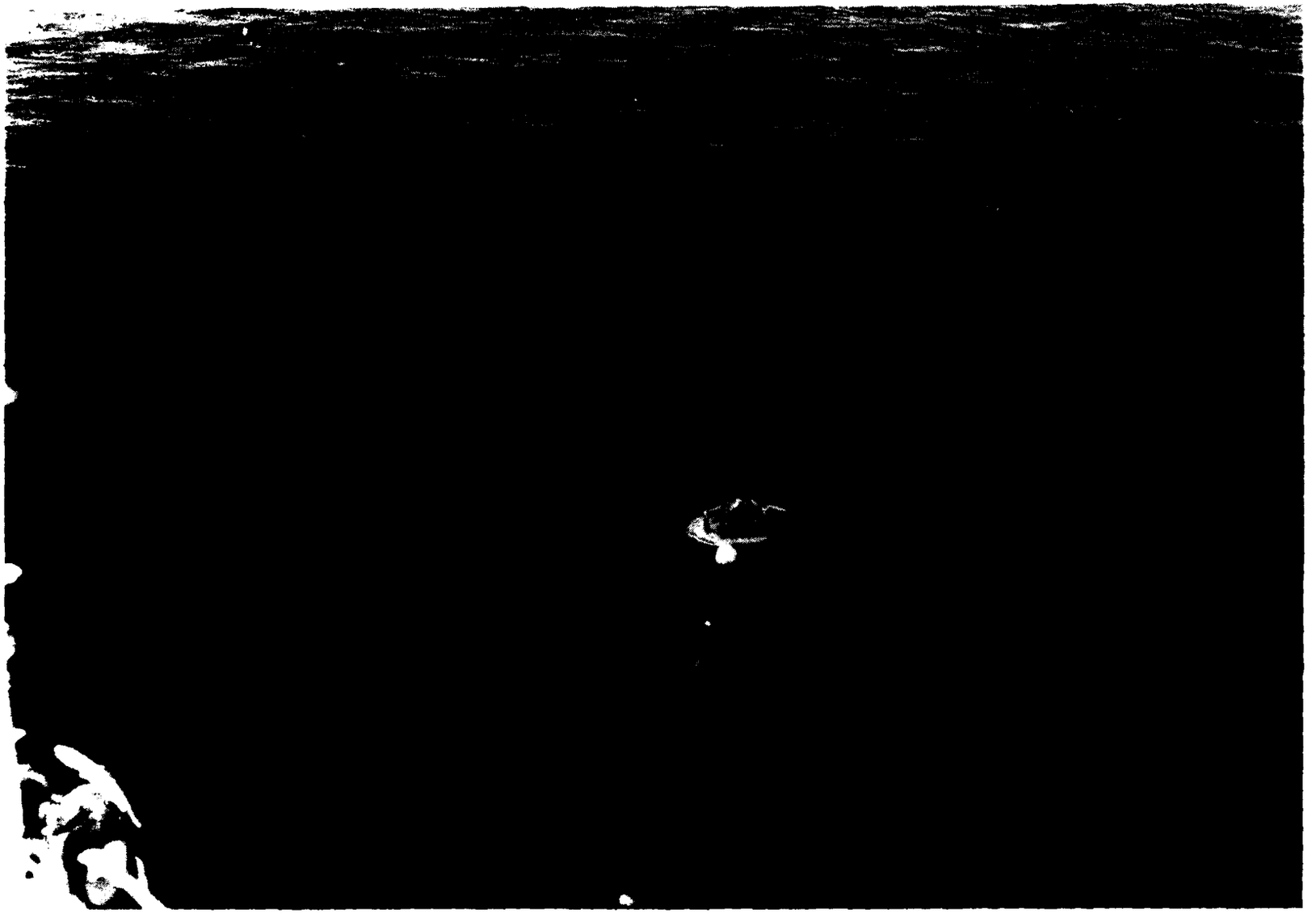

Figure 11. Surface Waves, 30 cm Long, Generated by the Circular Wave Generator.

with the wave slope-sensor on board the wave follower.

All data sets that required careful time correlations included the time code signal in their recording systems. For example, the same time signal was recorded simultaneously on the NRL radar system and on the wave follower recording system. The time code is also provided on the L-Band SAR images.

Collocation of sensors was another important consideration where comparisons between different measuring systems were required. For example, at small incidence angles, stereo-photographs and the laser-optical slope measurements were obtained over ocean patches in close proximity to each other. At larger incidence angles, radar backscatter and stereo-photographs overlapped in footprints. With these measurements recordings of wind stress, wind vector, current, air and water temperatures and surface energy were obtained simultaneously.

C. Airborne Measurements

Three types of aircraft participated in the TOWARD experiment. The aircraft and their corresponding measurement systems are briefly discussed below:

1. NASA CV-990 with JPL: L-Band SAR

This L-Band Synthetic Aperture Radar, with optical and digital recording and processing capabilities, was incorporated as a primary element in the TOWARD experiment. The system characteristics are given in Table 1. All flights followed a standard pattern, shown in Figure 12. Leg-1 of this pattern is shown in Figure 5. The nominal altitudes were 11,585, 6,098 and 2,134 m; they were flown to vary the aircraft range to velocity ratio. Variation of the latter was achieveable in the range 15-50 s.

The data processing characteristics of this system, in both optical and digital modes, are given in Table 2.

2. Marine Corps RF-4B with X-Band SAR

Less essential for TOWARD objectives, but needed for preparation of a later X-Band experiment, were X-Band SAR images obtained by the Marine Corps RF-4B aircraft. The X-Band system characteristics are given in the Science Plan. The flights that were executed in Phase-I are shown in Table 3. Each flight pattern was executed by two aircraft flown in tandem.

3. Army OV-1(D) with X-Band Real Aperture Radar (RAR)

Also, less essential for TOWARD objectives, but required for a later X-Band experiment are the RAR images obtained with two Army OV-1(D) aircraft. These aircraft participated only in Phase II of TOWARD. Initial flights at 5,500 and 3,000 m produced low quality images over the ocean. Later flights at 300 m produced satisfactory images.

Table 1. System Characteristics of JPL L-Band Synthetic Aperture Radar on the CV-990 Aircraft.

Center frequency	1.225 GHz
Wavelength	24.5 cm
Pulse length	4.9 μs
Bandwidth	19.3 MHz
Peak power	4 kW
Antenna azimuth beam width	18°
Antenna range beam width	75°
Antenna beam center gain	12 dB
Nominal altitude	6 km - 12 km
Nominal ground speed	225 m/s
Sweep time - optical	55 μs
Sweep length - optical	25 mm
Nominal PRF	700 pps
Swath width - Quad Pol mode	7 km
Resolution (4 looks)	
Slant range x azimuth - digital	8 m x 13 m
Slant range x azimuth - optical	23 m x 15 m
Incident angle	nadir to 57°
Polarization	HH, VV, HV, VH
Linear dynamic range - power	22 dB digital, 12 dB optical
Azimuth pixel spacing	11.0 m
Slant range pixel spacing	7.5 m
Ground range pixel spacings	15 m at 30°; 9.8 m at 50°
Number of pixels (range x azimuth)	927 x 1024

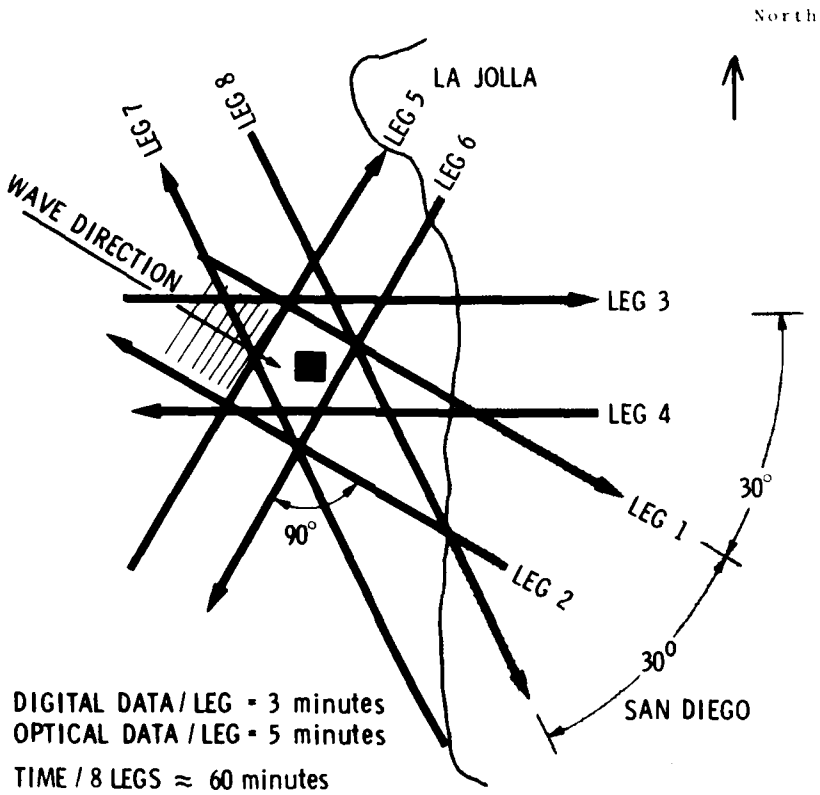

Figure 12. CV-990 SAR Flight Paths Over the Tower.

Table 2. Nominal SAR Data Processing Characteristics for L-Band SAR.

4 OPTICAL Channels = HH - VV - HV - VH

4 DIGITAL SUBFRAMES = HH - VV - HV - VH

Angle of Incidence at Center of Image = 35°

Optical/Digital Slant Range Coverage = 7 km (Quad Pol Mode)

Optical/Digital Slant Range Coverage = 13 km (Dual Pol Mode)

Optical Along Track Coverage = 60 km

Digital Along Track Coverage (Raw) = 30 km

Digital Along Track Coverage (Image) = 11 km

Digital Image Size = 927 pixels range x 1024 pixels azimuth

Optical Image Size = 50 mm cross track, 1:250,000 along track

RFP = 3 x (CV-990 Ground Speed in m/s)

= 600 @ 200 m/s, 750 @ 250 m/s

Digital Image Pixel Spacings = 7.5 m Slant Range x 11.0 azimuth

Table 3. Aircraft Flights During Phase-I of TOWARD. The Flight Intervals are Noted for Each in Pacific Daylight Time, and Pacific Standard Time Before and After 02 am 28 October 1984, Respectively.

Date	CV-990	RF-4B
2 October 1984		1046 - 1156
6 October 1984		1505 - 1600
7 October 1984		904 - 958
17 October 1984	1253 - 1536	
31 October 1984	1257 - 1542	1500 - 1614
4 November 1984	1512 - 1700	1131 - 1231
7 November 1984	1356 - 1640	

A summary of all flight missions executed in Phase II are given in Table 4. As shown, simultaneous flights with all aircraft occurred only on 19 March 1985. Three simultaneous X-Band SAR and RAR flights were executed on 19, 20 and 26 March 1985. Of these, the first two days produced acceptable SAR images but low quality (high altitude) RAR images. The third day produced high quality RAR images (low altitude), but no SAR images (data was destroyed in SAR processor).

The environmental conditions encountered during Phases-I and II flight days are given in Table 5 and Table 6, respectively.

Table 4. Aircraft Flights During Phase-II of TOWARD. The Flight Intervals are Noted in Pacific Daylight Time, and Pacific Standard Time Before and After 02 am 28 October 1984, Respictively.

Date	CV-990 (SAR)	RF-4B (SAR)	OV-1(D) (RAR)
13 March 1985			1322 - 1628
18 March 1985			1235 - 1423
19 March 1985	1301 - 1559	1345 - 1439	1355 - 1525
20 March 1985		1438 - 1602	1301 - 1421
24 March 1985			1310 - 1456
25 March 1985			1257 - 1444
26 March 1985		1420 - 1517	1243 - 1435
27 March 1985	1318 - 1558		

Table 5. Environmental Conditions During Flights in October-November, 1984: Phase-I. Noted Times are in Pacific Daylight Time and Pacific Standard Time Before and After 02 am 28 October 1984, Respectively.

Date	17 Oct 1984	31 Oct 1984	4 Nov 1984	7 Nov 1984
Time Analyzed	1250 - 1413	1300 - 1600	1512 - 1625	1412 - 1625
Wind Speed (knots)	15	6-8	5-7	10
Wind Direction (deg)	~275	~280	~300	~250
Mean Current (cm/sec) (5 m below surface)	<5	<5	<5	~10
Significant Wave Height (cm)	126	124	158	110
Air T (°C)	17.2	17.5	18.5	17.5

Table 6. Environmental Conditions During Flights in March, 1985: Phase - II. Noted Times are in Pacific Standard Time.

Day in March 1985	13	18	19	20	24	25	26	27
Analyzed Time	1320-1630	1230-1420	1300-1530	1300-1600	1310-1500	1300-1450	1240-1520	1320-1600
Wind Speed (knots)	7-4(2)	5-10(1)	8	8	4-6	8	7	8
Wind Direction	180-290°	300-310°	265-(3) 280°	300-310°	280-(3) 300°	240°	240-(3) 260°	230-(3) 260°
Mean Current (cm/sec) (5 m Below Surface)	<3	4-8	<3	<5	<3	<3	1-7	3-6
Significant Wave Height (cm)	88	79	143	129	85	127	144	104
Air T (°C)	11-14(1)	11.5-13(1)	13.7	13.6	13.5	13.4	13.7	13.3

(1) Increasing (2) Decreasing (3) Veering

III. DATA ANALYSIS APPROACH

An assessment of the TOWARD data sets indicates that they are adequate for addressing the objectives stated for the experiment. The available data sets are shown in Figure 13 in relation to the TOWARD objectives. Here, four primary objectives are stated. For each, various complementary data sets are utilized to address the related issues. The periods of recordings are given in Figure 14.

The objectives stated for TOWARD all relate to understanding the physics of SAR imaging of the ocean surface. The data analysis strategy aims at: (1) testing individually the hydrodynamics, radar backscatter and SAR imaging models, (2) using these models to simulate SAR images of the ocean surface, and (3) testing the simulation procedure by comparing the simulated images with actual SAR images of that ocean surface. Eventually, when successful SAR simulations are achieved, the inverse technique will become possible (by iteration if not by direct inversion) for using SAR to provide information on the ocean surface.

Three discipline review committees (members listed at the front of this report) were established to provide advice for the data analysis effort. The committees contribute by: (1) assigning priority to the data sets being analyzed, and those to be compared with each other, (2) insuring that the required data sets and requisite analyses are applied to resolve the relevant issues, and (3) allowing adequate testing of the differing hypotheses before final conclusions are formulated.

Initial priority in data analysis was assigned to those data sets needed to validate the SAR imaging models. For this purpose priority was assigned to those days where good-quality SAR images were obtained under desirable environmental conditions. For example, high priority was assigned to the data sets recorded on 31 October 1984. On this day a dominant swell propagated through the tower site, the SAR images of ocean waves were of good quality, and in-situ and tower-based radar measurements had been recorded successfully during the flight period.

During the SAR overflights the near-surface and in-situ measurements at the tower site were coordinated to: (1) yield data sets that complemented the SAR data (for example, tower-based radars were set at the same incidence angles, 35°, as the tower location in the SAR image) and (2) provide ocean surface measurements that could be used as input for simulating the SAR image. Here, the emphasis was on providing data sets that could be utilized for validating the "velocity bunching" vs. the "distributed surface" models.

The L-Band SAR images from all flights were carefully scrutinized to determine the influence of environmental parameters on SAR imaging. Optical images were used to scan a large area of the ocean in the vicinity of the NOSC tower. Digitally-processed images were compared with optically processed ones to establish the gain achieved with digital processing. From these standard products, 10 digital frames were selected from the Phase-I flights for detailed focusing studies. The selected 10 frames are shown in Table 7. For each frame, 15 focus settings were prescribed by the SAR Committee. Each focus step was

Data Sets	Test SAR Imaging Theories	Test Radar Back-scatter Models	Understand Hydro-Dynamic Modulation of Short Waves	SAR Detection of Surface and Subsurface Features
1. Laser Slope Sensor System	•	•	•	•
2. Stereo Photograph	•	•	•	
3. Surface Tension	•	•	•	•
4. Directional Spectrum of Long Waves	•	•	•	•
5. Meteorological Data	•	•	•	•
6. Thermistor Chain			•	•
7. Subsurface Current			•	•
8. Multi-Freq. Tower Radars			•	•
9. L-Band SAR	•	•		•
10. X-Band SAR	•			•
11. X-Band RAR	•	•		•

Figure 13. Matrix of TOWARD Science Objectives vs. Acquired Data Sets.

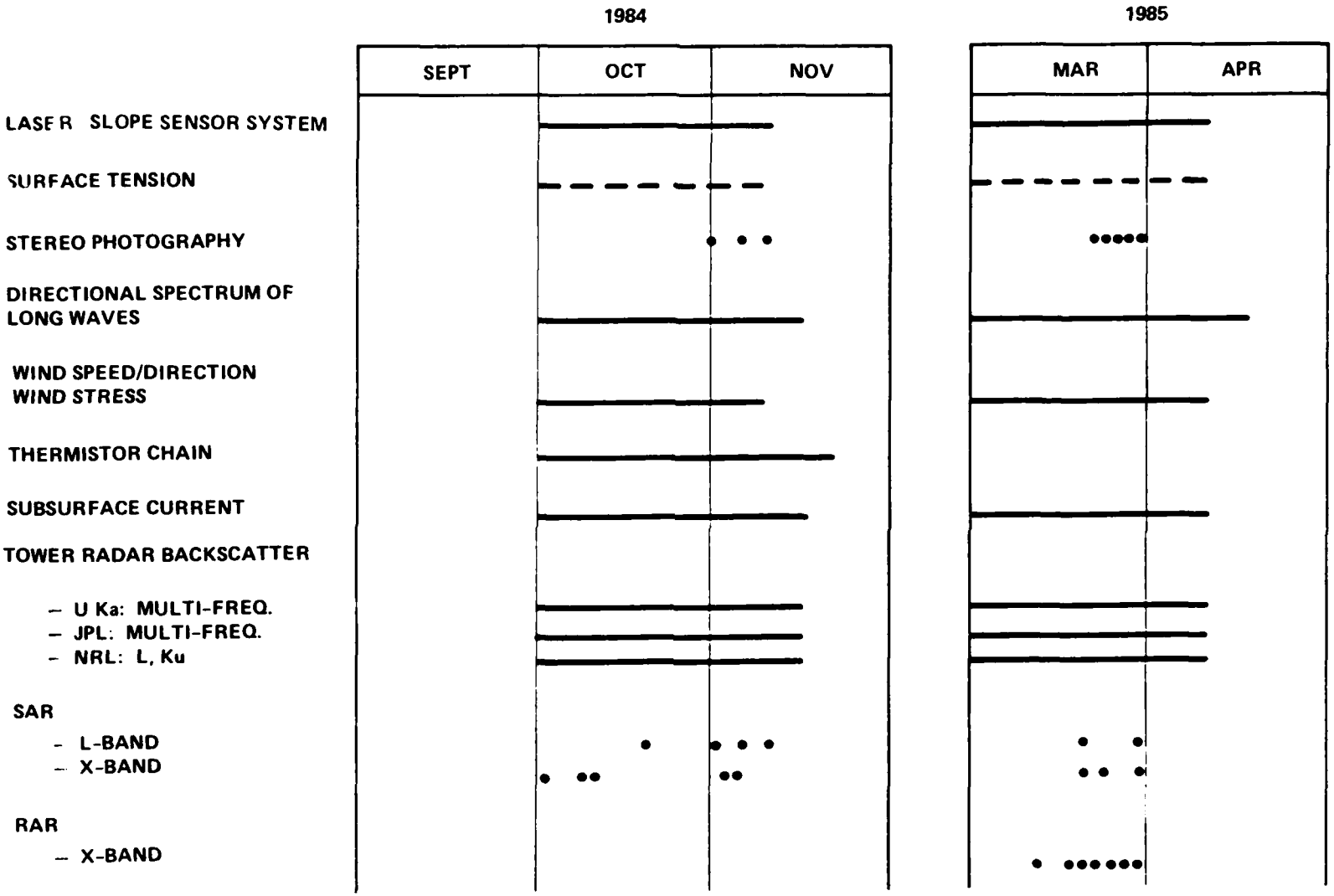

Figure 12. TOWARD Data Summary .

set equal to 0.33 of the phase speed, C, of the dominant wave. Hence, the prescribed focuses covered the range from -2.33 C to +2.33 C. A nominal value for C is 11.0 m/s.

Table 7. SAR Frames Especially Processed for Focusing Studies.

Aircraft Altitude (m)	17 Oct 1984	31 Oct 1984	4 Nov 1984	7 Nov 1984
2,134		Legs 4,7		
6,098	Leg 2	Leg 1	Leg 2	Leg 2
11,585		Legs 1,2,4,7		

In the intervals without SAR overflights the tower measurements were coordinated to provide fundamental understanding of the hydrodynamics of modulated short waves by long waves and to understand the mechanisms of radar backscatter from the ocean surface. Here, simultaneous measurements with the different tower radars, stereo-cameras, and wave follower with laser-optical slope sensor were recorded. For example, at small incidence angles, the stereo-cameras and the laser-optical slope sensor were operated simultaneously over ocean patches in close proximity of each other. For other (higher) incidence angles radar backscatter measurements and stereo-photographs were obtained in overlapping footprints. With the above measurements, recordings of the ambient environment (e.g. wind stress, wind speed and direction, current both near the instantaneous water surface and at 5.0 m below the mean water level, air and water temperatures and surface energy) were obtained at the same location.

It is important to note here that understanding the processes involved in SAR imaging of surface waves has an important bearing on understanding SAR imaging of subsurface processes. Microwaves probing the ocean surface penetrate only a thin layer (of order of one wave length) of the ocean surface. SAR detection of long surface and/or subsurface oceanic features is achieved strictly through interaction of short surface waves with the current fields that are generated by the larger scale processes (e.g. surface waves, internal waves or bathymetric changes). The short surface waves respond to the total local current. In Chapter VI the influence of surface waves on SAR resolution degradation is discussed. Direct measurement of resolution degradation due to surface motion has not been possible to date. Estimation of this quantity is presently dependent on the model used for SAR imaging of surface waves. Resolution degradation is found to be substantial (up to 60 m in Sea State 2) so as to make assessment of imaging subsurface processes, with length scales less than 240 m, questionable (see Chapter VI, Table 16).

The TOWARD data sets, shown in Figure 13, provide an adequate set for addressing issues related to SAR imaging of internal waves. This data set will be elevated in priority following completion of the tasks related to testing of the SAR imaging models.

Other data sets of interest include analysis of SAR and RAR images (needed for planning of a future experiment), and decay rate of short waves obtained with the "Bobbing Buoy" (needed for understanding characteristics of ship wakes in SAR images).

IV. IN-SITU MEASUREMENTS: OBJECTIVES, DATA SUMMARY AND EARLY RESULTS

The primary uses for the in-situ measurements are:

1. Provide a direct measure of the ocean surface for comparison with remote observations.

2. Use in-situ measurements as input in simulation models of radar backscatter and SAR imaging.

3. Investigate hydrodynamic processes in the near surface layer.

An adequate set of in-situ measurements was incorporated in the TOWARD experiment, as described in TOWARD Science Plan (Shemdin, 1984). This chapter summarizes the data sets acquired and discusses the early results for: directional long surface waves and subsurface current in (A), laser-optical measurement of short surface waves in (B), stereo-photography in (C), surface tension in (D), atmospheric/meteorological measurements in (E), and internal wave measurements in (F).

A. Directional Long Waves and Subsurface Current

Long wave directional properties (with directional resolution ± 25°) were measured by a square array of pressure sensors, approximately 6m on a side, placed 5 m below the mean water surface. Details of these measurements are given by Guza in Volume II. The data sets acquired by this system are listed in Table 8a for Phase-I and in 8b for Phase-II. These tables include measurements of the subsurface current by a current meter, also placed 5 m below the mean water surface.

The wave height spectra, computed for overflight days in Phase-I, are given in Figure 15. Their corresponding directional distributions are given in Figure 16. Wave height spectra for eight flight days in Phase-II and their corresponding wave directional distributions are given in the Appendix. The flight on 31 October 1984 produced good quality images where the surface waves are highly visible. The data set on this day are given priority to facilitate early testing of SAR imaging models. The L-Band SAR images obtained on other flight days are also of good quality. The waves are less visible in most, however, presumably because of different environmental conditions. The correlation between detectability of surface waves and the local environment is an objective in TOWARD. The spectra shown in Figures 15 and 16 provide the ambient background against which the SAR images can be examined.

The directional wave measurements on all flight days were of good quality, and the available data sets cover almost the entire period of measurements in both Phase-I and II.

Sample measurements of the two horizontal components of current are given in Figure 17 for the flight on 31 October 1984. As can be seen the current was $\leq$ 5 cm/s in the cross-shore direction and $\leq$ 10 cm/s in the longshore direction on this day. This condition ($\leq$ 10 cm/s) pervailed during all the flight days.

Table 8a. Directional Long Waves and Current Data Summary, Phase-I.

Data	Time	Data Quality	Remarks
9-23-84	1406 - 2206	Good	Currents not measured
9-25-84	0904 - 1704	Good except 1519 - 1545	
9-26-84	0904 - 1532	Good	
10-6-84	0943 - 1743	Good	Wave heights and currents have been analyzed for all flight days for comparison with SAR images
10-7-84	0201 - 1001	Good	
10-17-84	0940 - 1413	Good	
10-19-84	1029 - 1647	Good	
10-20-84	0847 - 1647	Good except 1311 - 1320, 1528 - 1536	
10-21-84	0847 - 1647	Good	
10-22-84	0847 - 1502	Good	
10-23-84	1517 - 2317	Good	Statistics of wave heights shown in Figure 6
10-24-84	0833 - 1633	Good	
10-25-84	0833 - 1633	Good	
10-26-84	0837 - 1537	Good	
10-27-84	0717 - 1517	Good except 0717 - 0722	
10-28-84	0717 - 1517	Good	
10-29-84	0717 - 1517	Good	
10-30-84	0717 - 1517	Good except 0900 - 1000	
10-31-84	0717 - 1947	Good	
11-1-84	1156 - 1956	Good	
11-2-84	0833 - 1633	Good	
11-3-84	0833 - 1633	Good	
11-3/4-84	2029 - 0330	Good	
11-4-84	0825 - 1625	Good	
11-4/5-84	1705 - 0105	Good	
11-7-84	0838 - 1638	Good	

Pacific Daylight Time to 27 October 1984 (inclusive)
Pacific Standard Time 28 October 1984 - 7 November 1984

Table 8b. Directional Long Waves and Current Data Summary, Phase-II.

Date	Time (PST)	Data Quality	Remarks
3-2 to 3-6-85 inclusive	0900 - 1700	Good	- Wave height analyzed on flight days
3-7-85	1130 - 1700	Good	
3-8 to 4-8-85	0900 - 1700	Good	- Wave height statistics shown in Figure 6

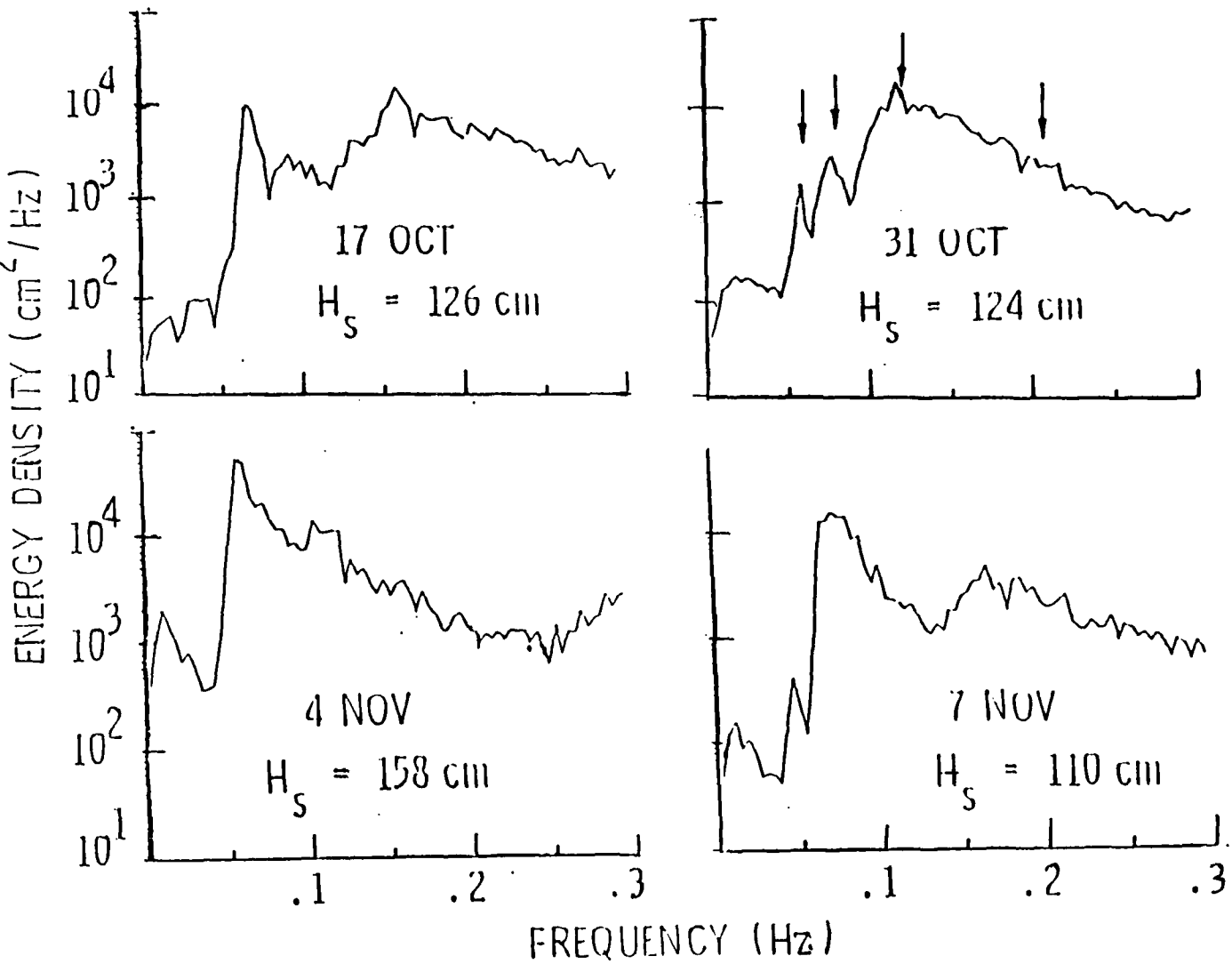

Figure 15. Wave Height Spectra for Four Overflight Days in Phase-I.

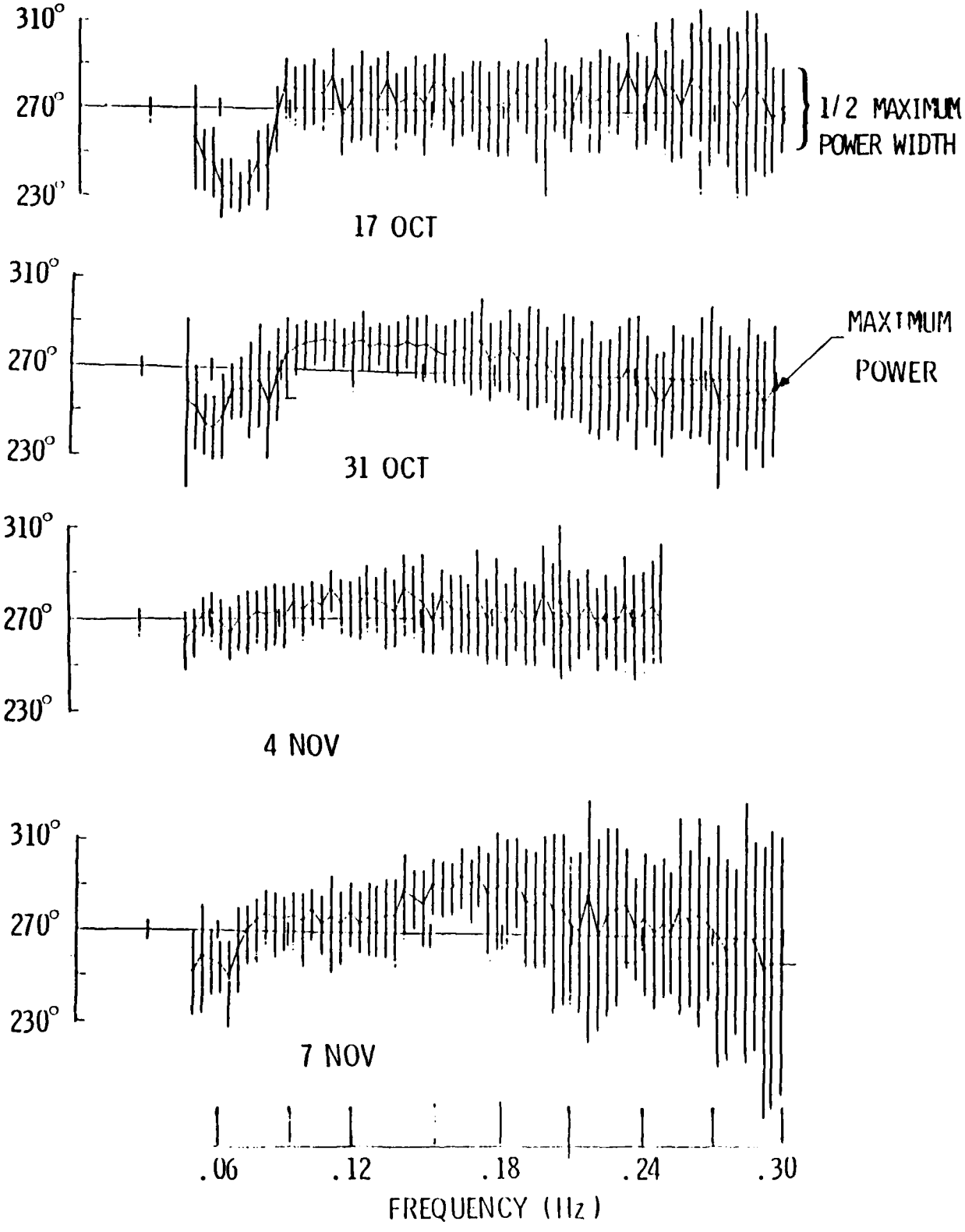

Figure 16. Wave Direction (at Maximum Power) and Angular Spread (at Half Maximum Power) vs. Frequency, Phase-I.

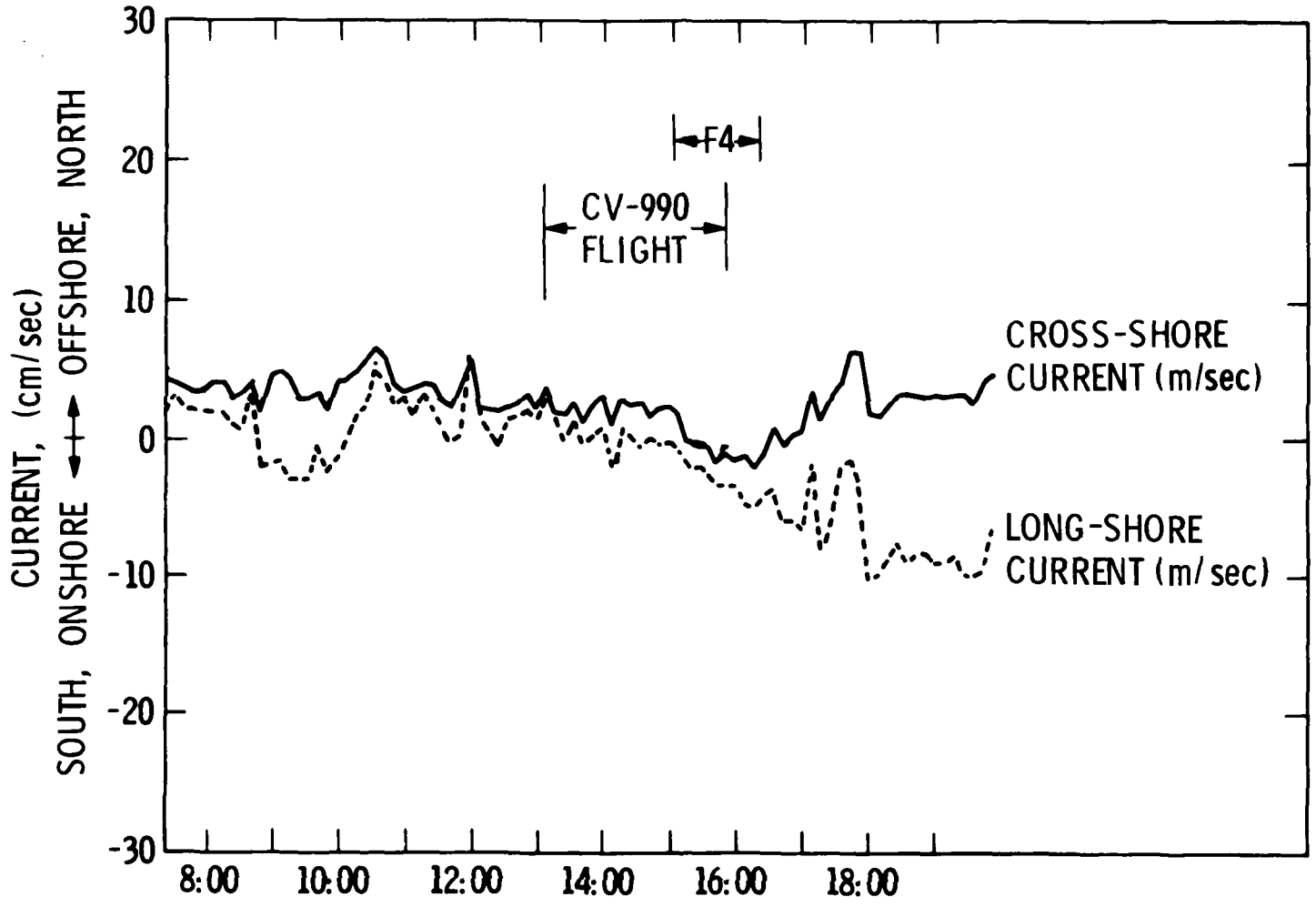

Figure 17. Time Histories of Subsurface Current During Flights of 31 October 1984, Time in PST.

B. Laser-Optical Measurements of Short Surface Waves

The laser-optical sensor was mounted on the wave follower instrument frame, as shown in Figures 7 and 8. The wave follower truss assembly was fastened to the tower structural extension (south side). Hence, the laser beam penetrated the water surface at approximately 6.5m from the tower legs when the instrument frame was pointed to the west, and 10.0m when it was pointed to the south. The details of the wave follower and instrumentation are given by Shemdin (1980) and Shemdin and Hoff (1986). More details regarding data analysis procedures are given by Hwang in Volume II of this report. Briefly, the laser-optical system consists of a laser mounted below the water surface with the beam pointing vertically upwards (see Figure 8). The two dimensional optical receiver is placed above the water surface, pointing down, and detects the position of the refracted laser beam, yielding two slope components of the water surface. The vertical displacement of the water surface is detected by a Reticon Camera. An electro-magnetic current meter, which measures two components of the horizontal current, is placed on the wave following instrument frame at 50 cm below the water surface. The data sets collected with this system are summarized in Table 9a for Phase-I, and Table 9b for Phase-II of TOWARD. As noted in these tables, the available data sets cover a range of wind speeds from 0 to 12 m/s, and provide surface truth for practically all the flights in both phases of the experiment. A typical time series is shown in Figure 18. The optical slope measurements in the two upper records clearly show the high frequency structure of the surface, which is not detected by the submerged pressure gage record shown in the lowest record in Figure 18.

The early results derived from the wave follower data are partially described by Hwang in Volume II. Important samples of completed analysis are included here.

A computation of the slope variance, $\overline{(\nabla\eta)^2}$, is given in Figure 19 as a function of the friction velocity, U_*. The TOWARD measurements are compared with similar field results given by Cox and Munk (1954) and Hughes et al (1977). The agreement is considered to be good. In addition to the slope variance, the TOWARD data provide time series of slopes, and hence slope spectra. Such results could not be produced by the photographic technique employed by Cox and Munk (1954), but could be produced by the method of Hughes et al (1977). The primary advantage of the TOWARD data set over Hughes et al is in the deployment of the laser-optical sensor on the wave follower. Such configuration allowed accurate slope measurements even in the presence of swell. Hughes et al measurements were obtained in a protected body of water where swell was generally absent. All three data sets show the slope variance to be linearly dependent on the wind-friction velocity. Hence, the TOWARD data confirm previous findings in this regard.

A desirable type of analysis is the determination of the probability density function, PDF, for the wave slope time series. This was executed for the components in the Principle Axis (defined as axis of symmetry in a 2-dimensional PDF distribution) and Cross-Axis directions. The results are compared with a Gaussian distribution, used for reference, as shown in Figure 20. The four panels a, b, c, and d correspond to U_* equal to 7.1, 16.6, 18.2 and 27.7 cm/s, respectively. At the lowest wind speed the PDF's for both Principal- and Cross-Axes appear to be Gaussian distributed. As the wind speed

Table 9a. Laser Slope Sensor System Data Summary, Phase-I.

Date	Time[1] (PDT)	Wind Speed (m/s)	Wind Direction (°)	Stereo-[2] Photography	Flights
10/17/84	1315 - 1345	7.5	285		CV990
10/20/84	1355 - 1455	6	265		
	2355 - 0025	4	120		
10/29/84	1435 - 1505	5	300		
	1520 - 1550	4.5	300		
10/30/84	1535 - 1605	3	290		
10/31/84	1030 - 1100	2.5	235		
	1300 - 1600	3-5	280-300	4 Series	CV990 RF-4B
11/03/84	1820 - 2045	2.5	270		
	2330 - 2400	3	25		
11/04/84	0030 - 0130	3	10		
	0945 - 1230	2	220	1 Series	RF-4B
	1530 - 1630	3	300	2 Series	
	1835 - 1930	1	175		
	2320 - 2350	2.5	0		
11/07/84	1625 - 1655	4	260	3 Series	CV990

[1] Pacific Daylight Time.
[2] Each series is composed of pre-set number (12-80) of stereo-photographs taken in sequence with a constant time lapse (1-2 seconds) between each succeeding pair.

Table 9b. Laser Slope Sensor System Data Summary, Phase-II.

Date	Time (PST)	Wind Speed (m/s)	Wind Direction (°)	Stereo-Photography	Flights
3/19/85	1400 - 1530	6	260		CV990 RF-4B, OV-1(D)
3/20/85	1000 - 1130	6	330		
3/21/85	1450 - 1500	3	310	1 Series	RF-4B, OV-1(D)
	2030 - 2230	0			
3/22/85	0340 - 0410	1.5	90		
	1145 - 1215	3	290	2 Series	
3/24/85	1330 - 1400	3	270		
3/25/85	1120 - 1150	5	235		OV-1(D)
	1340 - 1700	7	240		
	1730 - 1800	6	230		
	1940 - 2010	2.5	180		
3/26/85	1011 - 1140	4	210	4 Series	RF-4B, OV-1(D)
3/27/85	1020 - 1050	8	225	1 Series	
	1330 - 1530	9±	225		CV990
3/28/85	0930 - 1130	12±	225	2 Series	
4/1/85	2100 - 2230	0			

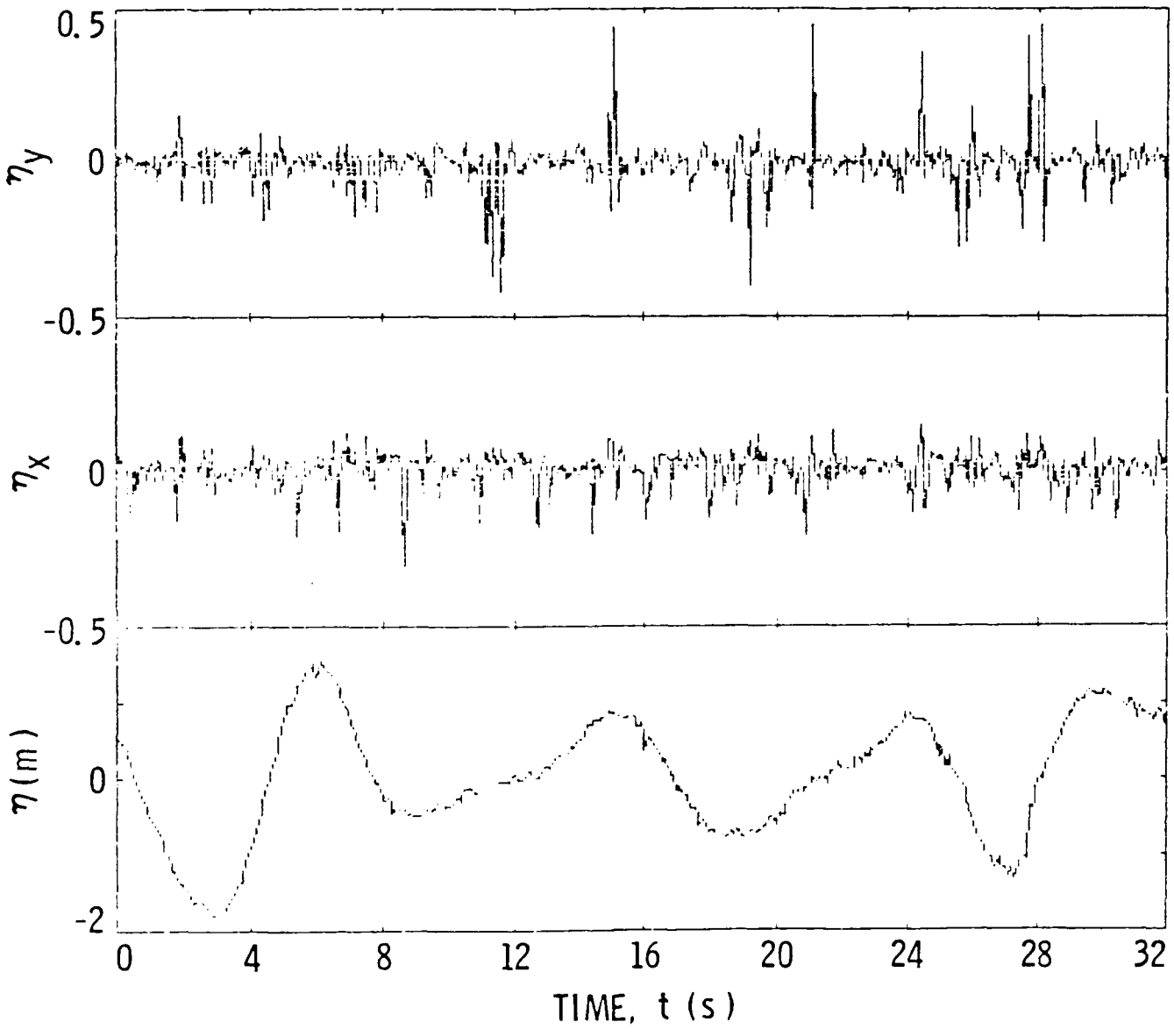

Figure 18. Sample Time Series from Laser Slope Sensor System. The Upper Two Traces Give the Up-Wind/Down-Wind Wind Slopes, Respectively. The Lower Trace Gives the Low Response Surface Elevation Measurements obtained with a Submerged Pressure Sensor.

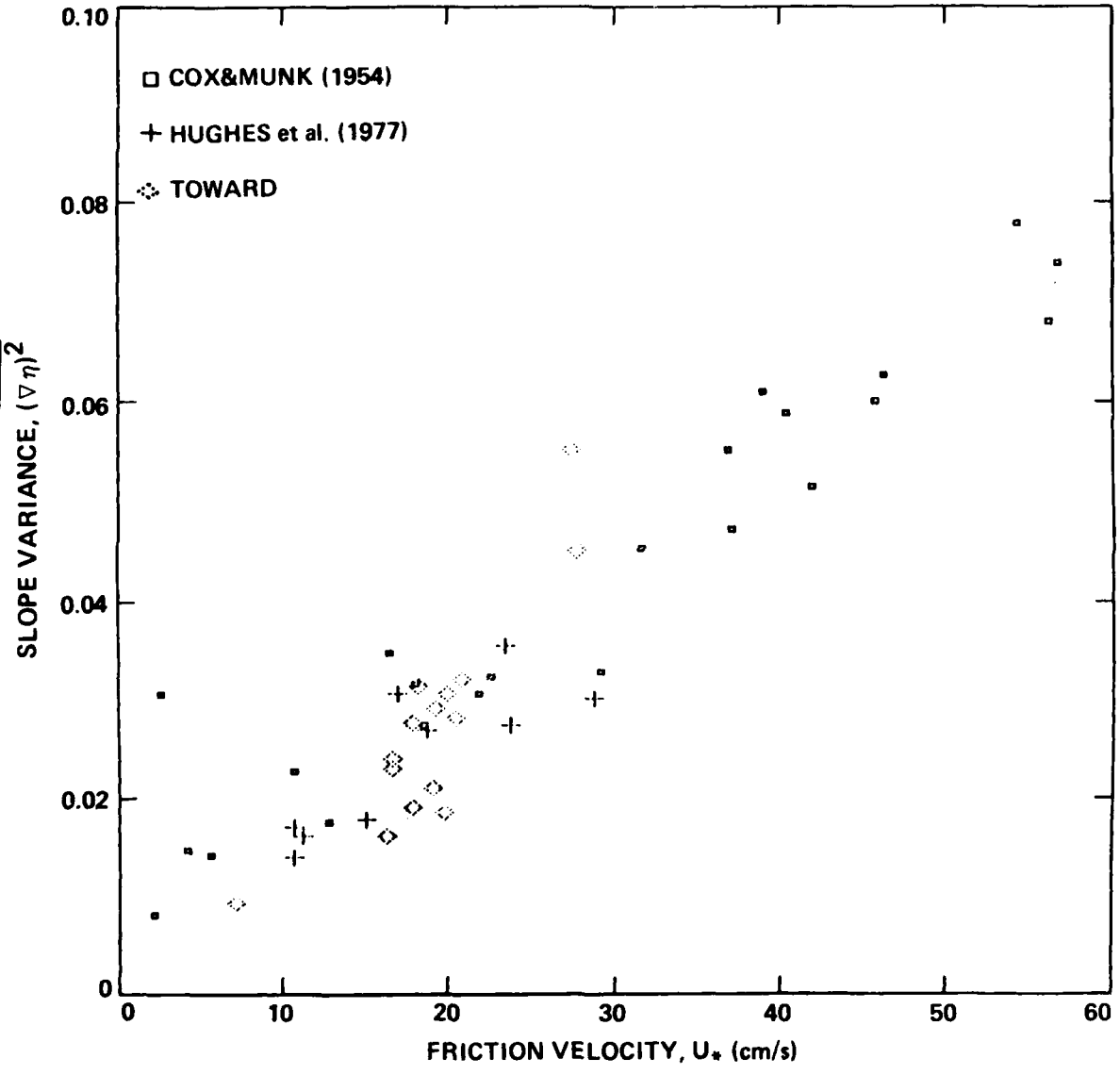

Figure 19. Correlation of Slope Variance with Wind Friction Velocity; TOWARD Data is Compared with Previous Field Investigations.

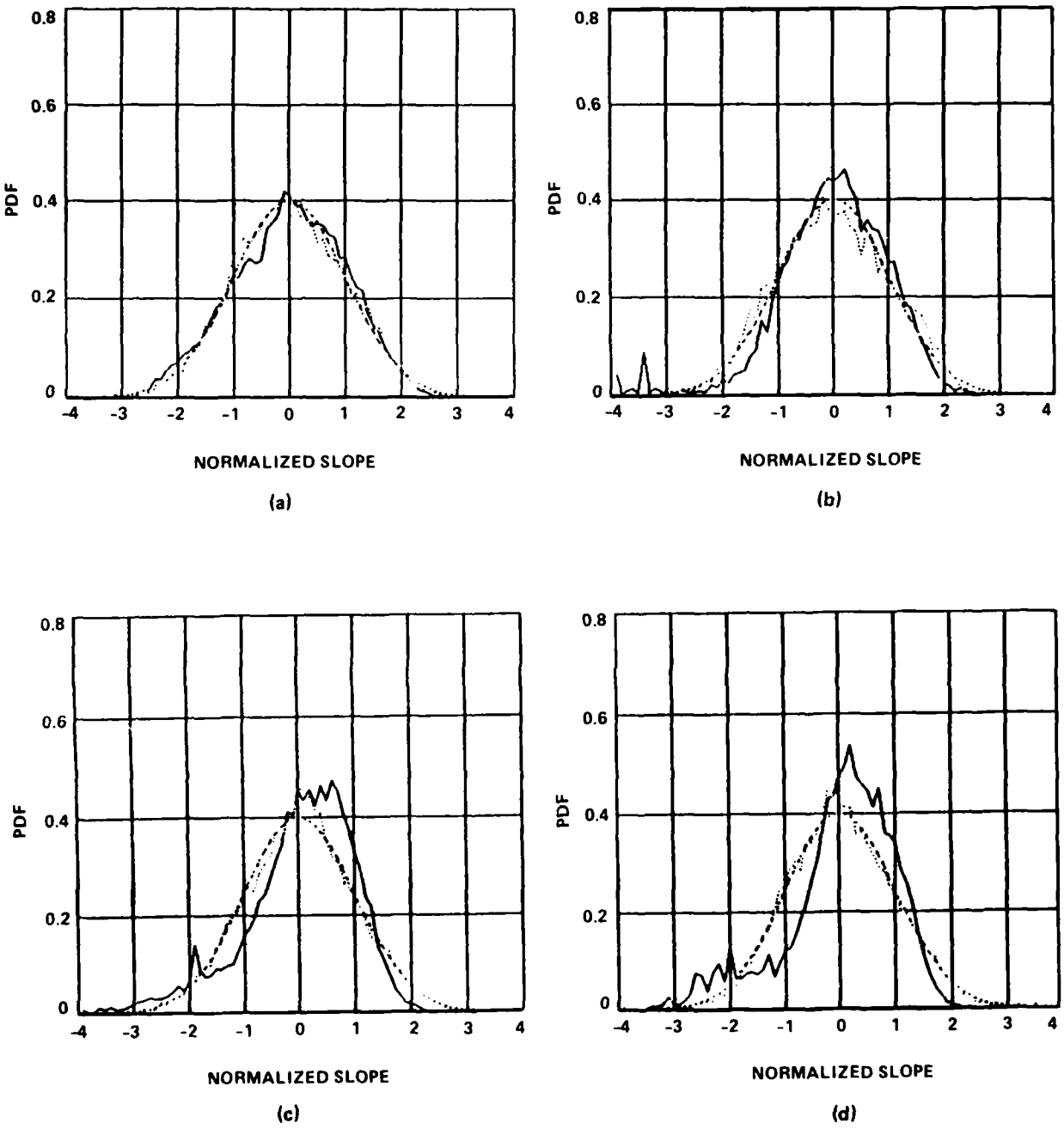

Figure 20. Probability Density Functions (PDF) in the Principle Axis (——) and Cross Axis (···) Directions, Compared with Gaussian Distribution (---). The Wind Speeds (U_{10}) and Shear Velocities (U_*) for the Panels are: (a) U_{10} = 3.2 m/s, U_* = 7.1 cm/s; (b) U_{10} = 4.1 m/s, U_* = 16.6 cm/s; (c) U_{10} = 5.6 m/s, U_* = 18.2 cm/s; (d) U_{10} = 5.9 m/s, U_* = 27.7 cm/s.

increases, deviation from the Gaussian distribution becomes more noticeable. Also, the PDF corresponding to the Principle Axis becomes more asymmetric with increasing wind speed.

To investigate this occurrence further, the time series are: (1) low-passed with a cut-off of 2.5 Hz and then the PDF computed, (2) band-passed between 2.5 and 7.5 Hz and then the PDF computed, and (3) high-passed above 7.5 Hz and then the PDF computed. The unfiltered time series and each of the filtered time series are shown in Figure 21. Each panel shows its respective Gaussian distribution for comparison. It is clear from panel (b) that the long waves are random, but somewhat skewed such that the up-wind slope is smaller than the down-wind slope. This is consistent with expected behavior of long ocean waves at moderate and high wind speeds.

In Figure 21(c) the PDF's indicate near Gaussian behavior; a departure from Gaussian is noticeable, however. L-Band Bragg waves correspond to frequencies in this band, and it is possible that waves 30 cm in length behave in the ocean as weakly coupled waves, under moderate wind conditions. The high-passed PDF's shown in Figure 21(d) are highly peaked, compared to the Gaussian distribution, and they suggest that the very short waves are possibly strongly coupled, which should be further investigated.

The frequency spectra of wave slopes, obtained from the time series, are shown in Figure 22 for four different wind speeds. In this figure the ordinate is the logarithm of frequency times the slope spectrum. The Phillips equilibrium slope spectrum is proportional to f^{-1} so that a spectrum conforming to Phillip's description would appear parallel to the horizontal axis in Figure 22, and independent of wind speed. The TOWARD results deviate from the f^{-1} description and show systematic dependence on wind speed.

Pierson and Stacy (1973) proposed a model which incorporates the dependence of the slope spectrum on wind speed. Comparisons of the TOWARD results with Pierson and Stacy's predicted slope spectra are shown in Figure 22. Here the agreement is less than satisfactory. The predicted spectra overestimate the wind speed required to generate a certain equilibrium slope by a factor of five at high wind speeds, and a factor of three to four at lower wind speeds. The Pierson and Stacy model relies in its derivation on wave height measurements obtained with capacitance wave gages, among others. These are known to have a low-frequencey response ($\lesssim$ 8.0 Hz). Hence, waves with higher frequencies are attenuated. The Pierson and Stacy model does not incorporate this defect in measurements. It is clear from the TOWARD results that significant wave energy exists at wind speeds below those predicted by the Pierson and Stacy model. An objective in the TOWARD hydrodynamic investigation is the development of a more realistic wave spectral model that is consistent with TOWARD observations.

Wave-slope frequency spectra can be transformed to wave-number spectra through a conversion process that is described in detail by Hwang (1986). Typical frequency spectra are shown in Figure 23a. The high-frequency tail slope is greater than -1.0, as observed before (Figure 22). The converted wave-number spectra are shown in Figure 23b. The high wave-number tail slope is -4.0. Of central importance to the objectives of this study is the modulation in the wave number spectra of short waves by long waves. The first of these results are given in Figure 24. The wave number spectra appear to preserve the

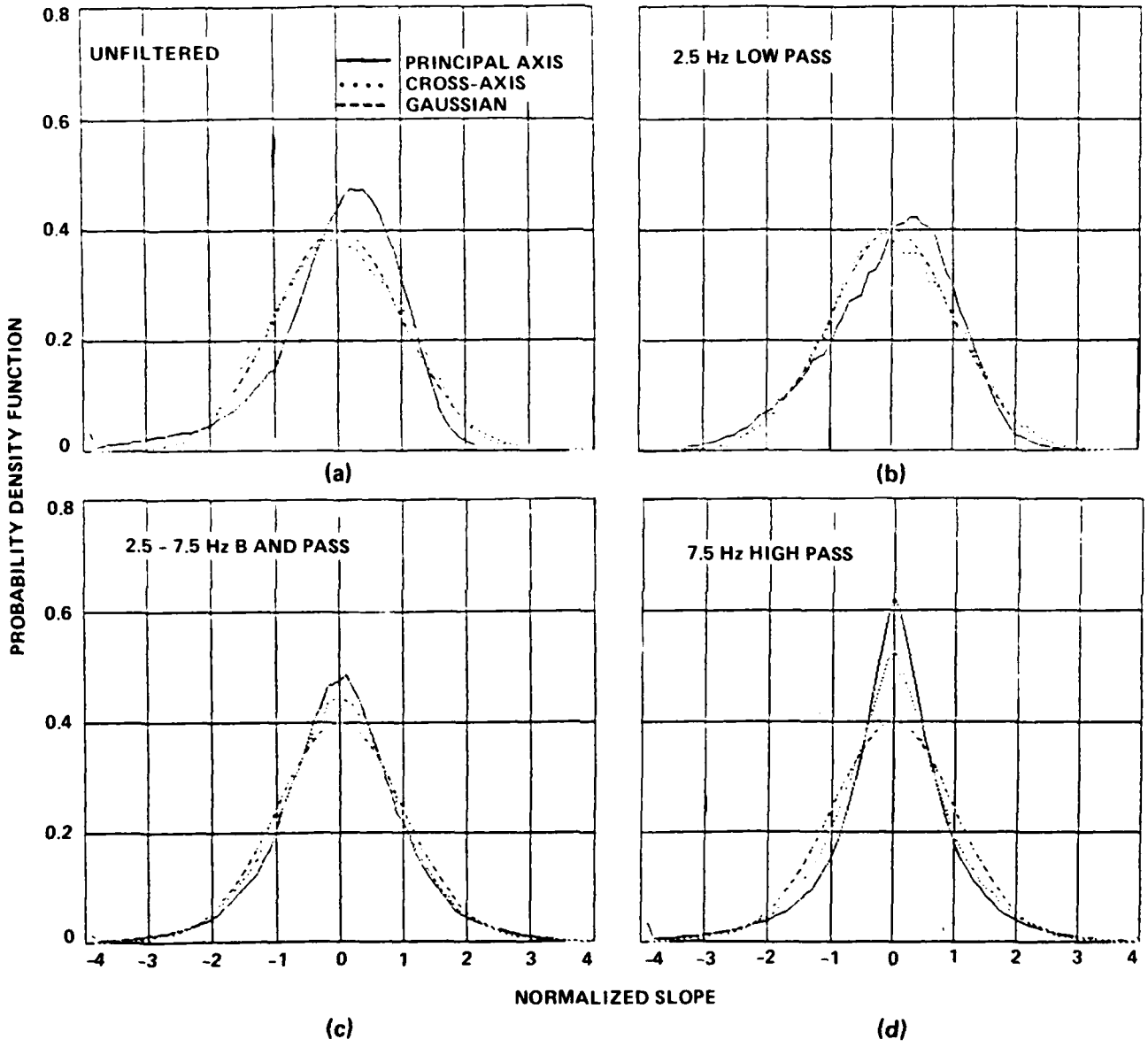

Figure 21. Probability Density Functions (PDF) for U_{10} = 6.2 m/s, U_* = 19.5 cm/s. Legend for Each Panel is as Indicated.

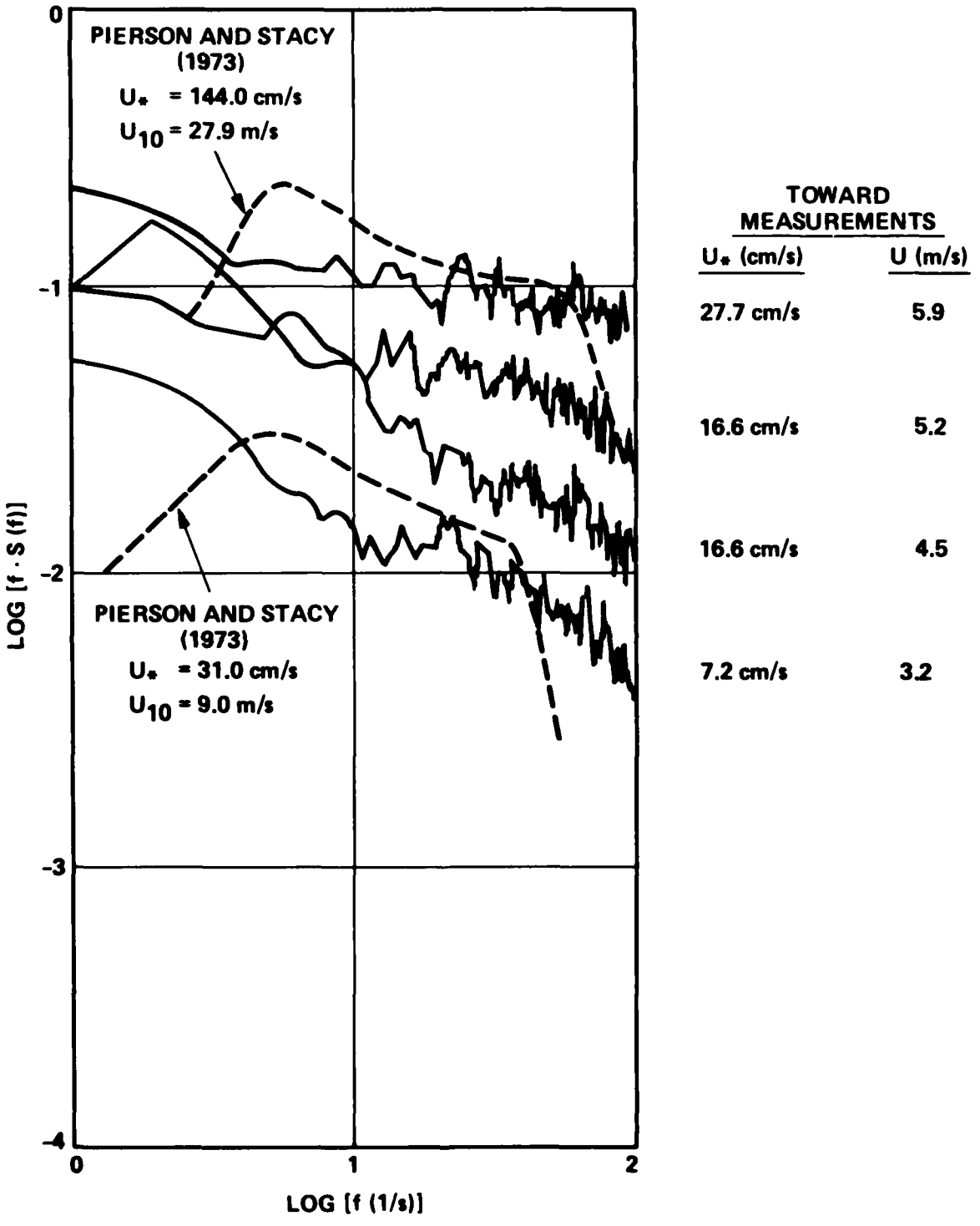

Figure 22. Dependence of Wave Slope Spectra on Wind Speed.
—— Toward Laser Optical Slope Measurements,
– – Predictions According to Pierson and Stacy (1973).

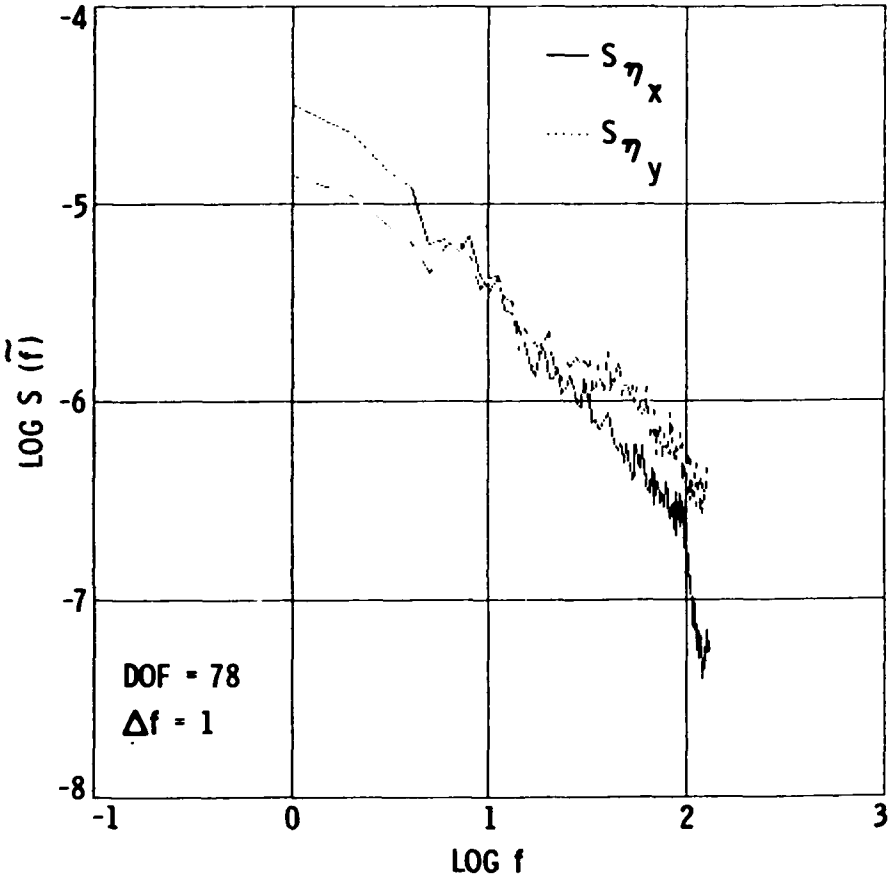

Figure 23a. Slope Spectra of Short Waves in Up-Wind/Down-Wind Direction, n_x, and Cross-Wind Direction, n_y. The Record Length is 60 seconds.

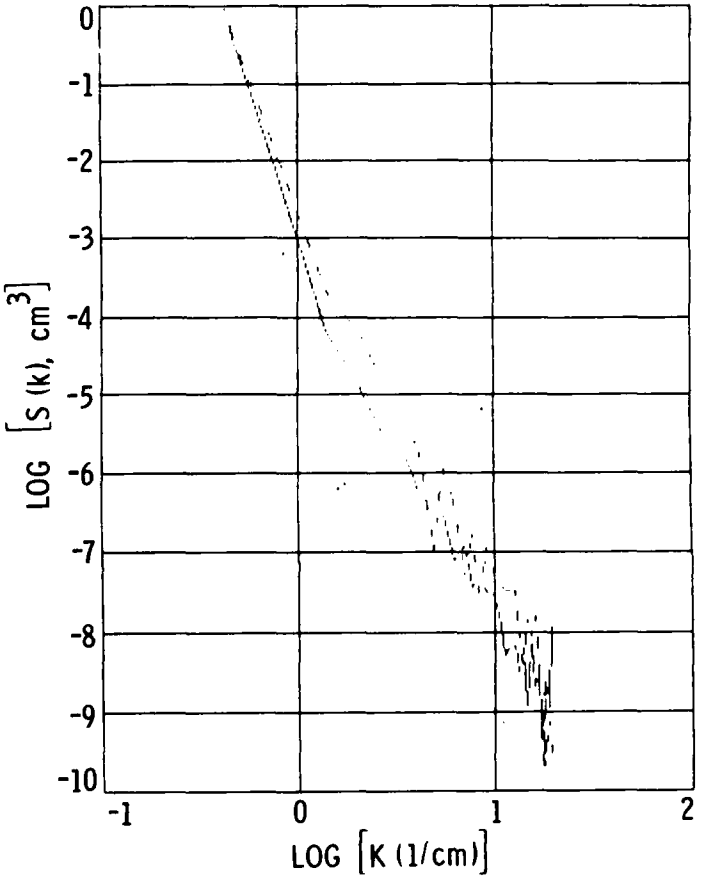

Figure 23b. Spectra in Frequency Domain of Figure 23a Converted into Wave-Number Domain.

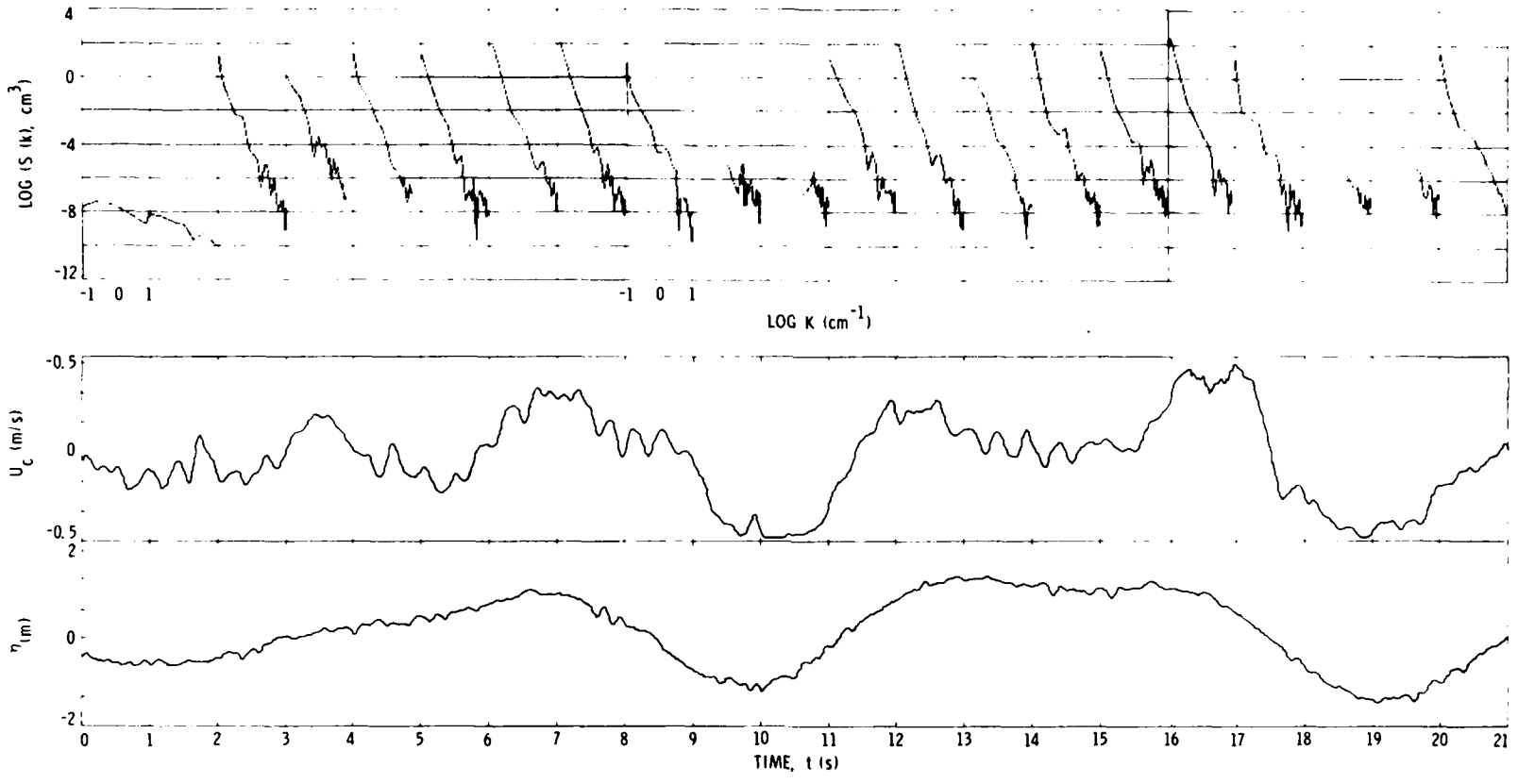

Figure 24. Modulated Wave Number Spectra (upper panel) at Different Phase Points Along the Long Waves. The Middle Trace is Horizontal Orbital Velocity of Long Waves. The Lower Trace is the Surface Displacement of Long Waves.

k^{-4} shape over most phase locations along the long waves (lower trace), except over the trough regions. There, the short wave energy appears to be absent. In between consecutive troughs the modulation in wave-number spectral level, preserving the k^{-4} shape, is over 2-decades in wave energy. More detailed investigation of this process is necessary before definitive conclusions can be drawn.

C. Stereo-Photography

Two Hasselblad cameras with 150 mm lenses were used to photograph a section of the ocean surface with an overlapping area of approximately 3m x 3m. This area is suitable for short ocean wave studies at L-Band, consistent with the primary objective of TOWARD. Primary emphasis was given in Phases I and II to the collection of data near the radar footprints. The cameras were operated from the main deck of the tower (see Figure 2) with a baseline, (camera separation) to height (vertical distance to the water surface) ratio of 0.4. This ratio is consistent with the stereo-data processing requirement to yield a surface elevation resolution of 3 mm. The periods during which the stereo-cameras were operated are given in the Appendix. A typical stereo-analyzed frame is shown in Figure 25 for photo-frame 24 on 27 March 1985. The brightness level at each x-y horizontal point in the data plane corresponds to the magnitude of the z-elevation. The stereo-photo analysis provides 300 scan lines along the x-direction; the point separation in y is 0.85 cm. From individual contours the mean surface elevation is constructed, as shown in Figure 25. These contours show a surface elevation rise of the order of 40 cm over a horizontal length of 200 cm, giving a mean surface slope in excess of 10°. The short wave structure is seen superimposed over the mean sloping surface. This combination of mean slope and high frequency surface elevation provides the information necessary for radar backscatter simulation.

While the stereo-generated surface does not preserve breaking-wave signatures (other than in showing plateau regions), such white water regions are observed in the individual photographs. In Figure 26 the region analyzed stereographically is superposed on the left photograph. Here, breaking waves appear at a crest region (plateau), and another small breaking patch appears in the maximum slope region.

To gain further insight on the nature of water surface roughness superposed over a sloping water surface, a single point scan (point A in Figure 25) is shown in Figure 27(a). The rise in mean water level is large compared to water surface displacement of short waves. Imposing a 50 cm running average on the scan in Figure 27(a) gives the result shown in Figure 27(b). Subtracting Panel (b) from Panel (a) gives the small scale roughness shown in Figure 27(c). The wave-number spectrum of the record in Panel (c) is shown in Panel (d). The latter exhibits a k^{-3} slope and a well defined peak at a wave length 25 cm long.

The results in Figure 27 suggest that the water surface, shown in the stereo-photograph, is composed of the following: (1) the small scale roughness has a peak at L-Band. The short waves (approximately 5 cm in wave height) are superposed on the long waves which have wave heights approximately 30 to 40 cm; (2) the wave number spectrum of the short waves has k^{-3} slope in the high wave-number domain. The accepted slope is k^{-4}, but direct measurements have not been available to date. Also, the short waves may be highly strained by the

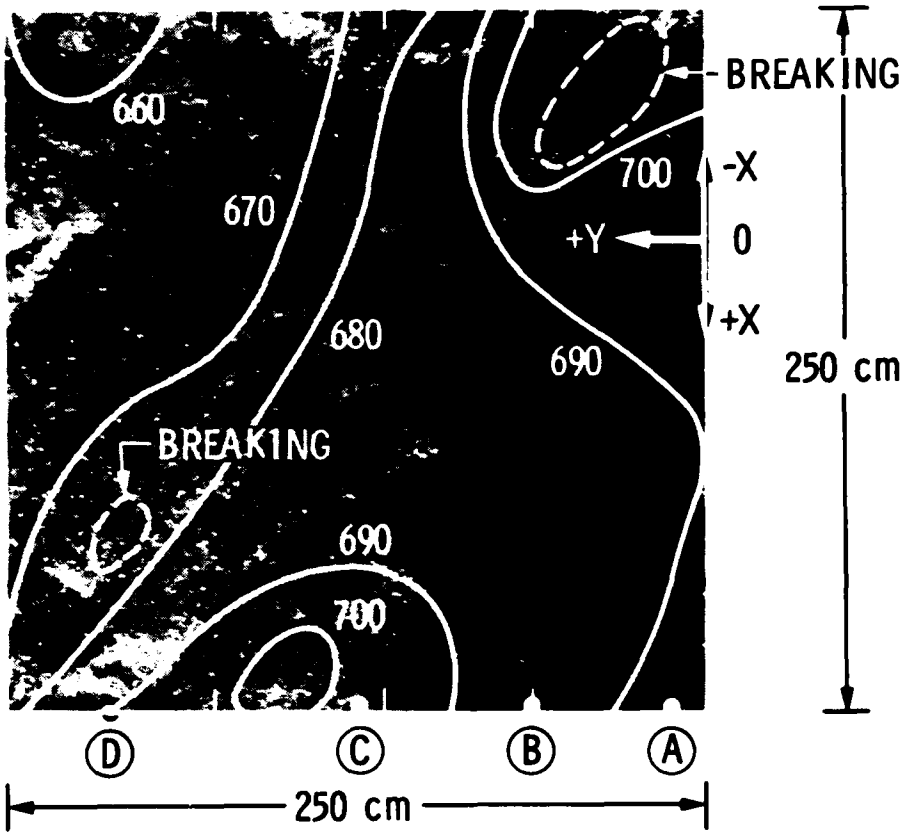

Figure 25. Map of Surface Elevation Determined from Stereo-Pair Frame 24 Acquired on 27 March 1985. The Contours Represent the Mean Surface Elevation Above an Arbitrary Datum. Intensity in the Frame Represents Small Scale Surface Elevation, Z, at Each Point in X-Y Plane.

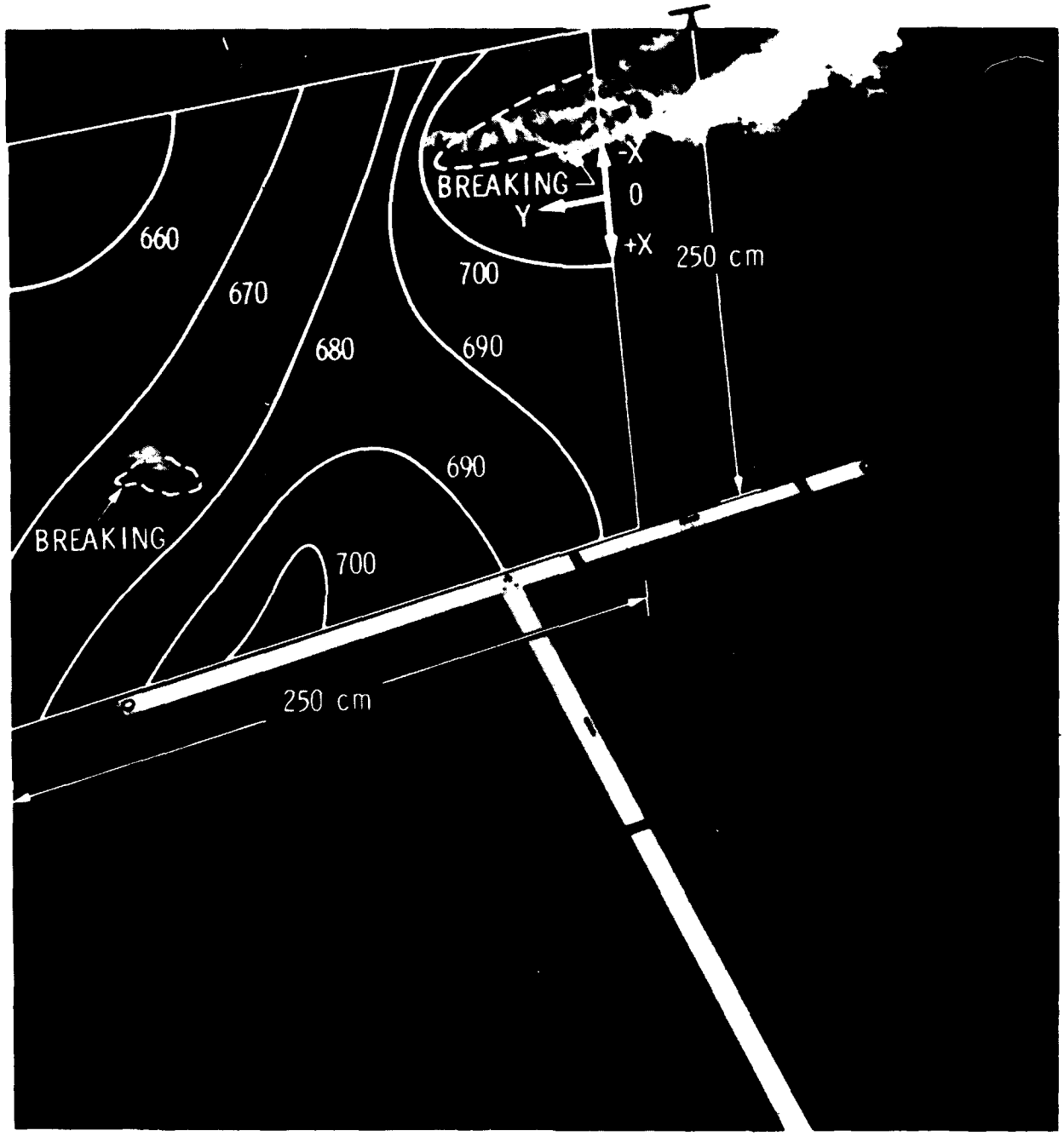

Figure 26. Photograph of Sea Surface Showing Wave Breaking. Superposed Surface Elevation Contours Are Derived From the Stereo-Pair Shown in Figure 25.

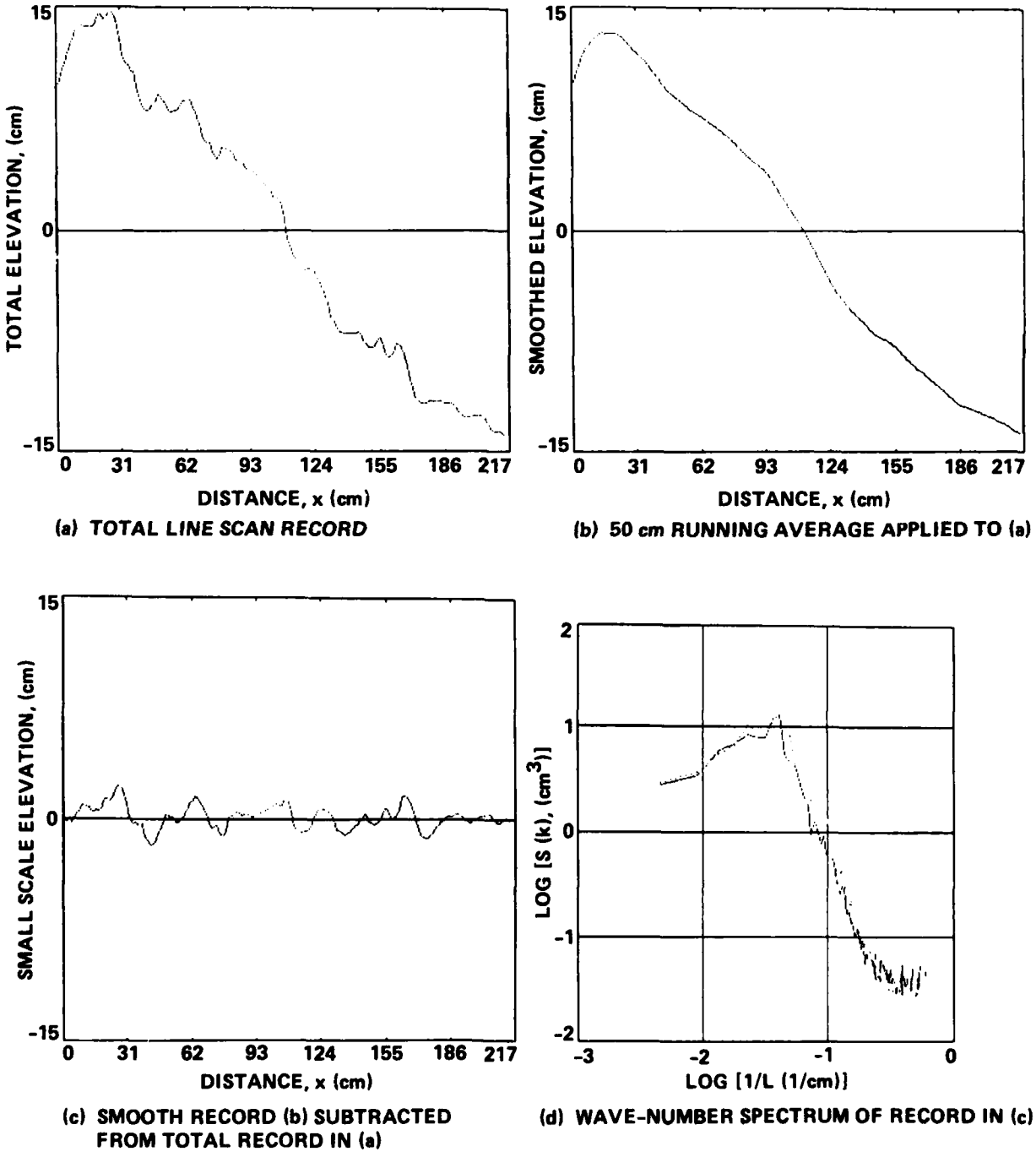

Figure 27. Line Scan Analysis of Stereo-Frame Shown in Figure 25.

long waves, yielding a modified spectrum. It is important to note that useful information on short waves can be obtained after the mean surface due to long waves is removed from the total record. Statistical reliability requires processing of several frames, which is now in progress.

A more precise determination of the wave number spectrum is obtained by utilizing the 2-D FFT technique. Here, the mean water (low pass) surface is computed first and subtracted from the total surface, yielding the small scale surface. The 2-D procedure yields the wave directional distribution. The 2-D FFT, applied to the small scale surface, produces the results shown in Figure 28. In Panel (a) the directionally-averaged wave number spectrum is shown. The slope of the high wave number region is k^{-3}, consistent with Figure 27(d). In panels (b), (c) and (d) the directional distributions for selected wave numbers, corresponding to wave lengths 18, 8 and 12 cm, are given, respectively. The distributions shown in panels (b) and (d) can be fitted with a $\cos^4\theta$ function. The distribution in panel (c) is more peaked and fits a $\cos^{16}\theta$ function.

D. Surface Energy

The technique for measuring surface energy in TOWARD is described in detail by Garrett in Volume II. The data sets collected with this device are given in Table 10 for both Phases I and II of TOWARD. A sample time history of surface energy change is shown in Figure 29. A substantial dip is observed at a location where an administered oil slick passed through the sampled region. A typical time series of the derived surface tension change is given in Figure 30. The remaining data sets are detailed by Garrett in volume II of this report.

Correlations between radar backscatter, short wave slope and surface tension measurements are in progress.

E. Stress and Drag Coefficient Measurements

These measurements are described in detail by Geernaert in Volume II. Briefly, the instrument set-up on the tower mast included the following (sensor elevations are indicated):

Sensor	Elevation (m) Above Mean Sea Level
1. Sonic Anemometer	22m
2. Lyman - α	19m
3. Cold Wire	22m
4. Hot film	22m
5. Bulk Air and Dew Point Temperatures	18m
6. Cup Anemometer	18m
7. Wind Vane	17m
8. Water Temperature	-3m
9. 40 Radiosonde Launches in March 85	

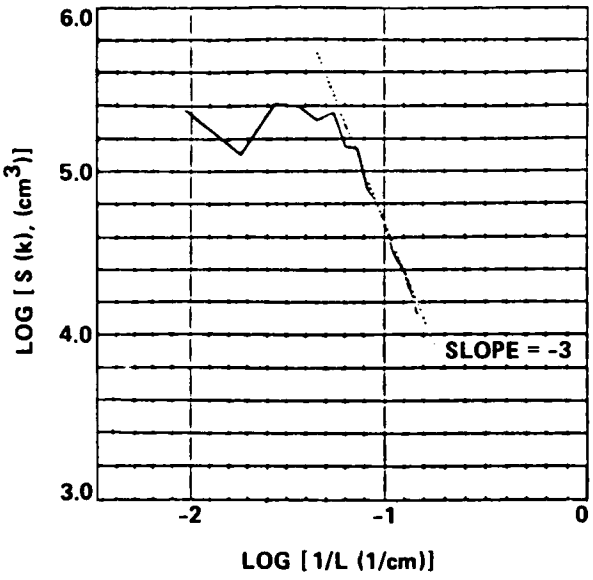

(a) DIRECTIONALLY-AVERAGED WAVE – NUMBER SPECTRUM

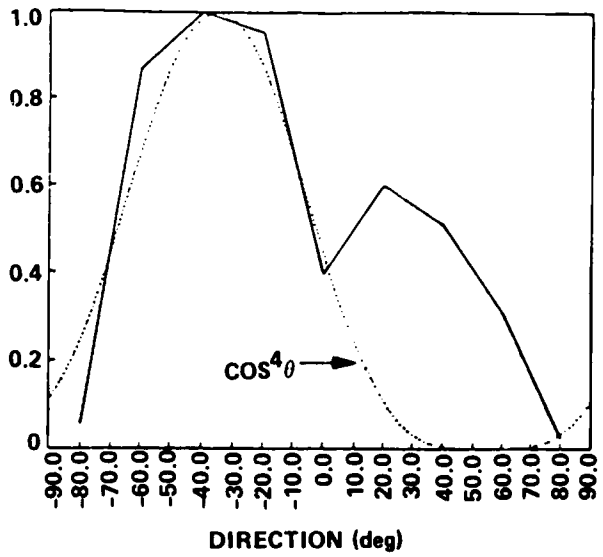

(b) DIRECTIONAL DISTRIBUTION OF 18 cm LONG WAVES

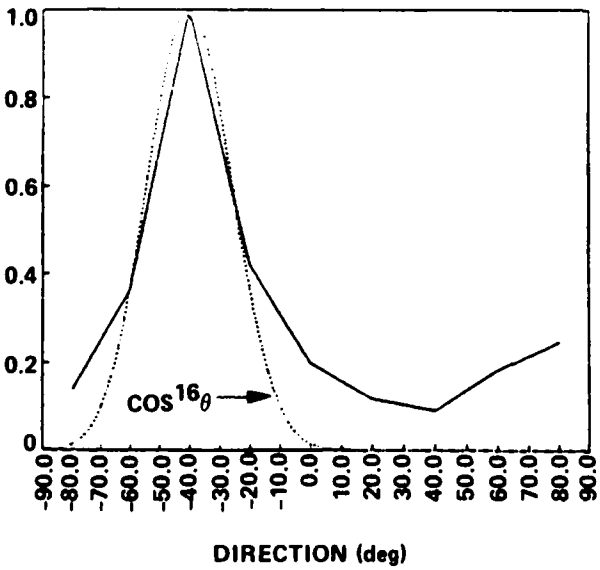

(c) DIRECTIONAL DISTRIBUTION OF 8 cm LONG WAVES

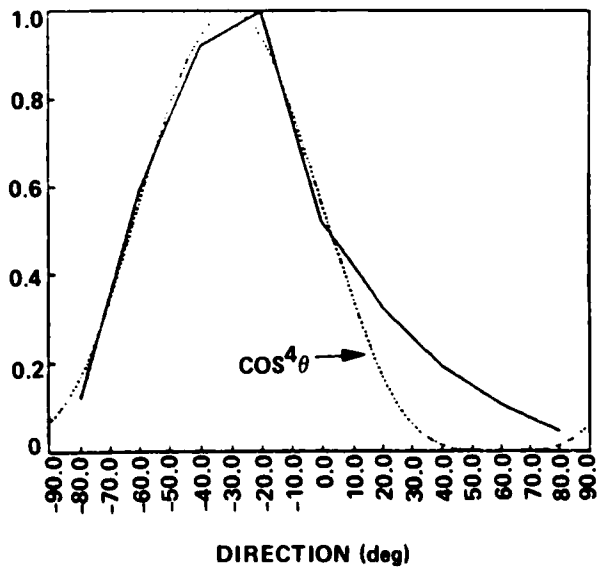

(d) DIRECTIONAL DISTRIBUTION OF 12 cm LONG WAVES

Figure 28. Results of Two-Dimensional Spectral Analysis Applied to Small Scale Surface.

Table 10. NRL Surface Tension Measurement System Data Summary. Time is in Pacific Daylight Time and Pacific Standard Time Before and After 02 am 28 October 1984, Respectively.

Date	Time	Date	Time	Date	Time
09-20-84	1620 - 1648	10-15-84	1616 - 1704	3-08-85	1015 - 1357
09-21-84	1624 - 1657	10-16-84	0933 - 1146	3-12-85	0915 - 1611
09-22-84	0836 - 0851		1833 - 1842	3-13-85	0853 - 1057
	0915 - 1013	10-27-84	0852 - 1414		1130 - 1622
09-24-84	0822 - 0958			3-14-85	0822 - 1059
	1013 - 1057	10-18-84	0915 - 1238		
	1105 - 1232		1315 - 1357	3-15-85	110 - 1539
	1240 - 1358		1416 - 1440		
				3-16-85	1013 - 1400
09-25-84	0814 - 0937	10-20-84	0940 - 1144		
	1014 - 1058		1315 - 1815	3-18-85	1032 - 1140
	1109 - 1333		1853 - 2223		
				3-19-85	1001 - 1223
09-26-84	0853 - 0856	10-23-84	0843 - 1006		1513 - 1637
	0907 - 1459		1152 - 1422		
			1634 - 1722	3-20-85	0826 - 1233
09-27-84	0847 - 1459				1505 - 1605
		10-24-84	0847 - 1128		
09-28-84	0839 - 1210		1208 - 1448	3-21-85	0943 - 1757
	1223 - 1501		1516 - 1654		
				3-22-85	0828 - 1257
10-02-84	0924 - 1044	10-25-84	0835 - 1256		1553 - 1630
	1053 - 1558		1454 - 1557		
				3-24-85	1208 - 1539
10-03-84	0906 - 1520	10-27-84	0847 - 1021		
			1124 - 1654	3-25-85	0823 - 1153
10-04-84	0842 - 0957				1246 - 1358
		10-28-84	1110 - 1250		1543 - 1555
10-06-84	1005 - 1150		1315 - 1558		1611 - 1746
	1129 - 1609				1819 - 1831
		10-29-84	1109 - 1619		
10-09-84	0556 - 0659			3-26-85	0929 - 1258
	0850 - 0918	10-30-84	0823 - 1056		1520 - 1558
	1341 - 1359		1120 - 1519		
	1424 - 1450				
		10-31-84	0936 - 1256		
10-11-84	1843 - 2008		1415 - 1457		
	2030 - 2105				
		11-02-84	1017 - 1622		
10-12-84	0841 - 1317				
	1651 - 1814	11-03-84	1319 - 1725		

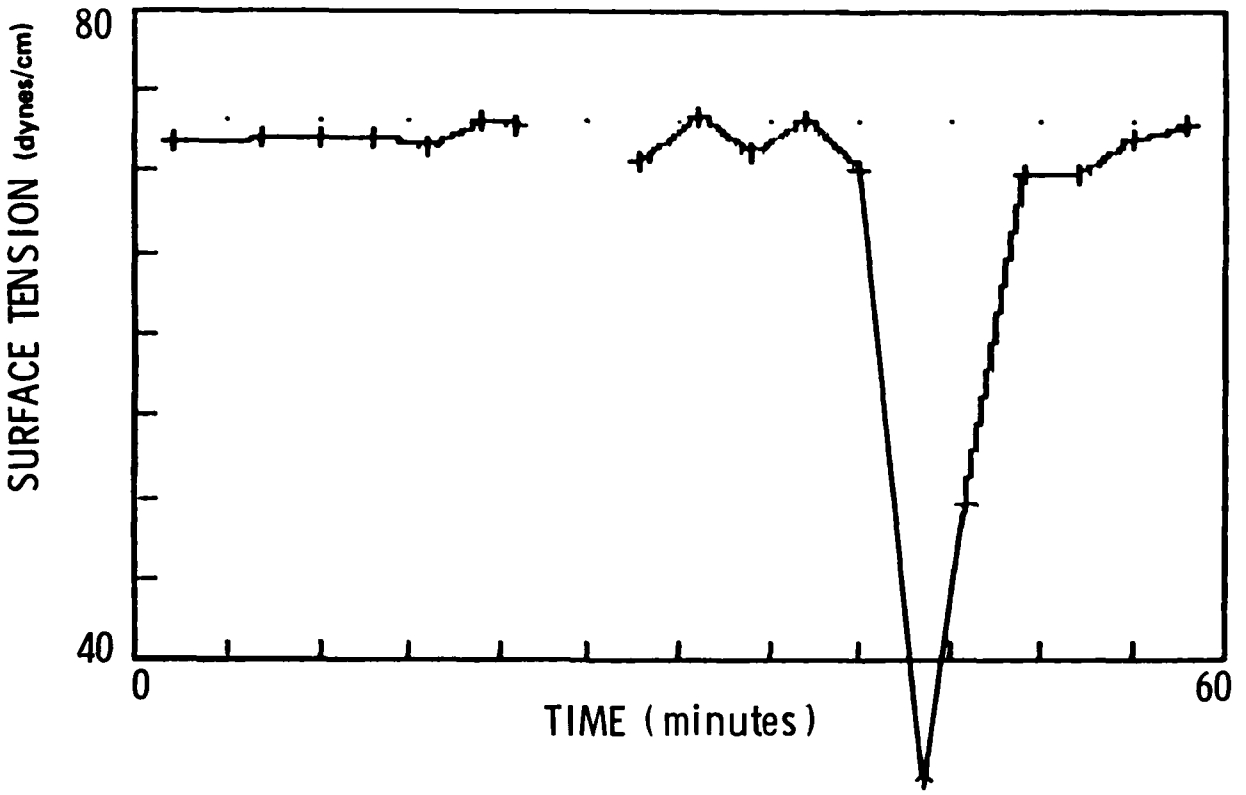

Figure 29. Time History of Surface Energy Showing a Noticeable Drop During Passage of an Administered Slick.

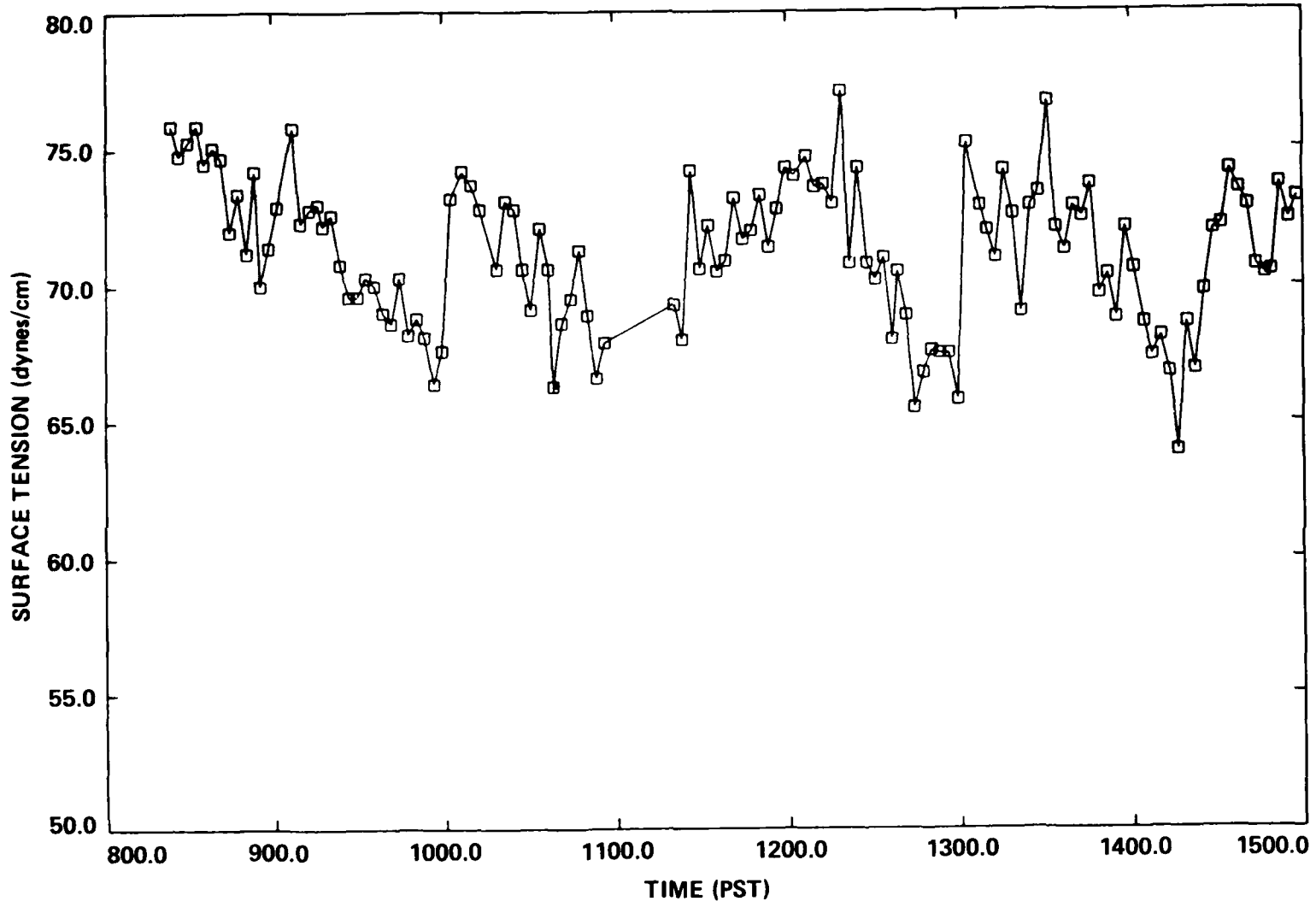

Figure 30. Sample Time History of Surface Tension Measured at the Tower by the Surface Energy Detection Device on 30 October 1984.

The meteorological conditions and data quality are summarized in Table 11. In general, sea breeze conditions were frequently encounterd. The associated sea breeze fetch was less than 50 km when the wind direction was from the west and less than 4-8 km when the wind direction was from the east. The flow distortion at the top of the mast was minimal for winds from west and north, but substantial for winds from south and east. The latter data sets were deleted in the analysis phase. Continuous data collection was obtained from 2 October to 7 November, 1984 in Phase 1 and from 4 March to 28 March 1985 in Phase II.

A detailed analysis, by Geernaert (Volume II) and Geernaert et al (1986), of the Drag coefficients, using the dissipation method, in the range 2-11 m/s, has yielded the following results:

1. The drag coefficient is constant in the range U_{10} = 4-10 m/s with magnitude equal to $1.14 \pm 0.4 \times 10^{-3}$. The drag coefficient increases when $U_{10} > 10$ m/s in a manner consistent with Smith (1980) and Large and Pond (1981).

2. The drag coefficient is generally larger for short fetches compared to long fetches. The available data set for this study is limited to $U_{10} < 4.0$ m/s.

3. Large drag coefficients are observed when cold fronts approach. Correlation of these with wave observations will be revealing.

4. The drag coefficient is large during the initial stage of sea breeze and diminishes as the cycle progresses in time.

F. Thermistor Chain Measurements

Continuous measurements from the thermister chain system, shown in Figure 9, are available throughout the periods of measurements in both Phases-I and II of TOWARD. The temperature measurements are presented in terms of time histories of isotherms varying in the water column at the tower site. The data segments that indicated presence of internal waves are shown in Table 12. A typical internal wave event is shown in Figure 31, as was observed on 7 October 1984.

The analysis of internal wave data is given important attention in light of dominant interest. The focus on resolving the SAR imaging mechanisms for surface waves has pre-empted the possibility of producing early results related to internal waves.

G. Summary and Conclusions Derived from In-Situ Measurements

It is clear from the above that extensive in-situ measurements are available to serve both as: (1) surface truth for radar observations, and (2) basic information, to investigate the near surface layer, and in particular the modulation of short waves by long waves. The measurements of short waves, using stereo-photography, was designed to measure wave lengths in the L-Band range (an adequate investigation of shorter waves, e.g. X-Band range, requires a different configuration of cameras and lenses). The directional long wave measurements are limited in their directional resolution. A high resolution array can enhance the quality of this data set. Nevertheless, comparisons between SAR derived and in-situ derived wave spectra are possible, as will

Table 11. Meteorological Data Quality Assessments and General Conditions during SAR Flight Days.

Flight	Wind Conditions		Strafification	Data Quality Based on Dissipation Measurements
10-2-84	S	3-4	N	G
10-6-84	NW	8-5	S	G
10-7-84	NW	5-7	N	G
10-17-84	NW	7-8	U	G
10-31-84	W	3-6	N	G
11-4-84	NW	2-4	U	G
11-7-84	W	4-5	S	G
3-13-85	W	4-5	N	G
3-18-85	NW	3-10	N	G
3-19-85	W	5-6	N	G
3-20-85	NW	5-7	N	G
3-24-85	W	3-4	S	G
3-25-85	SW	6-7	S	G
3-26-85	SW	4-5	S	G
3-27-85	SW	5-8	S	I

Legend:

South West
North West
South
West
Windspeed (m/sec)

Stable
Neutral
Unstable

Good
Intermittent

Table 12. Internal Wave Events Data Summary.

	Data	Time (GMT)	
	09-06-84	1800 - 2000	
		2000 - 2200	
		2200 - 2230	
	09-07-84	0800 - ?	
		1549 - 1700	
	09-20-84	1100 - 1300	
	09-25-84	1900 - 2100	
*	09-26-84	1500 - 2200	
	10-02-84	1600 - 1800	
		2100 - 2300	
	10-06-84	1700 - 2000	
		2200 - 2400	
	10-07-84	1200 - 1300	
*		1450 - 1800	
	10-13-84	1600 - 1800	
		2000 - 2200	
	10-16-84	1300 - 1600	
	10-17-84	1700 - 2300	
	10-20-84	2300 - 0300	(10-21-84)
	10-23-84	1600 - 1930	
	10-24-84	1700 - 2400	
*	10-25-84	1700 - 2300	
	10-27-84	1900 - 2300	
	10-28-84	2300 - 0020	
	10-29-84	1900 - 2000	
	10-30-84	2200 - 2400	
	11-02-84	2300 - 0100	(11-03-84)
	11-04-84	0100 - 0400	
	11-05-84	0000 - 0400	
	03-15-85	2200 - 2300	
	03-20-85	2300 - 2400	
	03-26-85	0300 - 0500	
	04-02-85	2200 - 2320	

*Strong Activities

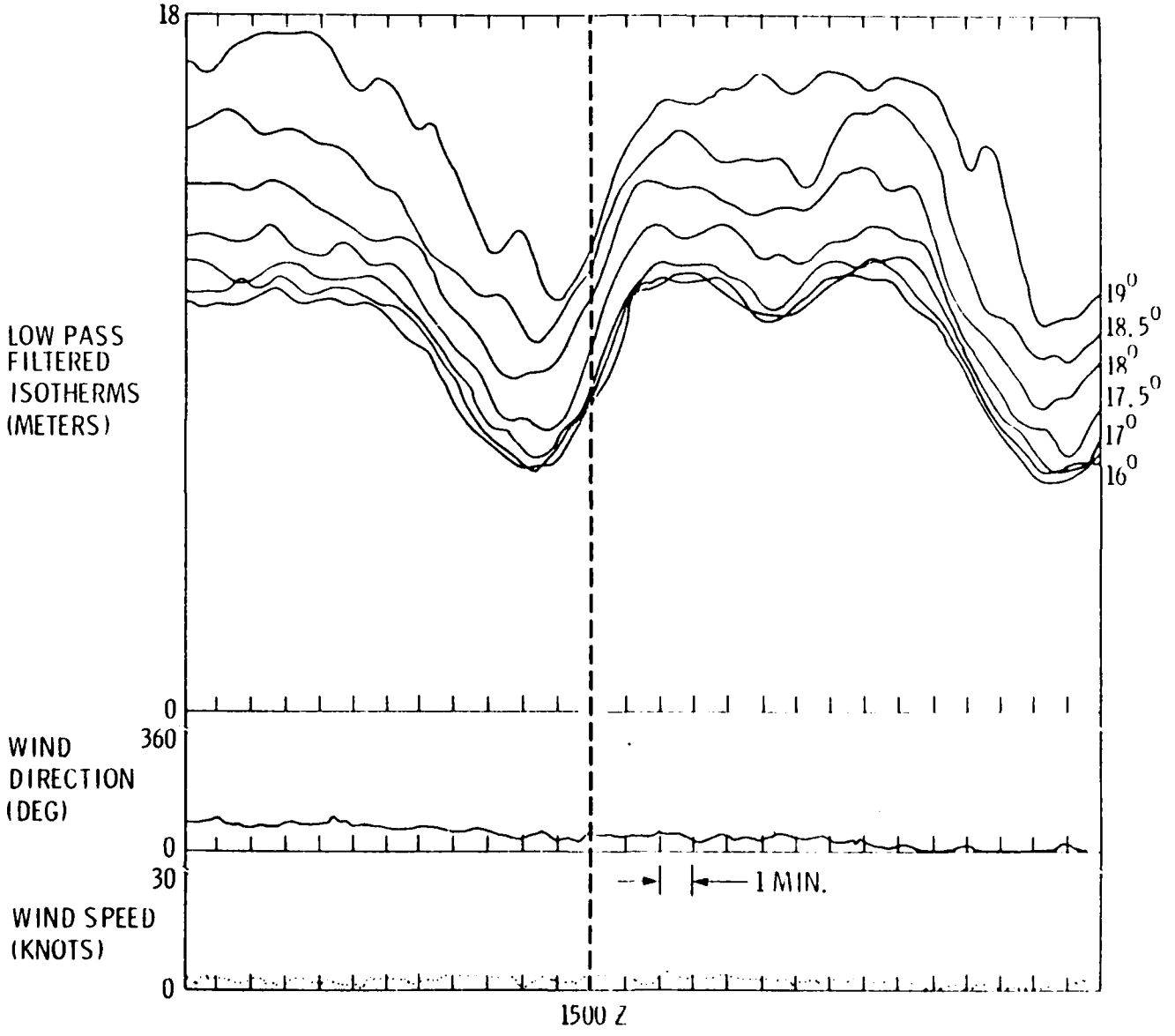

Figure 27. Time History of Isotherm Elevations Showing Internal Wave Structure on 7 October 1984.

be demonstrated in chapter VII.

The preliminary conclusions derived from analysis of in-situ measurements to date are:

1. The dominant long wave energy during the SAR flights was from direction 290°, which corresponds to the window north of San Nicolas, and south of Santa Rosa Islands. These waves are imaged by SAR as practically undirectional. The directional wave array shows more directionally distributed wave energy at the same time and location.

2. PDF's of slope measurements indicate near Gaussian distribution for wave frequencies less than 2.5 Hz, and non-Gaussian distribution for waves high-passed above 7.5 Hz. Non-Gaussian behavior is normally associated with strongly nonlinear wave-wave interaction.

3. Slope frequency-spectra of short waves indicate that the Pierson and Stacy (1983) model overpredicts wind speed, for a given slope intensity, by a factor of 3-5.

4. Direct measurement of the directional wave-number spectrum of short waves is possible with stereo-photography. The first frame yields the high wave-number slope to be k^{-3}, and a directional distribution that can be approximated by $\cos^4\theta$. Statistical averaging obtained from analysis of more frames is required to confirm these observations, and is in progress.

5. The meteorological obervations indicate that the drag coefficient depends on fetch and is higher for small fetches. The drag coefficient also depends on storm conditions, being higher during the passage of a front than after (when steady winds prevail, for a long period of time).

The measurements of surface tension are valuable in their own right; they represent the first open ocean time series of surface tension recorded to date. The observations were sampled every three minutes. Hence, the data set is suitable for detecting surface tension variability with time scales greater than six minutes. Internal waves and processes with longer time scales can be investigated. Surface tension variability along the profile of a surface wave can not be obtained with this data set.

The internal wave measurements were restricted to a single station. The temperature profile and the horizontal current vector at 5 m below the water surface were measured. The salinity change with depth is known to be negligible at this site, so that time series of the density profile can be derived from the temperature profile. Because of finite depth considerations, the internal waves can be assumed to be parallel to the bottom contours. These assumptions allow the development of space-time models that characterize the internal waves being detected with the thermistor chain. Correlations with radar backscatter and short surface waves can be computed to determine the modulation of short surface waves by internal waves, subject to these stated assumptions.

V. RADAR BACKSCATTER MEASUREMENTS: OBJECTIVES, DATA SUMMARY AND EARLY RESULTS

The primary objectives for obtaining direct radar backscatter measurements in TOWARD are to:

1. Determine the effect of radar backscatter modulation by long waves on synthetic and real aperture radar imaging of the sea surface.

2. Improve understanding of the mechanisms responsible for radar backscatter from the sea surface (e.g. Bragg, specular and wedge), and to assess the relative contribution of sea spikes in relation to less spurious fluctuations.

3. A non-SAR objective is to provide a data set sufficiently complete to enable assessment of limitations of existing scatterometer models.

To achieve these objectives, simultaneous measurements were incorporated with parallel radar systems operated by the University of Kansas, Naval Research Laboratory, and Jet Propulsion Laboratory. In addition short wave slope measurements were obtained with the laser-optical sensor and with stereophotography. Such a collection of simultaneous measurements, under various environmental conditions, provides a unique opportunity for addressing the stated objectives.

A. Jet Propulsion Laboratory System

The Jet Propulsion Laboratory radar was described in the Science Plan (Shemdin, 1984). It was operated from the main deck of NOSC tower, which restricted its operating range of azimuthal angles and reduced its signal to noise ratio. A summary of the acquired data sets are given, in tabular form, in the appendix. Analysis and comparison with other radar data sets is in progress.

B. Naval Research Laboratory System

The Naval Research Research Laboratory radar operated a pulsed L-Band system in both phases I and II. it was placed at 35° incidence angle and in HH mode during the SAR overflights. The data collected are of high quality and form an essential element toward validating SAR imaging theories.

A K_u-Band CW radar was operated during Phase II only. The objective for deployment of this radar was to put to advantage the meteorological and oceanographic measurements for use in evaluating the functional dependence of radar cross-section on wind speed when other environmental parameters are varied. The system was coherent so that amplitude and phase information could be recorded on an analog magnetic tape recorder for later analysis. Both mean cross-sections and modulation transfer functions are computed from the recorded data.

The pulsed L-Band system used for SAR simulation was also coherent; its output was recorded on analog tape. During periods in between flights (by far the majority of the time), this system was used to record data for use in investigating mean radar cross-sections and the modulation transfer function.

A complete log of data acquired is given in the Appendix. Times of aircraft overpasses are also noted in these tables. Data analysis and comparison with other data sets is in progress.

C. University of Kansas System

The University of Kansas radar was described in the Science plan; it was operated from the upper deck of NOSC tower. An extensive set of measurements was obtained during phases I and II of TOWARD. The data sets are summarized in tabular form in the Appendix. The tables specify periods of measurement, incidence and azimuthal angles, frequency and relation to wind or wave directions. All data sets have been processed and are being used for analysis and comparison with other radar data sets. The first results discussed below are almost exclusively based on this data set. A summary comparison of the three radar systems used in TOWARD is given in Table 13.

Table 13. Tower Radars System Characteristics.

	U. Kansas	NRL	JPL
Frequencies (GHz)	1.5,5,10,15	1.5,14.0(1)	3-18
Polarization	VV,HH	VV,HH	VV,HH
Surface Wave Property Measured	wave height	orbital velocity	wave height
Backscattered Signal Measured	power	power	total signal (can process to power)

(1)Phase-II only

D. Data Analysis and Early Results

Initial priority in radar-backscatter data analysis was given to day 31 October 1984, in support of the priority established by the SAR committee. The early results rely on these data sets; other days have now been analyzed

An important element toward understanding the mechanisms of radar-backscatter is a firmer understanding of sea spikes, their frequency of occurrence, relative contribution to the total radar backscatter, and whether they are generated by specular or Bragg mechanism. A sea spike was defined in the preliminary analysis as instantaneous return in excess of 6 dB above the

average returned power. The University of Kansas data set acquired on 31 October 1984, was analyzed to investigate the influence of sea spikes on the radar cross-section, σ_o. Five records at L-Band and five records at X-Band were studied to determine the influence of sea spikes on σ_o. Samples of these L-Band and X-Band records are shown in Figures 32 and 33, respectively. The result of the analysis is shown in Table 14.

The results in Table 14 indicate that sea spikes have no significant influence at L-Band. The X-Band analysis, also shown in Table 14, indicates presence of more frequent spikes in the record. Comparisons between University of Kansas data sets and those acquired by NRL and JPL are in progress.

To investigate the contribution of sea spikes to total radar backscattered power at X-Band, an extensive data set was analyzed at different wind speeds and look angles (relative to wind and wave directions). These are summarized in Table 15. The frequency of occurrence of sea spikes varies in the range 1-5% of the total points sampled. An example of the distribution of spikes in bins greater than 6dB is given in Figure 34 for a wind speed of 4.5 m/s. In this example the spikes occurred 1.16% of the sampled times and increased the total power by 0.17dB or 4.0%.

The wind speed dependence is shown in Figure 35, where at 6.5 m/s wind speed the frequency of occurrence of all spikes becomes 3.36%, and the spikes contribution to the total power becomes 0.8db or 20%. The frequency of occurrence of spikes decreases as the threshold is increased above 6dB, as expected. Whether such a decrease in frequency of occurrence can be explained in terms of radar backscatter mechanisms remains to be investigated.

At frequencies above X-Band one may expect higher occurrence of spikes (since hardly any spikes are observed at L-Band). Examples of such occurrence are given for 14.6 GHz radar at two different wind speeds. The results for a wind speed of 3.5 m/s are given in Figure 36, where spikes contribute negligibly to the total return power. In Figure 37, similar results are given for 7.0 m/s wind speed. Here, the spikes occur 12.31% of the time and increase total power by 2.4 dB or 73%.

Another objective in radar backscatter analysis is the determination of whether and, if so, how radar backscatter is modulated by the long ocean waves in the cross-wind and cross-wave direction. Differing views exist on this point because it is an argument in support of the "Velocity Bunching" hypothesis for SAR imaging of the ocean surface. Using University of Kansas time series, wave height (from radar ranging technique) and backscattered power are shown in Figure 38. From these records the modulation transfer function, M_a, is computed from (subscript a refers to wave amplitude)

$$M_a(\Omega) = \frac{H_{pa}(\Omega)}{K\ P\ H_{aa}(\Omega)} \quad ,$$

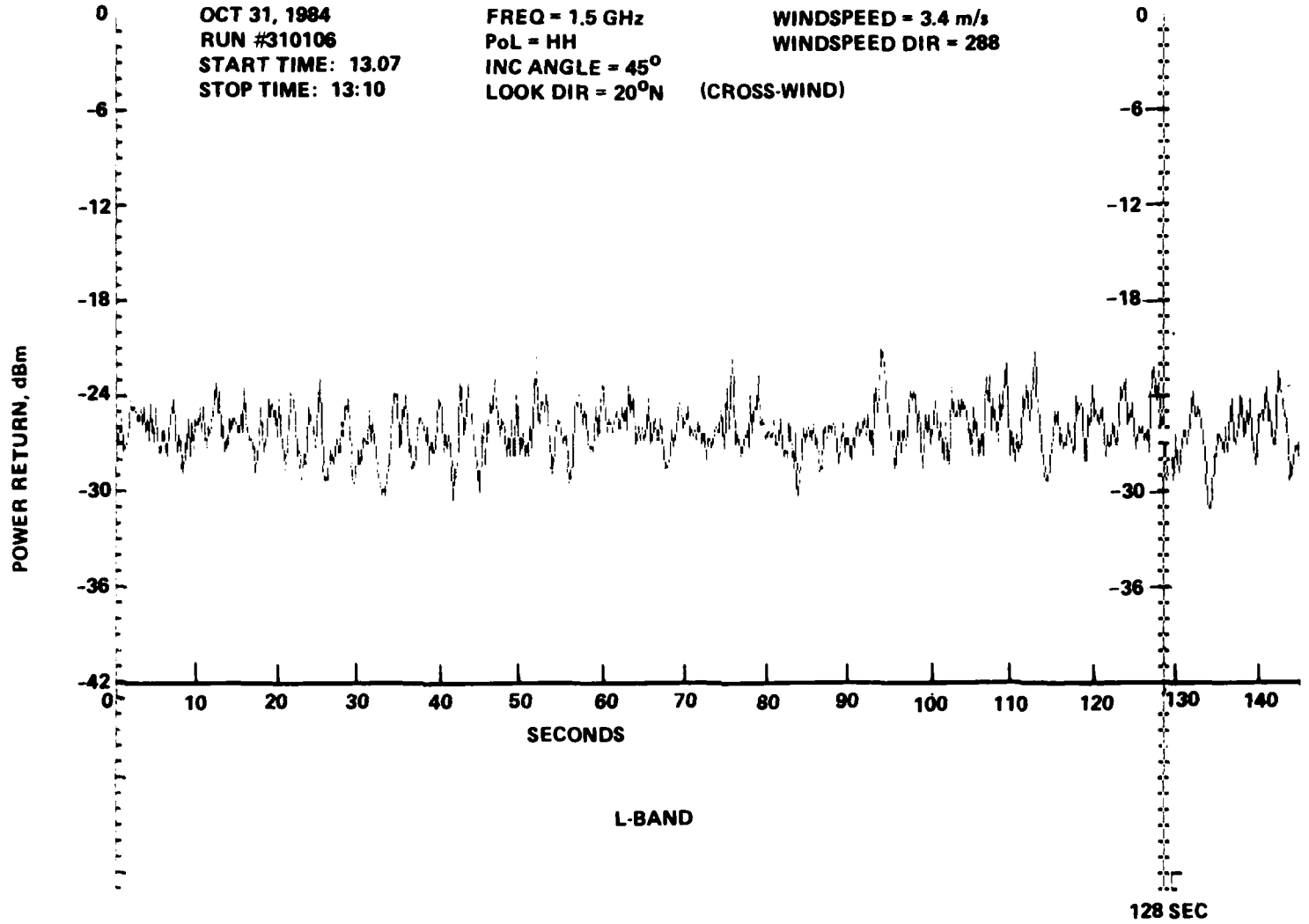

Figure 32. Time History of L-Band Power Return Used in Sea-Spike Analysis. Record Specifications are Shown in Inset.

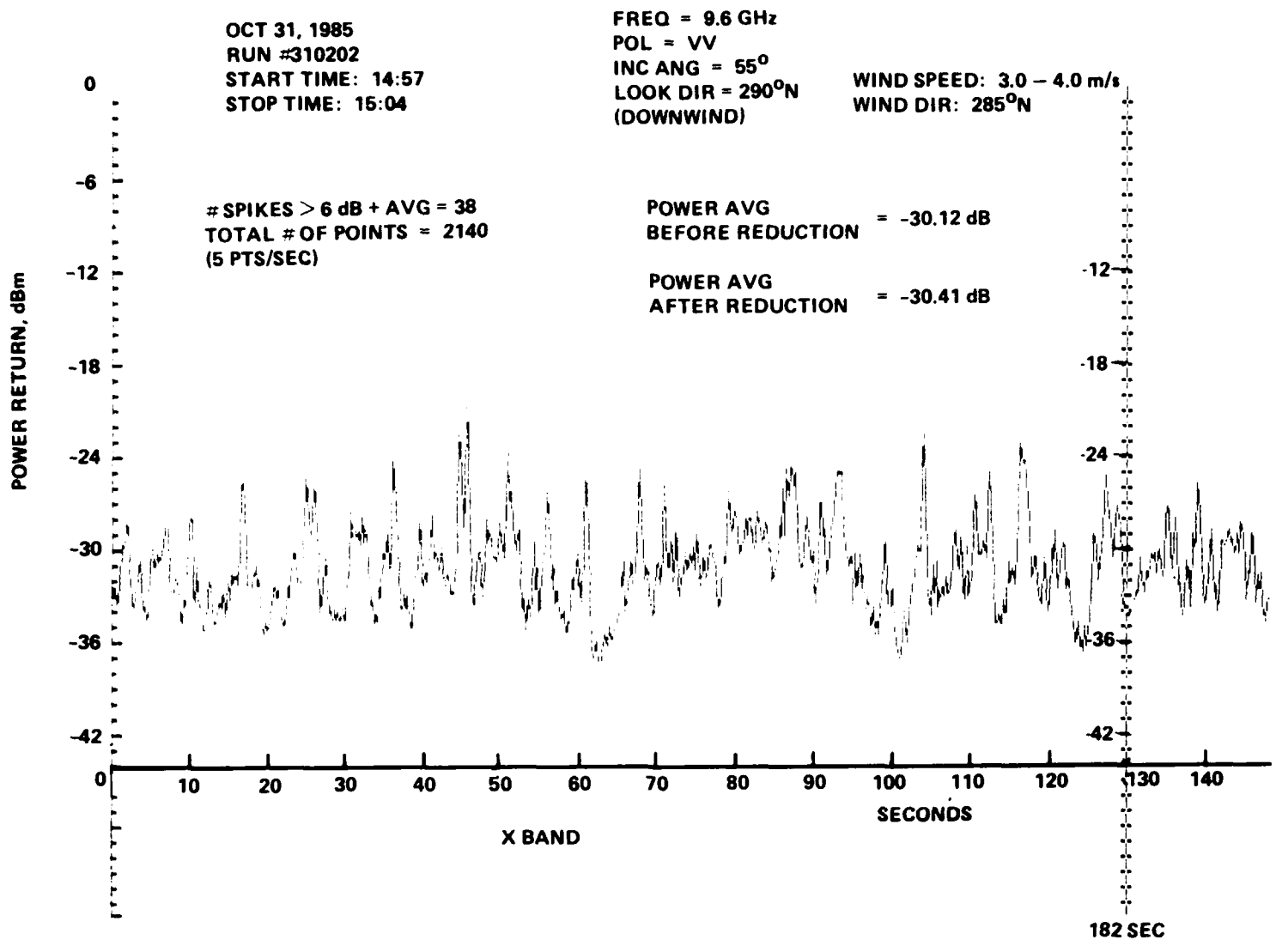

Figure 33. Time History of X-Band Power Return Used in Sea-Spike Analysis. Record Specifications are Shown in Inset.

Table 14. Analysis of Radar Backscatter for "Sea Spikes" with University of Kansas Multi-Frequency Radar. All the Records were obtained on 31 October 1984 between 13:00 and 16:00 PST. The Wind Speed was 3-4 m/s. Sampling Interval of 0.2 s was used.

Run No.	Number of Spikes	Total Number of Samples	Pre-Removal Average Power (dBM)	Post Removal Average Power (dBM)	Frequency (GHz)
		L-Band: 1.5 GHz; Incidence Angle: 45°, Look Direction: Cross-Wind; Polarization: HH			
310106	0	1120	-25.930	-25.931	1.5
310107	1	2975	-24.811	-24.821	1.5
310108	0	2960	-26.430	-26.440	1.5
310110	0	1420	-26.00	-26.02	1.5
310111	0	1680	-25.62	-25.62	1.5
		X-Band: 9.6 GHz; Incidence Angle: 55°, Look Direction: Down-Wind; Polarization: HH			
31202	38	2140	-30.135	-30.417	9.6
31204	22	2605	-32.287	-32.438	9.6
31206	19	1230	-30.878	-32.122	9.6
31207	39	2920	-29.796	-30.017	9.6
31211	107	4580	-29.736	-30.146	9.6

Table 15: Contribution of Sea Spikes to Total Radar Backscattered Power at X-Band.

Frequency = 9.6 GHz, POL = VV, Incidence Angle = 45°

Windspeed (m/s)	Look Angle W.R.T. Wind	Look Angle W.R.T. Wave	Percent Ratio of Spikes/Total Samples	Date/Run #
4.5	15°	80°	5.80%	260120
	15°	80°	3.57%	260117
	45°	20°	1.16%	260121
	45°	25°	1.30%	260119
	45°	20°	3.98%	260115
	90°	25°	1.34%	260122
	90°	25°	1.57%	260116
	160°	80°	2.60%	260113
5.0	0°	60°	3.58%	270215
	0°	0°	2.96%	220012
	0°	0°	3.61%	220011
	30°	20°	4.41%	270211
	30°	40°	4.97%	270212
	50°	60°	4.02%	270213
	50°	60°	3.81%	370210
	80°	70°	2.79%	270214
5.5	15°	80°	3.41%	260123
	45°	20°	4.04%	260124
6.5-7.0	90°	0°	3.36%	270002
	90°	0°	3.44%	270009
7.5-8.0	10°	60°	3.05%	270205
	10°	60°	3.60%	270203
	30°	40°	3.35%	270206
	30°	40°	2.93%	270202
	50°	60°	4.22%	270207
	80°	70°	2.28%	270208
	140°	70°	1.41%	270204

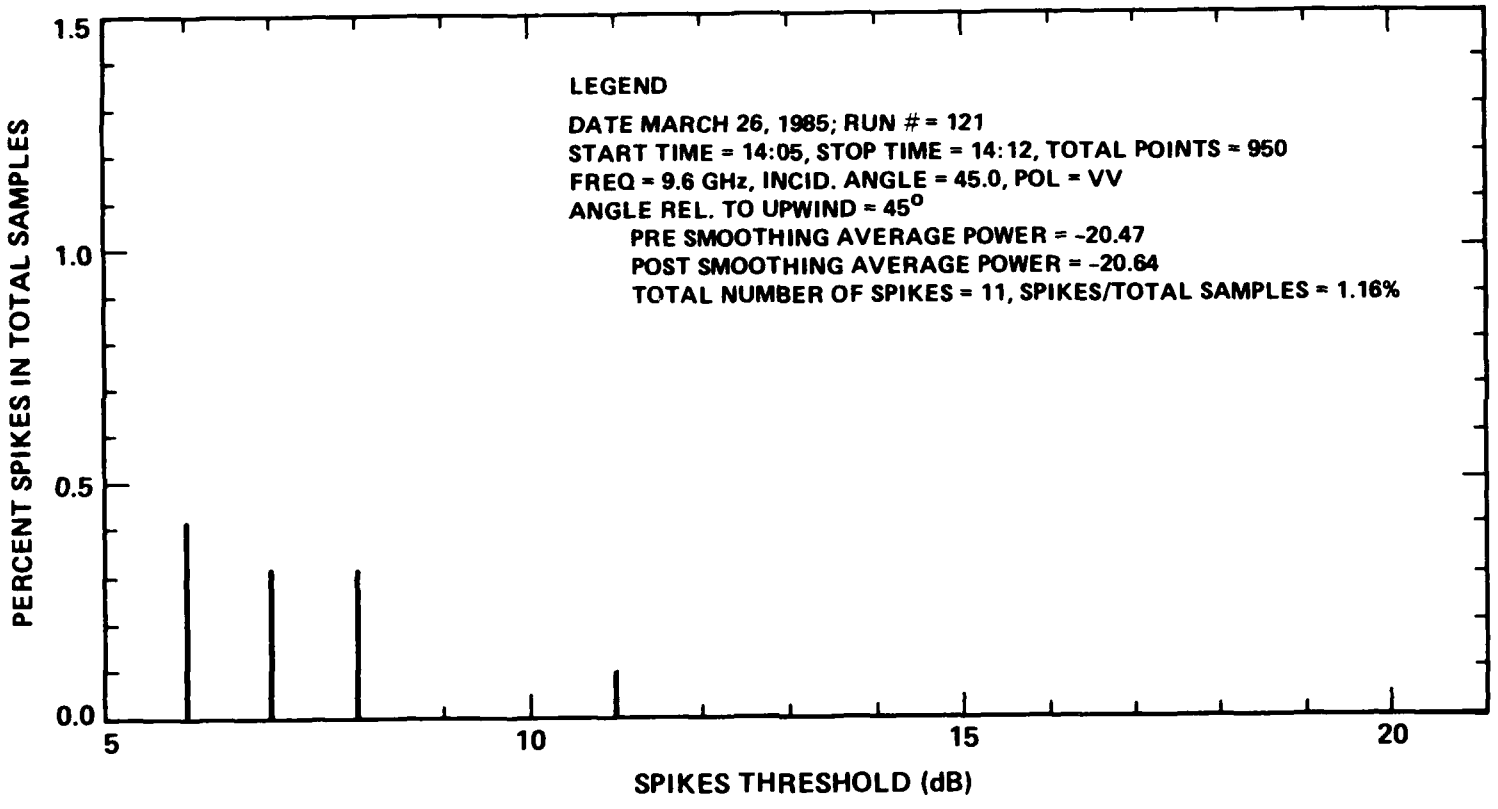

Figure 34. Sea Spikes Analysis for X-Band Radar; Wind Speed = 4.5 m/s .

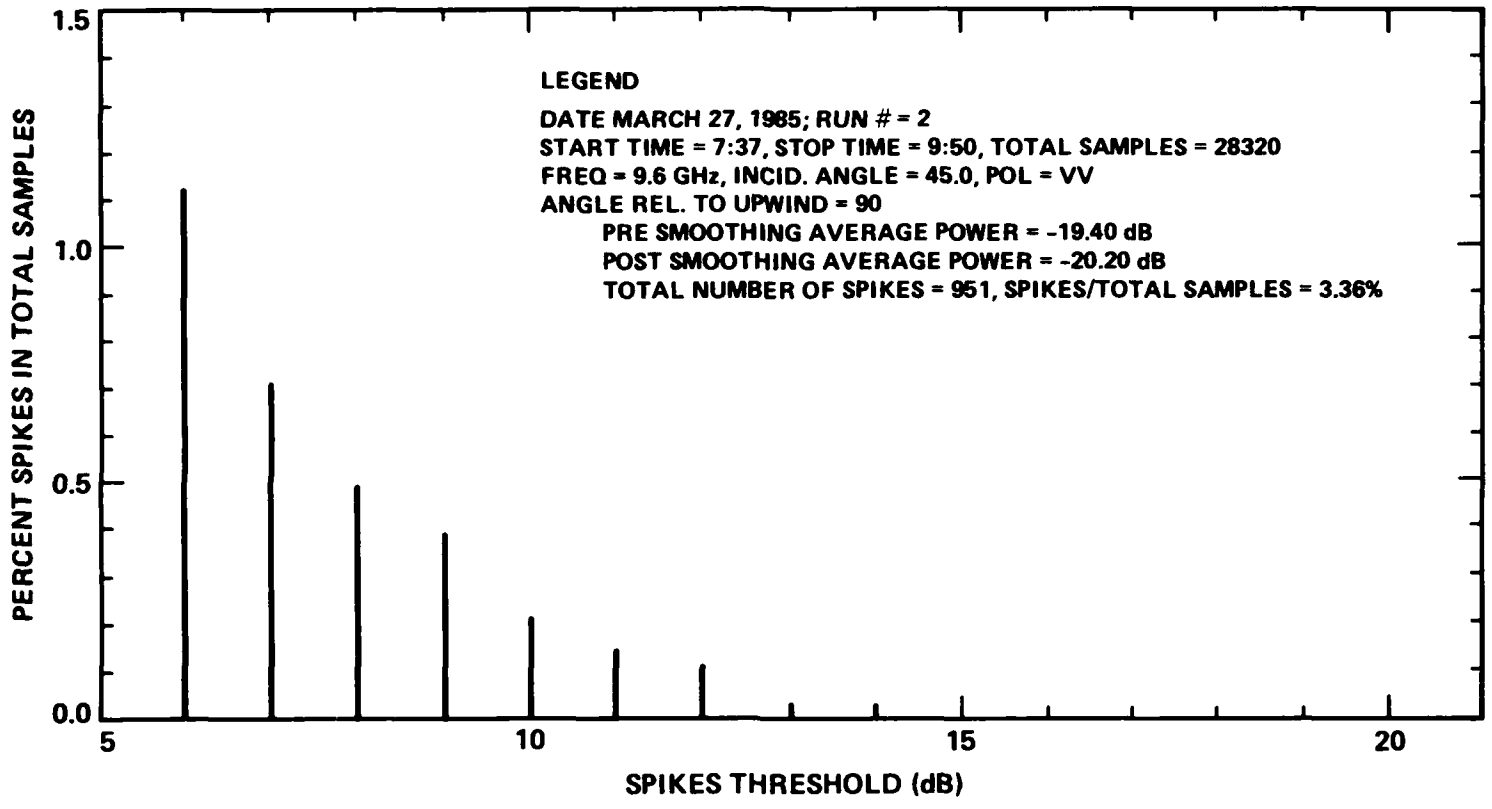

Figure 35. Sea Spikes Analysis for X-Band Radar; Wind Speed = 6.5 m/s.

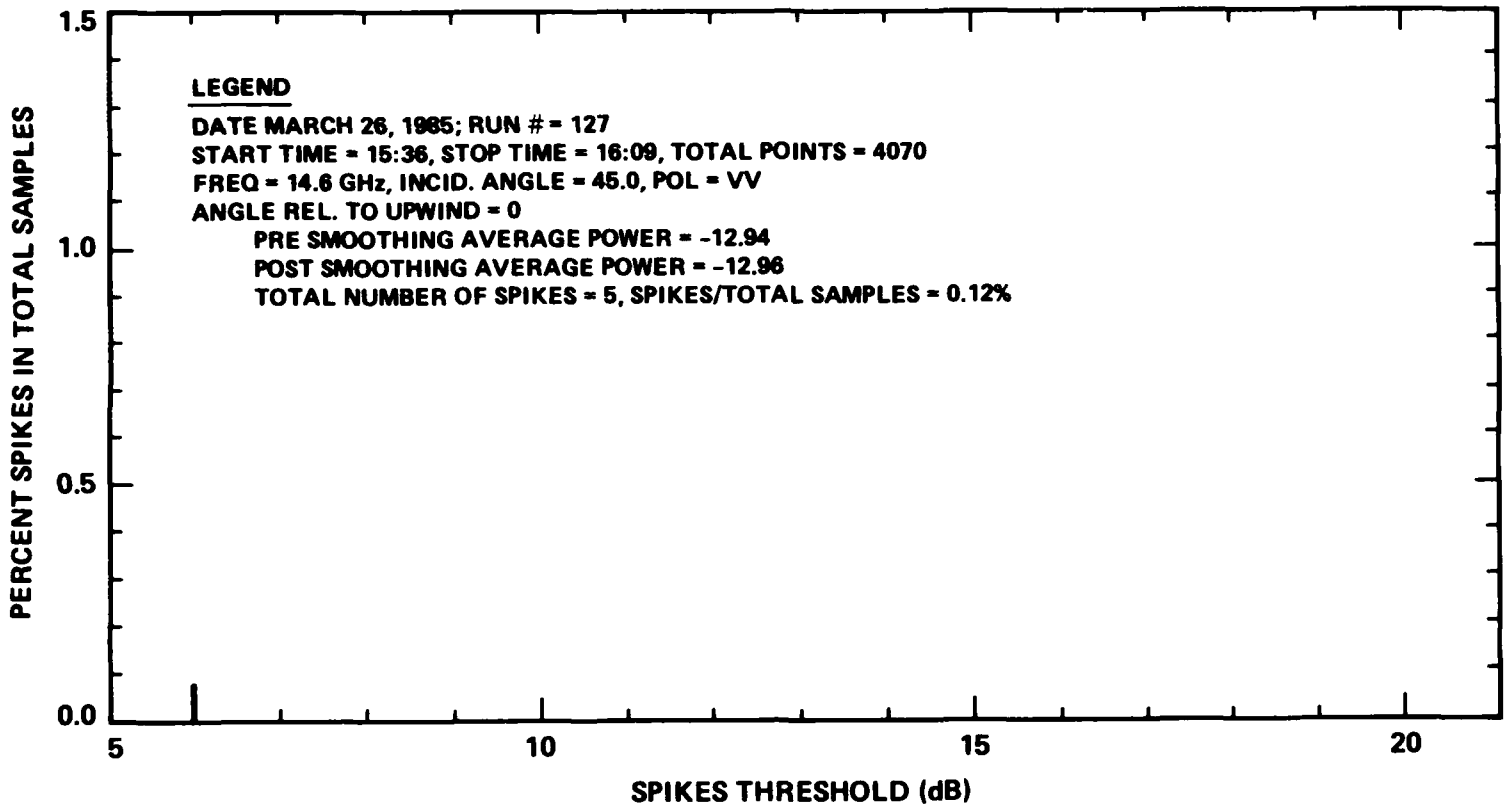

Figure 36. Sea Spikes Analysis for X-Band Radar; Wind Speed = 3.5 m/s.

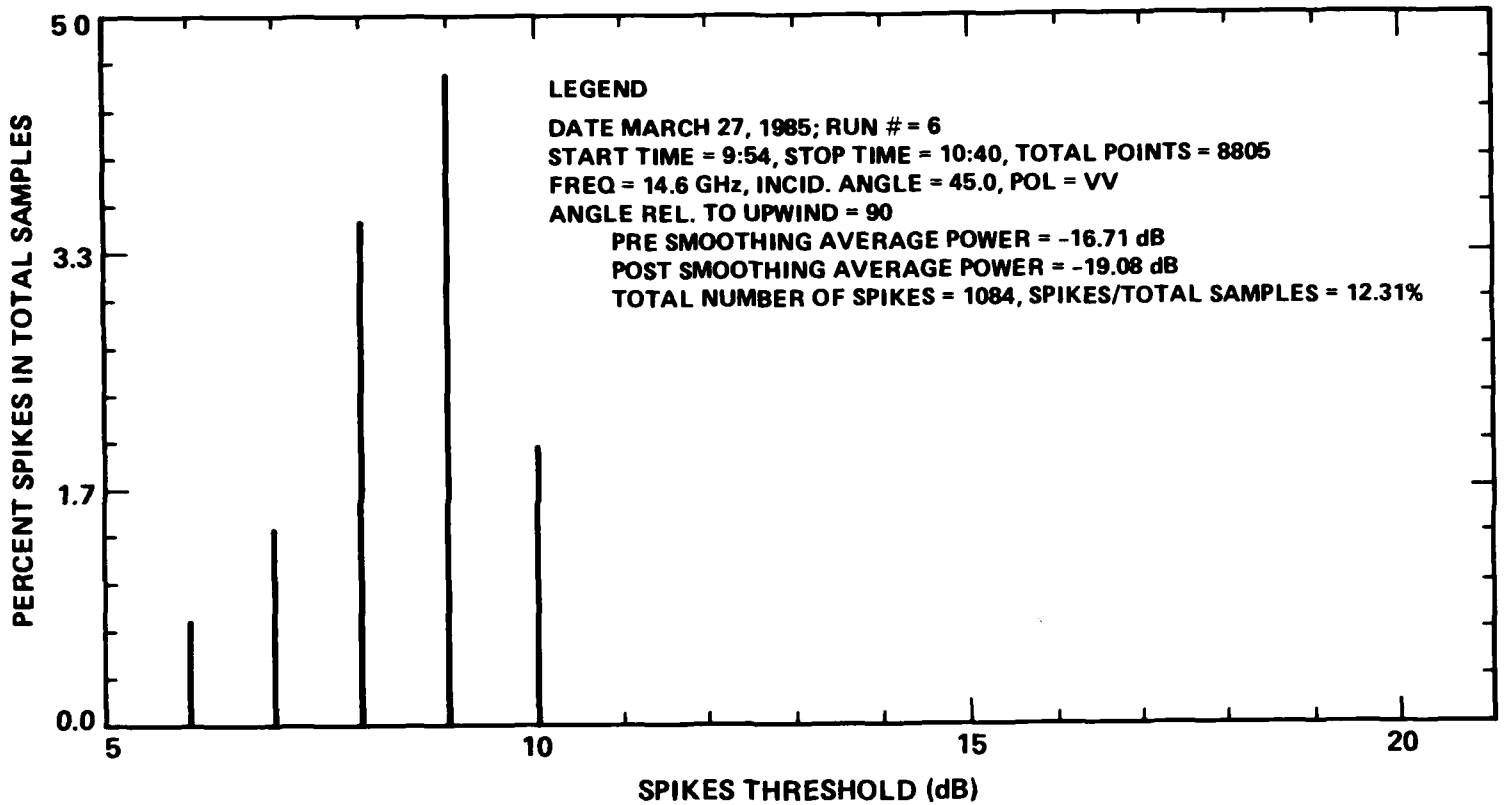

Figure 37. Sea Spikes Analysis for X-Band Radar; Wind Speed = 7.0 m/s.

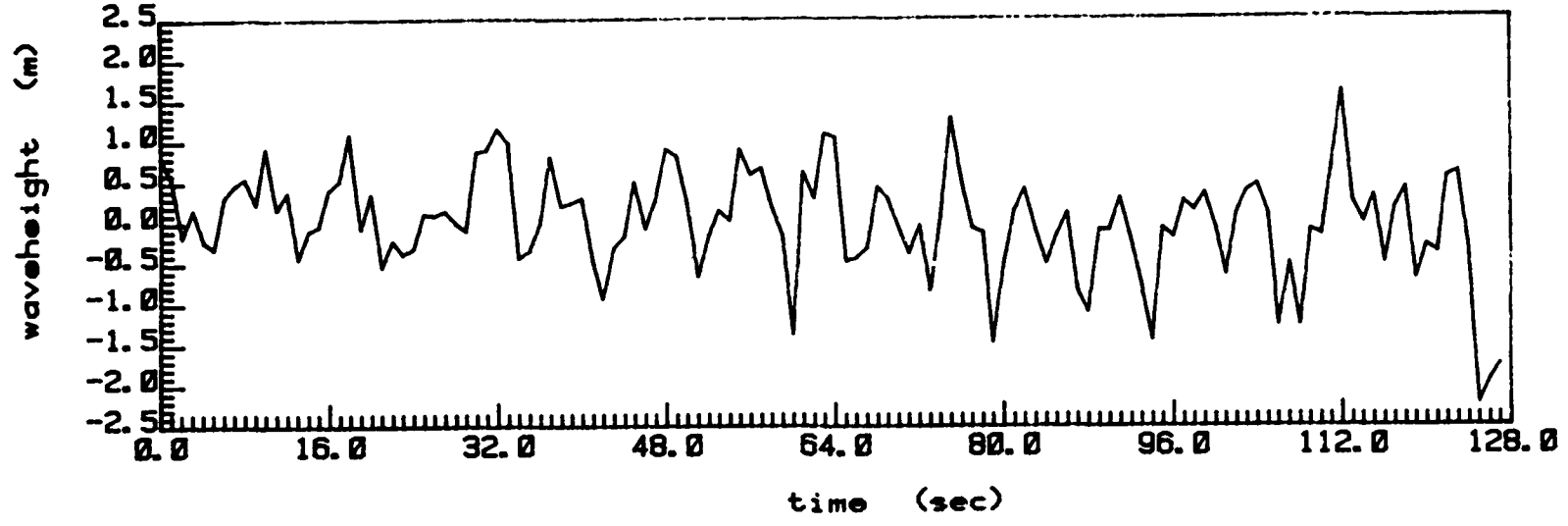

(a) WAVE HEIGHT RECORD OBTAINED USING RADAR RANGING TECHNIQUE

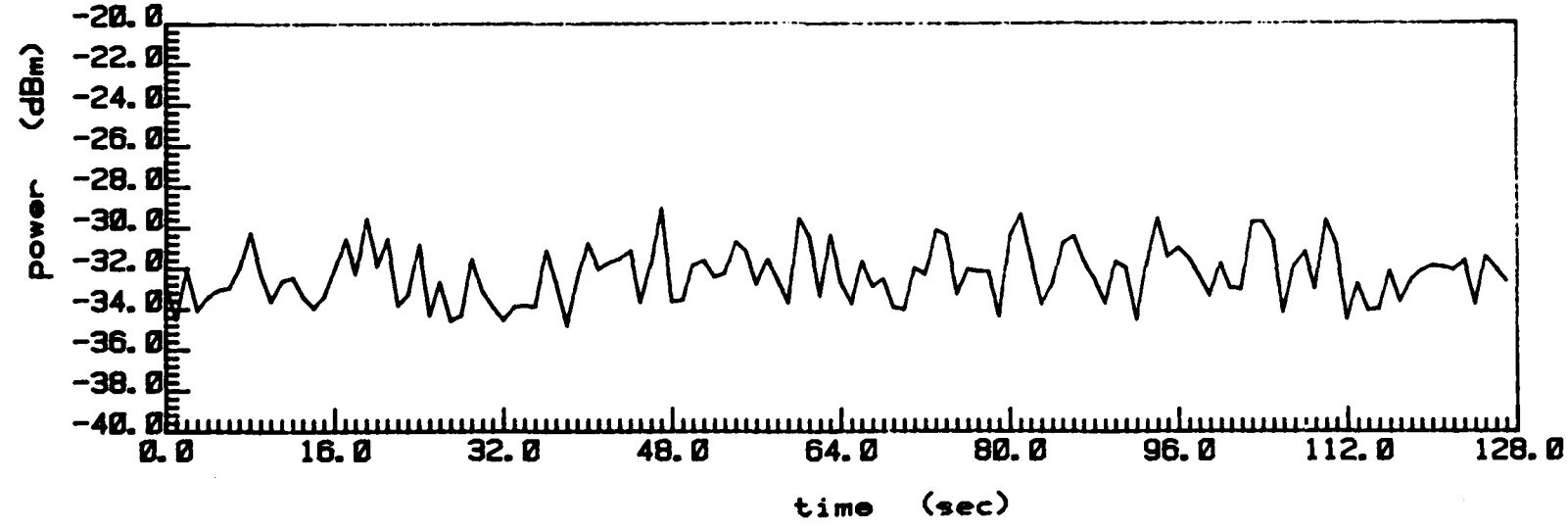

(b) BACKSCATTERED POWER RECORD

Figure 38. L-Band Tower Run 200-105, on 20 October 1984, 10:08 - 11:09 PST, HH - Polarization, 55° - Incidence Analysis Cross-Wind Direction.

where Ω and K refers to long-waves frequency and wave-number, respectively, H_{pa} is the cross-spectrum of backscattered power and amplitude of the long waves, and P is the mean backscattered power. The wave height spectrum, coherence and MTF obtained from the two records in Figure 38 are given in Figure 39. Panel (a) in Figure 39 indicates presence of a dominant long wave at frequency 0.12 Hz. Panel (b) indicates high coherence levels between wave height and radar backscatter. Panel (c) suggests the peak energy in the modulation transfer function is at the dominant frequency of the long waves. Finally, Panel (d) indicated that the modulation peak in radar backscatter leads the wave displacement by 80° at the dominant frequency.

Another example computed from the data set obtained during the SAR flight of 31 October 1984 is shown in Figure 40. The radar look angle was approximately perpendicular to both wind and wave direction (azimuthally travelling waves). Panel (a) shows the peak in wave height spectrum at 0.14 Hz. Panel (b) shows a corresponding peak in the power spectrum of returned power at 0.14 Hz. Such correspondence is not confirmed in the NRL data. Further resolution of this issue is an element of the data analysis in progress.

E. Summary and Conclusions Derived from Radar Backscatter Data

The available data sets obtained with radars deployed on the NOSC tower form a data base adequate to explore a variety of problems needed for understanding the mechanisms of radar backscatter from the sea surface. Results obtained from analyses of data can be summarized as follows:

1. At L-Band spikes occur infrequently in low to moderate wind speeds, and contribute negligibly to the mean backscattered power.

2. The frequency of occurrence of spikes increases with higher radar frequencies and higher wind speeds. Such an increase also corresponds to an increase in the contribution of spikes to the mean backscattered power.

3. The mechanism responsible for generating spikes is not yet explained definitevely.

An important issue, for which the necessary data sets from TOWARD are available, is the significance of the modulation in radar backscatter induced by long azimuthal waves. Comparisons between the NRL, JPL, and University of Kansas data sets are in progress with the aim of establishing consensus on this issue.

Other insights are expected to emerge when radar backscatter measurements are compared with measured slopes of short waves. Here, modulation of short waves by long waves can be computed from the radar data set and from the laser slope data set independently. Agreement vs. disagreement in the computed modulations will be revealing.

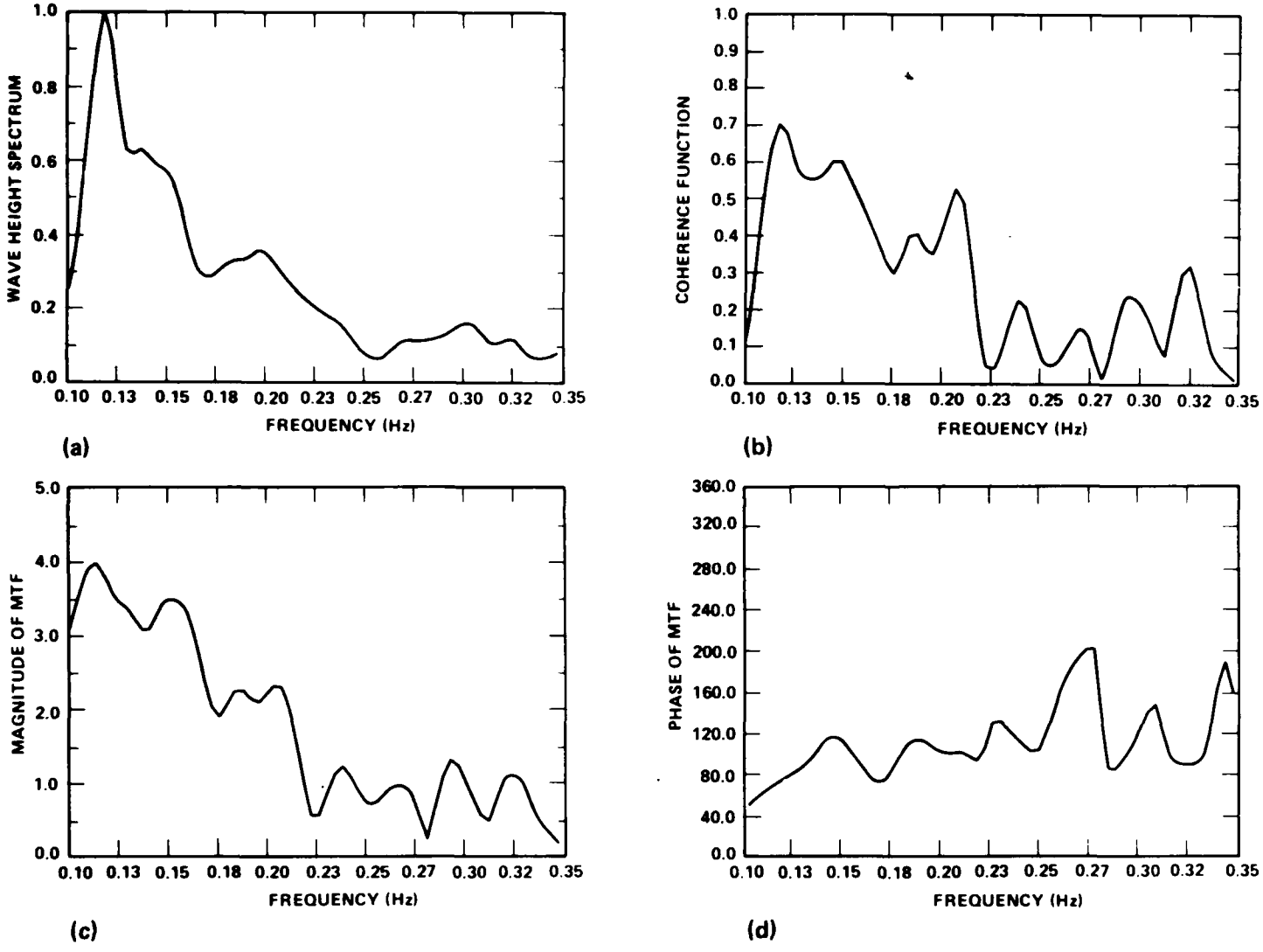

Figure 39. Auto- and Cross-Correlations of Wave Height and Radar Backscattered Power, Shown in Figure 38. (a) Wave Height Spectrum Normalized with Respect to Peak, (b) Coherence, (c) Magnitude of MTF and (d) Phase Lead of MTF Relative to Wave Displacement.

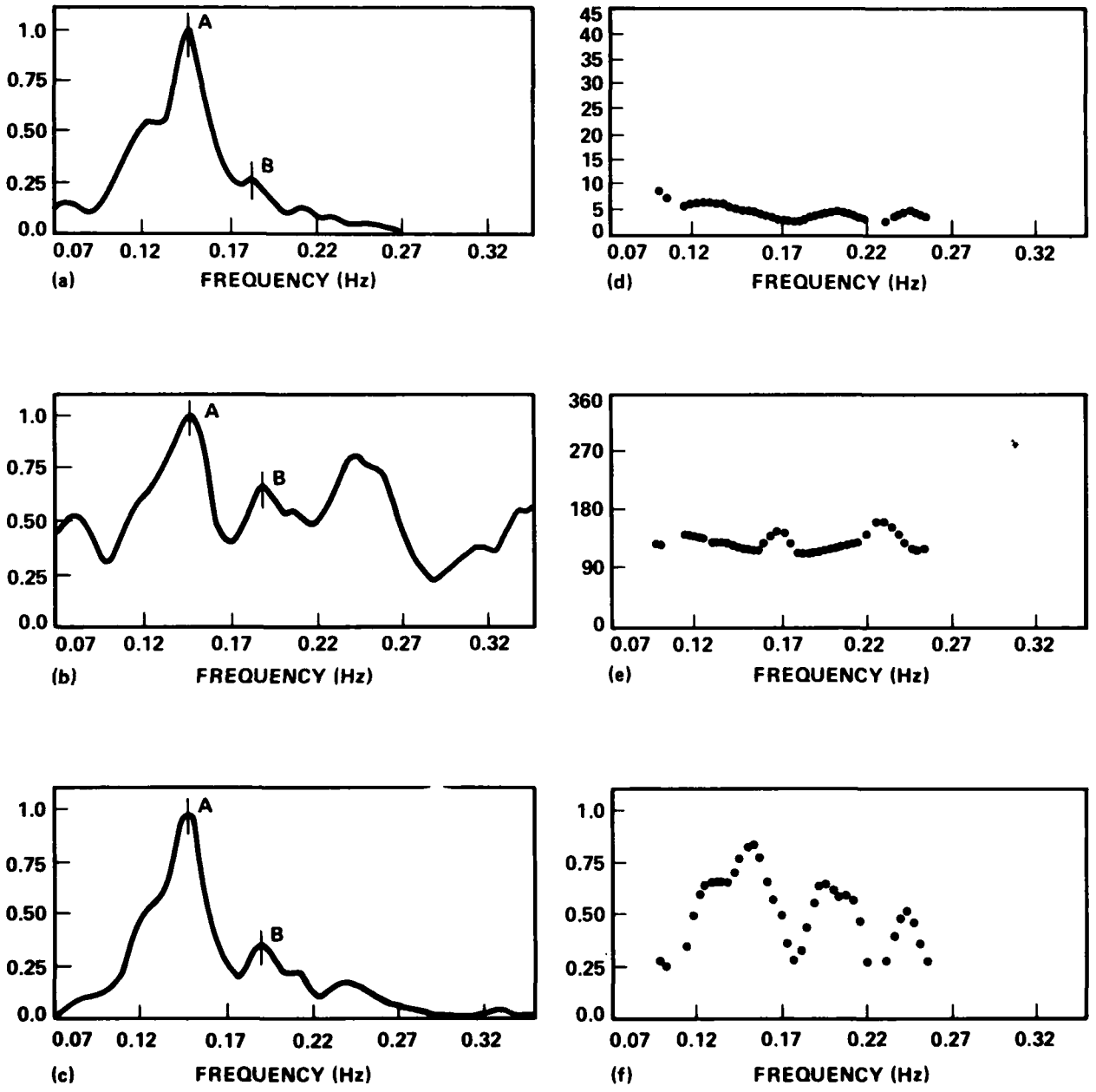

Figure 40. L-Band Tower Run 108, on 31 October 1984, Auto- and Cross-Correlations of Wave Height and Radar Backscattered Power. Wind Speed = 3.5 m/s, Wind Direction = 287°, Wave Direction = 290°. Radar Look Direction = 20°, Incidence Angle = 45°, Polarization - HH. (a) Wave Height Spectrum, (b) Radar Backscattered Power Spectrum, (c) Cross-Spectrum of Radar Power and Wave Height, (d) Modulation Transfer Function, Ma, (e) Phase of Ma, and (f) Coherence.

VI. SAR IMAGING ARGUMENTS

There is considerable interest in understanding the theoretical basis for SAR imaging of the ocean surface. The early work of Larsen, Moskowitz and Wright (1976) probably marks the beginning of this trend. Their analysis remains valid to date for the assumptions they stipulated. Hence, it is reviewed here to underline departure from their theoretical approach in applications where their assumptions are no longer valid. In this chapter, SAR imaging arguments are presented in (A) when the ocean surface is flat, i.e. no surface waves, and in (B) when surface waves are present. The impact of surface waves on SAR resolution is discussed in (C).

A. SAR Ocean Imaging Arguments of a Flat Sea Surface

Larsen et al (1976) considered imaging of a flat ocean surface (no surface waves). The ocean was assumed to have a current distribution of the form shown in Figure 41.

The Doppler frequency shift, $\Delta\omega$, was determined to be

$$\Delta\omega = 2\,k \cdot (\vec{V} + \vec{U}),$$

$$\Delta\omega \approx 2\,k \cdot \left(V \frac{y'}{R'} + U_x\right), \tag{1}$$

where k is the radar wave number, V is aircraft velocity, U is surface current, R' is horizontal component of range and y' is target displacement in aircraft coordinates. The Doppler shift is related to the x-component of current, U_x, and platform speed (see Figure 42).

The voltage received in radar platform coordinates is given by

$$e(t) \sim \int \rho(y', t) \exp\left[i\Delta\omega\,(y')\,t\right] dy' \quad . \tag{2}$$

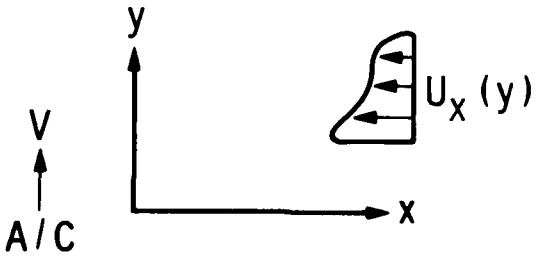

Figure 41. Schematic of Surface Current Distribution in Larsen et al (1975).

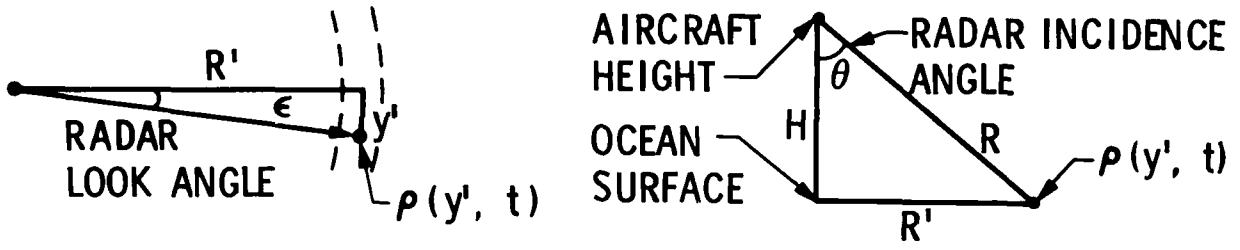

Figure 42. Schematic of SAR Horizontal and Vertical Geometry.

The transformation to earth coordinates is specified by:

$$y = y' + Vt.$$

A transformation of variables is introduced

$$s = 2kt\ (V/R') \quad ,$$

so that the Doppler Shift in Equation (1) becomes

$$\Delta\omega \approx -s\ V + \frac{s}{t}\left(y + \left(\frac{R'}{V}\right) U_x\right) \quad , \tag{3}$$

or

$$(\Delta\omega)t \approx -s\ Vt + s\left(y + \left(\frac{R'}{V}\right) U_x\right) \quad . \tag{4}$$

When $\rho(y', t) = \rho_o$, a constant representing a homogeneous roughness, Equation (2) is used to calculate the radar backscatter voltage in earth ordinates

$$e(s) \sim \int \rho_o \exp\left[is\left(y + \frac{V'}{V}\ U_x\right)\right] dy \quad , \tag{5}$$

where the quadratic error term, exp [-isVt] has been removed (normally done by matched filtering in SAR systems).

Introducing another coordinate transformation

$$r = y + \left(\frac{R'}{V}\right) U_x \quad ,$$

the voltage return has a Fourier integral from

$$e(s) \sim \int \frac{\rho_o \exp [irs]}{[1 + (\frac{R'}{V}) \frac{d U_x}{dy}]} dr \ . \qquad (6)$$

For demonstration purposes, if the derivative term in the denominator is small, i.e.,

$$(\frac{R'}{V}) \frac{d U_x}{dy} << 1 \ ,$$

Equation (6) is approximated by

$$e(s) \sim \int [1 - (\frac{R'}{V}) \frac{d U_x}{dy}] \exp [irs] dr \ . \qquad (7)$$

The Fourier transform, I(y), provides voltage intensities in the image domain

$$I(y) \sim 1 - (\frac{R'}{V}) \frac{d U_x}{dy} \ . \qquad (8)$$

If one considers a sea region that is quiescent and defines $I_o(y)$ to correspond to $\frac{d U_x}{dy} = 0$, then $I_o(y) \sim 1$, and the modulation in the image domain becomes.

$$\frac{\delta I}{I_o} = \frac{(I - I_o)}{I_o} \sim (\frac{R'}{V}) \frac{d U_x}{dy} \ . \qquad (9)$$

Using the incidence angle, θ, to relate range, R, to horizontal component of range R'

$$R' = R \sin \theta$$

the "velocity bunching" argument, as coined by Larsen et al (1976), is defined for no surface waves as

$$\left(\frac{\delta I}{I_o}\right)_{V.B.} = \left(\frac{R}{V}\right) \sin\theta \frac{d U_x}{dy} \quad . \tag{10}$$

For a Real Aperture Radar (RAR), intensity modulation in the image can be defined in terms of a hydrodynamic modulation which is assumed to be related to radar backscatter, σ_o, modulation i.e.,

$$\left(\frac{\delta I}{I_o}\right)_{RAR} = \left(\frac{\delta I}{I_o}\right)_{HYDRO} = \frac{\delta\sigma_o}{\sigma_o} \quad . \tag{11}$$

For SAR, the intensity modulation in the image can be determined as the sum of the real aperture modulation (amplitude) and velocity bunching contribution (phase):

$$\left(\frac{\delta I}{I_o}\right)_{SAR} = \left(\frac{\delta I}{I_o}\right)_{RAR} + \left(\frac{\delta I}{I_o}\right)_{V.B.} \quad . \tag{12}$$

It is noted that the above arguments have been stipulated for an ocean surface that is flat.

B. SAR Ocean Imaging Arguments in Presence of Surface Waves

In the presence of surface waves it is shown below that the SAR imaging process is somewhat more complex than described above for a flat surface. We now consider azimuthally travelling surface waves superimposed on a surface having the same mean current distribution described in Figure 41. This is shown schematically in Figure 43.

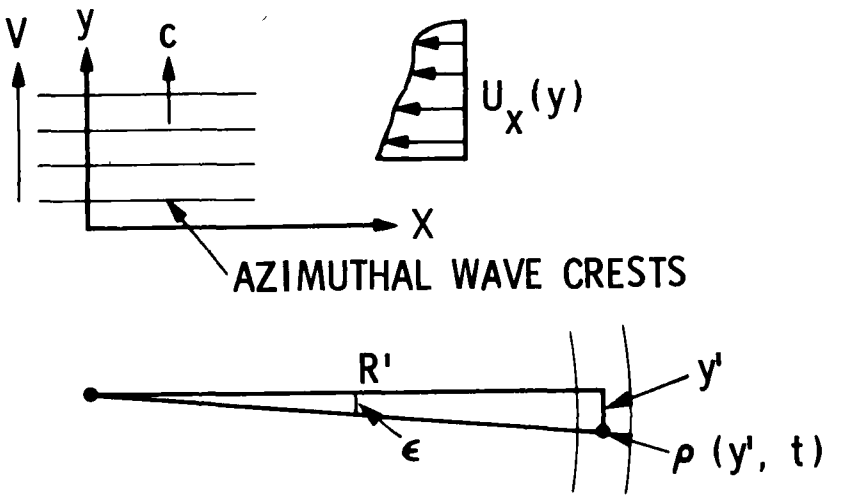

Figure 43. Schematic of SAR Geometry in Presences of Waves and Current.

The vertical displacement of the water surface is defined by η. Under such conditions the Doppler frequency shift becomes

$$(\Delta\omega) \approx 2\ k\ \left(\frac{Vy'}{R'} + U_o\ \frac{y'}{R'} + U_x + \frac{d\eta}{dt}\cos\theta\right) \quad , \tag{13}$$

where U_o is the horizontal orbital velocity of swell and $\frac{d\eta}{dt}$ is the vertical orbital velocity. Denoting $\frac{d\eta}{dt} = V_o$ and using the change of variables specified before, the phase variable becomes (assuming $U_o << V$)

$$(\Delta\omega)t \approx -svt + s\left(y + \frac{R'}{V}\ U_x + \frac{R'}{V}\ V_o\cos\theta\right) .$$

In the presence of swell, Equation (2) becomes

$$e(s) \sim \int\rho(y,t)\ \exp\left[is(y + \frac{R'}{V}\ U_x + \frac{R'}{V}\ V_o\cos\theta)\right]\ dy, \tag{14}$$

where the quadratic term exp [isVt] is again filtered out. Since

$$V_o = V_o(y,t) \quad ,$$

Equation (14) is nonlinear. It must be evaluated accurately if the ocean to image transfer function is to be defined in the presence of surface waves. In the theoretical approach by Alpers and Rufenach (1979) the integral in Equation (14) was solved by assuming the integrand to be piecewise constant. The latter assumption ascribes to their solution a similarity with the "velocity bunching" argument introduced by Larsen et al (1976). This assumption allows the solution for the transfer function to take place on a patch (area large compared to Bragg waves and small compared to long ocean waves) by patch basis, where each patch is composed of roughness elements that are independent of the neighboring patches. The patches are shifted in the image plane along the azimuthal axis by

$$\Delta y = \left(\frac{R'}{V}\right)\ V_o\cos\theta \quad , \tag{15}$$

where the variables are as defined before. The displacement of the patches, in this approach, is considered sufficient to form an image of the long waves even if the ocean surface roughness is uniform in the azimuthal direction.

The measured backscatter modulation at different focus settings given by Jain and Shemdin (1981), for an azimuthally traveling wave, suggests motion of the backscatter pattern with a velocity that is of the order of the phase velocity of long waves. Their results, based on MARSEN data, are shown in Figure 44. A simulation based on a simplified solution of Equation (2) using the "velocity bunching" approach, by Plant (1982), is compared in the same figure with the experimental results of Jain and Shemdin. The Plant simulation does not reconcile motion of the sea surface to the order of the phase velocity of long waves. The latter magnitude of surface motion can be inferred from the SAR equation, given in Equation (14), where $\rho(y,t)$ can be viewed as a roughness pattern that propages with the wave phase velocity.

The predictions provided by the different theoretical approaches constitute a central argument for executing the TOWARD experiment. The intent is to resolve the theoretical discrepancies through detailed comparisons with measurements. Comparisons with the TOWARD results are presented in Chapter VII (see for example Figure 57 for comparisons between TOWARD, MARSEN and "Velocity Bunching" simulation).

C. Degradation of Resolution

An important by-product from an accurate solution of the SAR Equation (14) is a correct estimation of the degradation of SAR resolution. A simplified solution of Equation (14) by Jain (1981), for a sinusoidal wave suggests that the Image Resolution, $\tilde{\rho}_a$, in SAR is degraded in the azimuthal direction by

$$\tilde{\rho}_a = \left(\frac{R}{V}\right) V_o \quad . \tag{16}$$

This form is also suggested by Beal et al (1983) based on experimental evidence. Note that Equation (16) is similar in form to Equation (15). Hence, in the"velocity bunching" approach the azimuthal shift, determined to be responsible for image formation of azimuthally traveling waves, is the degraded resolution in the nonlinear solution for sinusoidal waves. Obviously, these differences are sufficiently fundamental to require an explanation.

Our ability to determine whether certain oceanographic features can be detected is of interest. Such ability is directly dependent on the SAR resolution and the length scales of processes being detected, provided that sufficient modulation in the image exists to define the feature. In the Marineland experiment Shuchman and Shemdin (1983) determined that for surface waves, a SAR resolution less than one quarter of a wavelength is required to detect surface waves. Extending this approximation to other ocean features (subject to later verification), it is reasonable to assume that a SAR resolution of at least one quarter of a feature length is necessary to detect the surface signature of that feature. Using this assumption, we may demonstrate with Equation (16) which ocean features can be detected with SAR in a given sea state. The ability of SAR to detect internal waves, bottom topography or current boundaries can be evaluated now. This is shown in Table 1 by computing SAR resolution for each of three sea states - calm, moderate and high.

From Table 16 it is seen that ocean features that are smaller than 80, 240 and 380 m in Sea States 1, 2, and 3, respectively, cannot be detected in a SAR

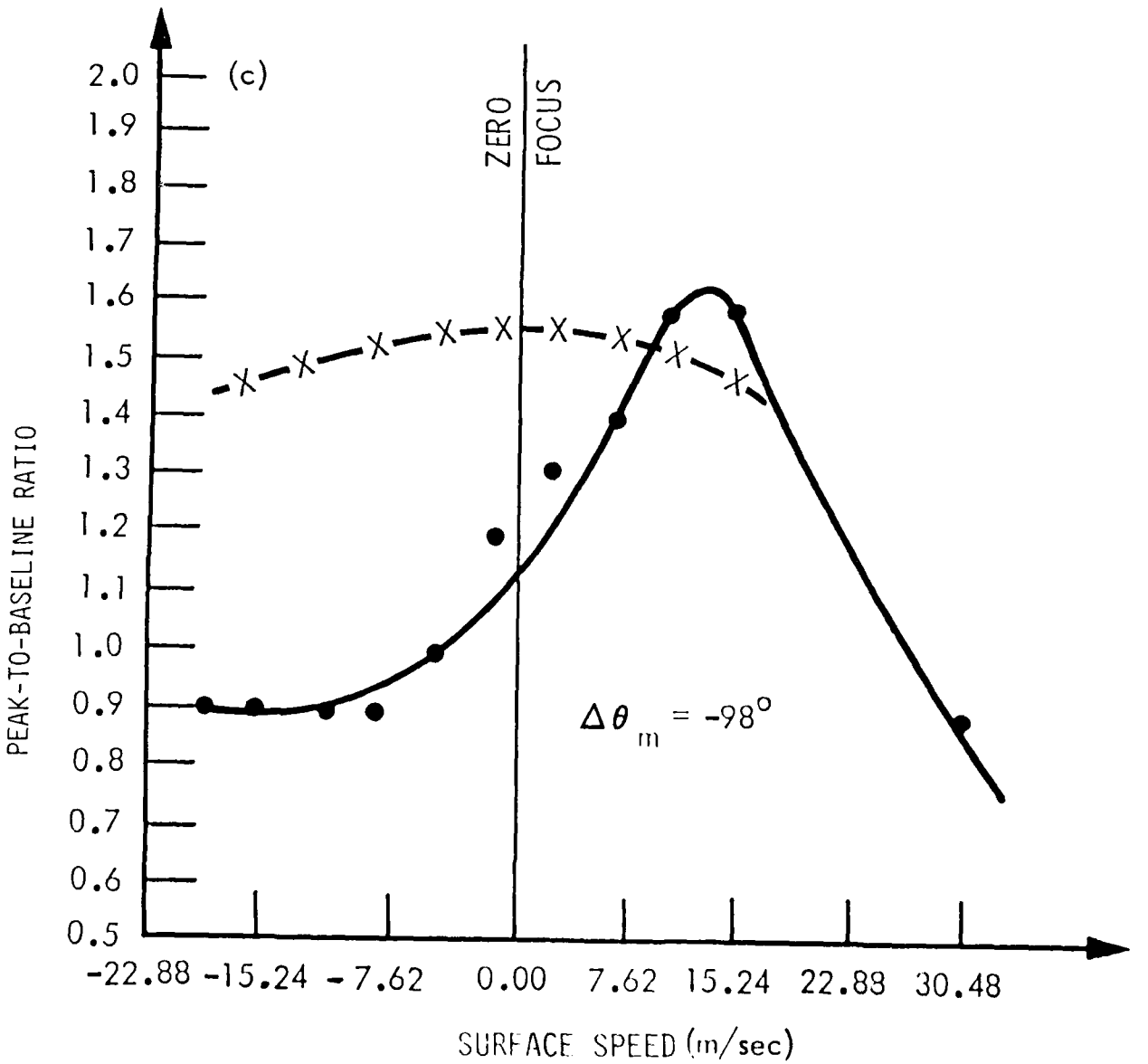

Figure 44. SAR Modulation Obtained from MARSEN Data for Azimuthal Waves as a Function of Focus, After Jain and Shemdin (1981). ●-Measurements, —Best Fit to Data, X-X-X- "Velocity Bunching" Simulation After Plant (1982).

Table 16. Effect of Surface Waves on SAR Detection of Ocean Surface Features.

(Sea State) →	(1) Calm	(2) Moderate	(3) High
Wind Speed (m/s)	2	5	10
Wavelength (m)	100	100	150
Wave Amplitude (m)	0.5	1.5	3.0
Wave Period (s)	8	8	10
U_o (m/s)	0.4	1.2	1.9
Assume R/V = 50			
Resolution, $\tilde{\rho}_a$(m)	20	60	95
Minimum Length to Identify Feature (m)	80	240	380

Table 17. Importance of Sea State in Detecting Ocean Surface Features.

(Sea State) →	(1) Calm	(2) Moderate	(3) High
Internal Waves			
Large (500 m)	N	U	I
Small (100 m)	N	I	I
Bottom Features (Scale - 500 m)	N	U	I
Current Boundaries (Scale - 1 km)	N	N	U

N - Neglible
U - Uncertain
I - Important

image when the R/V ratio exceeds 50. This ratio is typical of the CV-990 aircraft operations with the JPL: L-Band SAR. In Table 17 length scales of important ocean features are shown, and when matched with the resolutions calculated in Table 16, the importance of sea state on imaging such features is highlighted.

It is clear from this assessment, and subject to verification of Equation (16), that in calm seas, sea state is not an important factor in detecting internal waves, bottom features or current boundaries. In calm seas the simplified solution of the SAR Equation (2), referred to as the "velocity bunching" approach is probably valid. However, in sea states greater than 1, the influence of surface waves may be profound, depending on the length scale of features being detected. Here, the complete solution of Equation (2) or (14) is necessary to assess detectability of an ocean feature. Of particular importance is the fact that the nonlinear nature of Equation (2) prohibits apriori filtering of ocean surface waves from other ocean features of interest. Consequently, the use of matched filters remains to be justified in extracting ocean signatures when the SAR resolution is degraded by surface waves.

The form given by Jain (1981) in Equation (16) is one of many representations proposed by SAR investigators. The various representations are based on differing theoretical arguments. Here, the more important ones are presented to highlight the differences in predictions, and hence the consequences of such differing predictions.

The theoretical resolution, also the absolute minimum, given for a SAR system is

$$\tilde{\rho}_a = \frac{\lambda}{2\beta} = \frac{D}{2} \quad , \tag{17}$$

where λ is radar wave length, β is azimuthal beam width, and D is aperture length. When the integration time is limited in the SAR processor, the theoretical resolution becomes

$$\tilde{\rho}_a = \frac{\lambda}{2} \frac{1}{T} \frac{R}{V} \quad , \tag{18}$$

where R is range, V is aircraft velocity, and T is integration time.

The resolution degradation beyond these theoretical limits, due to surface waves, is given by different authors. Their results are compared here as a preliminary step toward comparing each with experimental results from the TOWARD experiment.

1. "Velocity Bunching" or "Oscillating Patch" Models

This form was proposed originally by Alpers and Rufenach (1979)

$$\tilde{\rho} = \tilde{\rho}_a \left\{ 1 + \left[\frac{4\pi}{\lambda} \left(\frac{T}{2} \right)^2 a_r \right]^2 \right\}^{1/2} , \tag{19}$$

where a_r is range acceleration which is equated to the vertical acceleration by

$$a_r = a_r \cos \theta \quad . \tag{20}$$

Lyzenga and Shuchman (1983) used the same form with the exception of a $(2/\pi)$ factor inside the inner bracket in Equation (19). When the coherence time of scatterers is smaller than the integration time of the processor, the resolution is proposed to be

$$\tilde{\rho}_a = \frac{\lambda}{2} \frac{1}{\tau} \left(\frac{R}{V} \right) \quad , \tag{21}$$

where τ is coherence time. Alpers et al (1985a) proposed the following form for τ

$$\tau = (2\pi\sqrt{2})^{-1} \lambda \langle U_r^2 \rangle^{1/2} \quad , \tag{22}$$

where $\langle U_r^2 \rangle^{1/2}_{\ldots}$ is the rms spread of the radial facet velocities within a SAR resolution cell. The degradation of resolution, as proposed by Alpers and Bruening (1985b), has the form

$$\tilde{\rho} = \left\{ \tilde{\rho}_a^2 + \left[\frac{\pi}{2} \left(\frac{R}{V} \right) a_r T \right]^2 + \left[\tilde{\rho}_a \frac{T}{\tau} \right]^2 \right\}^{1/2} . \tag{23}$$

Lyzenga and Shuchman (1983) proposed another form for computing resolution degradation when the scatterers are moved by a velocity, U, namely

$$\tilde{\rho} = \tilde{\rho} \left[1 + \left(\frac{4\beta^2 R\, U}{\lambda V} \right)^2 \right]^{1/2} . \tag{24}$$

Here, U can be assumed to be the orbital velocity of long waves for the purpose of estimating the degradation of resolution by this mechanism.

2. "Distributed Surface" Models

Harger (1985) derives a different form for resolution degradation by surface waves, as follows

$$\tilde{\rho} = \tilde{\rho}_a \left[1 + \frac{4}{\tilde{\rho}_a 4} \left\{ \frac{1}{\hat{K}} \left(\frac{V_{\rho 20}}{V} \right) - \frac{1}{2A \tilde{\beta} K_{20}^2} \right\}^2 \right]^{1/2},$$

where $V_{\rho 20}$ and K_{20} are wave phase-speed and wave-number of long waves, respectively,

$$K = 2 \frac{K_o}{R}, \text{ where } K_o = \frac{2\pi}{\lambda} \quad , \tag{26}$$

and

$$\tilde{\beta} = 2K_o \cos \theta \quad . \tag{27}$$

The form proposed by Jain (1981) for resolution degradation, given in Equation (16), falls in this category of "distributed surface" models. The empirical result given by Beal et al (1983) is similar in form to that given by Jain (1981).

A graphical comparison of the predicted resolution degradations is given in Figure 45, as function of sea state. The radar parameters used are indicated as legend in the figure. They correspond to the JPL: L-Band SAR aboard the NASA CV-990 aircraft, and the SAR processing parameters used in image processing for TOWARD. The sea state parameters used are those defined in Table 16. The TOWARD SAR flight of 31 October 1984 corresponds to Sea State 2. It is clear from Figure 45 that significant differences exist (one order of magnitude at Sea State 2) in the available theoretical predictions of resolution degradation. It is an objective in TOWARD to determine, based on experimental evidence, which theories are in agreement with field observations.

The dominant wave conditions on 31 October 1984 in TOWARD are given in Table 18, which also outlines the SAR processing parameters used (T = 1.74 s). Here, the "orbiting patch" model predicts a resolution of 70.2 m, while the "distributed surface" model (Harger, 1985) predicts 6.2 m. The processed resolution over land is 4.6 m.

A possible test for these models is to process the same image at the highest resolution ($\tilde{\rho}_a$ = 0.9 m). This would require 8.9 s in integration time. For such processing Harger predicts the resolution to be 24.1 m. There is question whether the orbiting patch model remains valid for such a long integration time.

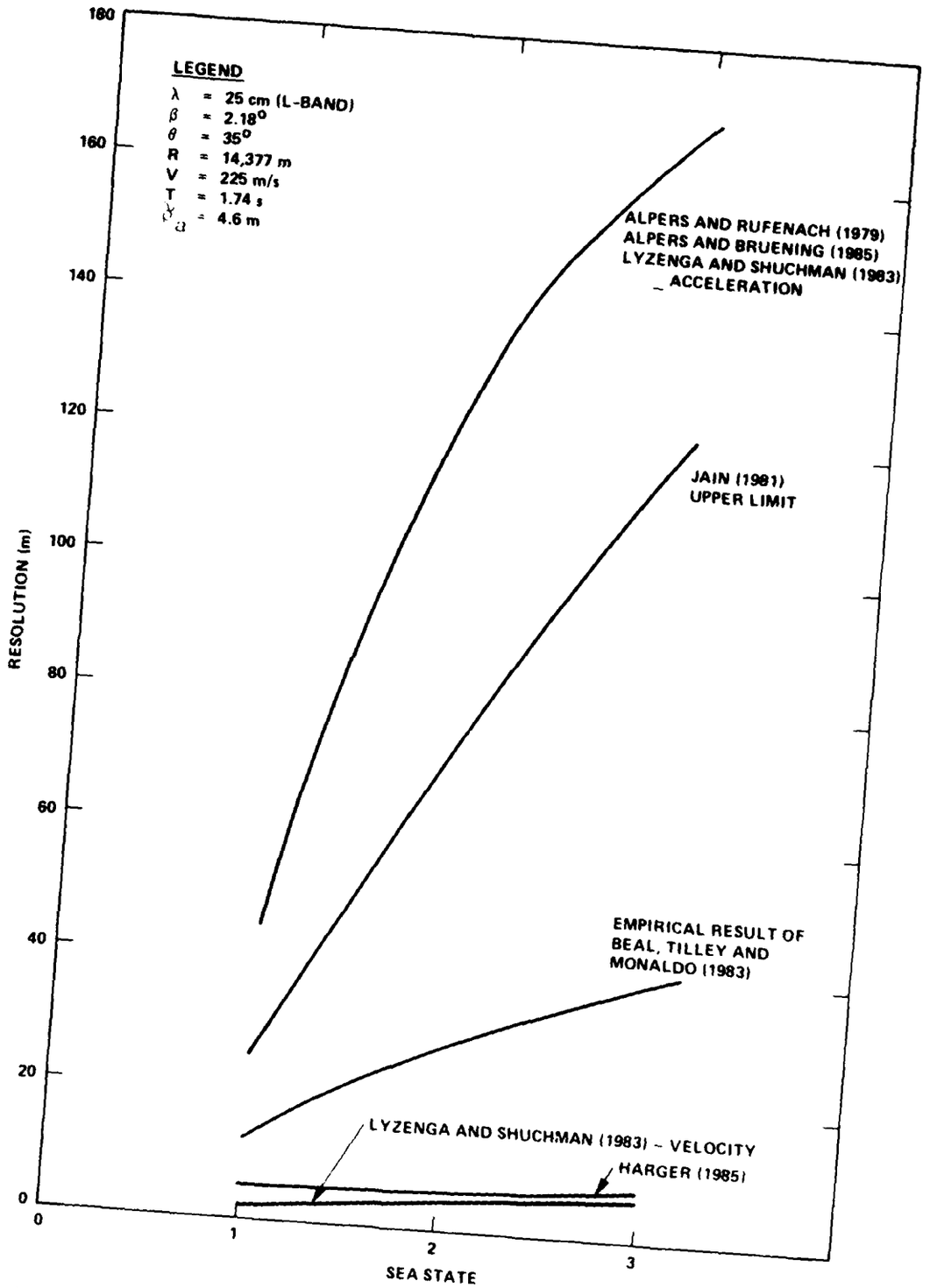

Figure 45. Comparison of Theoretically-Predicted Resolution Degradation as a Function of Sea State.

Table 18. Degraded Resolution Predicted by Various Models for Sea Condition on 31 October 1984.

WAVE LENGTH ≈ 122 m; WAVE PERIOD ≈ 9.0 s

WAVE AMPL. ≈ 1.0 m; PHASE SPEED ≈ 14.0 m/s

ORBITAL VELO. ≈ 0.7 m/s; ORBITAL ACCEL. ≈ 0.49 m/s^2

	$\beta = 1.55°$ $T = 1.74$ s $\tilde{\rho}_a = 4.6$ m	$\beta = 8°$ $T = 8.9$ s $\tilde{\rho}_a = 0.9$ m
	RESOLUTION (m)	
Alpers and Rufenach (1979) Alpers and Bruening (1985) Lyzenga and Shuchman (1983) - Acceleration	70.2	359
Lyzenga and Shuchman (1983) - Velocity	2.4	12.4
Jain (1981) - Upper Limit	44.7	44.7
Harger (1985)	6.2	24.1

VII. SAR MEASUREMENTS: DATA SUMMARY AND EARLY RESULTS

A. Discussion

Progress towards understanding how SAR images the ocean surface has suffered in the past from lack of data sets that are sufficiently complete and acceptable in data quality to resolve the outstanding issues. Partial data sets have been interpreted to support one hypothesis or theory over another. Experimental results have been accepted sometimes as credible by proponents of a hypothesis and discounted as unreliable by proponents of another. The TOWARD experiment was staged to provide a complete data set, i.e. in-situ, radar backscatter and SAR, and sufficiently detailed processing to enable validation of the different theories.

The JPL L-Band SAR was selected as a critical instrument because of established performance and associated capabilities to record and process SAR data in both analog and digital modes. The L-Band frequency is especially suited for resolving ocean surface motions so as to determine whether motions of the scale of wave phase-velocity are important in the SAR imaging process. The characteristics of this radar system and associated image processing features are give in Chapter II. The standard flight pattern executed during the experiment is given in Figure 12. This pattern was flown at three consecutive altitudes by the CV-990 aircraft. A complete sequence of legs flown is shown in Figure 46 for the flight on 31 October 1984. During this flight the wind was from direction 290°T and a swell was propagating in the vicinity of the tower from direction 290°T.

In Phase-II, the typical flight sequence with the CV-990 aircraft is given in Figure 47 for the flight of 19 March 1984. Here, the wind direction was from 270°T and the dominant swell was from direction 290°T.

The U.S. Marine Corp X-Band system was operated on board their RF-4B's during TOWARD. The system characteristics were given in the TOWARD Science Plan (Shemdin, 1984). The flight days for the F-4's are given in Table 3 and 4 of this report for Phases I and II, respectively. The flight pattern of the RF-4B on 19 March 1985 is given in Figure 48. The processing of the X-Band SAR images has been assigned second priority, compared to L-Band, because of emphasis placed on resolving contradictions in existing SAR imaging theories. This data set will be useful in the planning stages of a dedicated experiment to understand SAR imaging of the ocean surface at X-Band.

Another airborne resource in TOWARD was an X-Band Real Aperture Radar (RAR) which was operated on board OV-1(D) aircraft. The objective here was to acquire simultaneous SAR and RAR images at X-Band. On 19 March 1985 the flight pattern executed by the two OV-1(D) aircraft is given in Figure 49. One aircraft executed the pattern at 11,000 feet altitude, and the other executed the same pattern, during the same period, at 18,000 feet altitude. The RAR images were found to be of good quality when the aircraft was flown below 8,000 feet. This finding evolved by trial and error so that the early simultaneous flights with the RF-4B's produced low quality RAR images. The later OV-1(D) RAR flights which produced good quality RAR images corresponded to failures of the RF-4B's SAR system to produce good quality images. Consequently, the objective of obtaining simultaneous RAR and SAR, both good quality,

DATE: 31 October 1984

PLATFORM: CV-990, Postflight

RADAR FREQUENCY: L-Band

WAVE DIRECTION: 300°

INCIDENCE ANGLE: 35°

WIND DIRECTION: 290°

PLATFORM ELEVATION: As Tabulated

PLATFORM SPEED: 450 knots

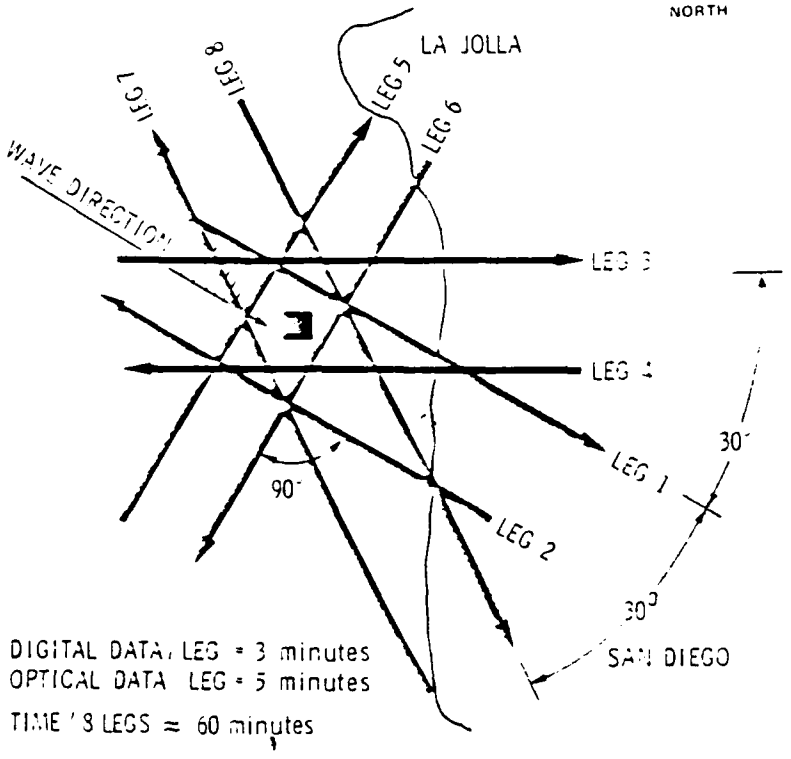

Flight Sequence

(Feet) Altitude	Run	Leg	Time	A/C Heading	Radar Look Direct.
7,000	1	7	1257	320	R - 050
7,000	2	1	1307	110	R - 200
7,000	3	4	1316	260	R - 350
7,000	4	2	1319	290	R - 020
20,000	5	7	1343	320	R - 050
20,000	6	1	1351	110	R - 200
20,000	7	4	1358	260	R - 350
20,000	8	2	1450	290	R - 020
20,000	9	6	1429	200	R - 290
38,000	10	7	1455	320	R - 050
38,000	11	1	1503	110	R - 200
38,000	12	4	1512	260	R - 350
38,000	13	2	1528	290	R - 020
38,000	14	6	1539	200	R - 290

Figure 46. Typical CV-990 Flight Pattern Executed in Phase-I.

DATE: 19 March 1985

PLATFORM: CV-990, Postflight

RADAR FREQUENCY: L-Band

WAVE DIRECTION: 290°

INCIDENCE ANGLE: 30°

WIND DIRECTION: 270°

PLATFORM ELEVATION: As Tabulated

PLATFORM SPEED: 450 knots

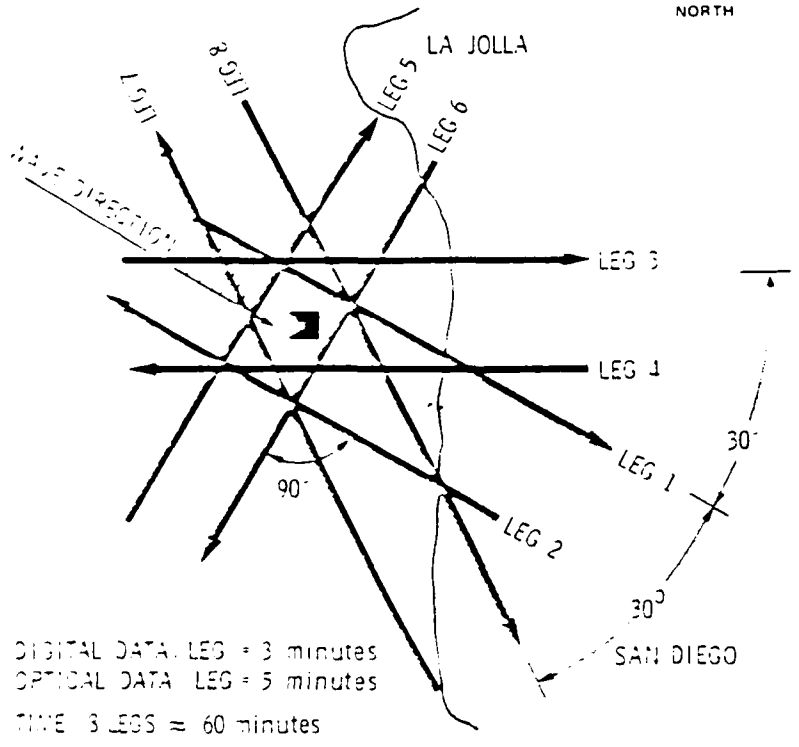

Flight Sequence

Altitude	Run	Leg	Time	A/C Heading	Radar Look Direct.
7,000	1	7	1301	320	R - 050
7,000	2	1	1309	106	R - 200
7,000	3	4	1317	264	R - 350
7,000	4	1	1325	106	R - 200
7,000	5	2	1333	292	R - 020
20,000	6	7	1349	320	R - 050
20,000	7	1	1350	106	R - 200
20,000	8	4	1409	265	R - 350
20,000	9	1	1418	103	R - 200
20,000	10	2	1427	290	R - 020
20,000	11	6	1445	205	R - 290
32,000	12	7	1458	316	R - 050
32,000	13	1	1509	109	R - 200
32,000	14	4	1520	265	R - 350
32,000	15	1	1529	107	R - 200
32,000	16	2	1538	289	R - 020
32,000	17	6	1553	209	R - 290

Figure 47. Typical CV-990 Flight Pattern Executed in Phase-II.

DATE: 19 March 1985

PLATFORM: RF-4, Postflight

RADAR FREQUENCY: X-Band

WAVE DIRECTION: 290°

WIND DIRECTION: 270°

PLATFORM ELEVATION: 15,000 Ft.

PLATFORM SPEED: 400 knots

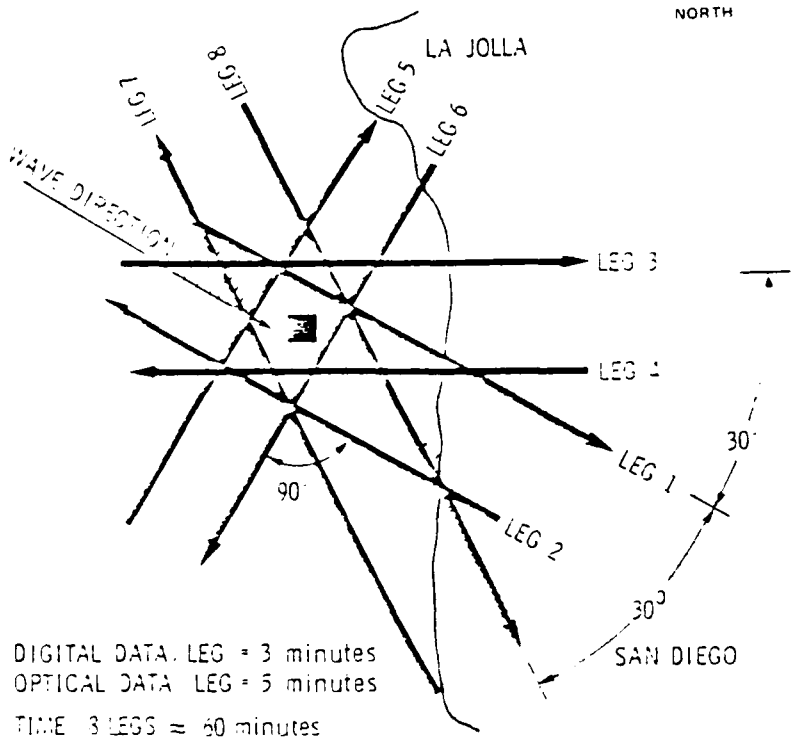

Flight Sequence

Run	Leg	Time	A/C Heading	Radar Look Direc.
1	6	1343	200	R - 020
2	2	1350	290	R - 020
3	4	1357	260	R - 350
4	8	1401	325	R - 235
5	1	1407	290	R - 200
6	3	1414	260	R - 170
7	7	1419	325	R - 055
8	5	1425	020	R - 110
9	1	1432	110	R - 200

Figure 48. Typical RF-4 Flight Pattern Executed on Phases-I and II.

DATE: 19 March 1985

PLATFORM: OV-1(D) - Postflight

RADAR FREQUENCY: X-Band

WAVE DIRECTION: 290°

WIND DIRECTION: 270°

PLATFORM ELEVATION: 11,000 Ft. and 18,000 Ft.

PLATFORM SPEED: 200 Knots

Flight Sequence

Run	Leg	Time	A/C Heading	Radar Look Direct.
1	6	1355	200	R
2	5	1402	020	R
3	8	1408	145	R
4	7	1418	325	R
5	1	1428	110	R
6	2	1436	290	R
7	3	1446	080	R
8	4	1458	260	R
9	3	1512	150	R

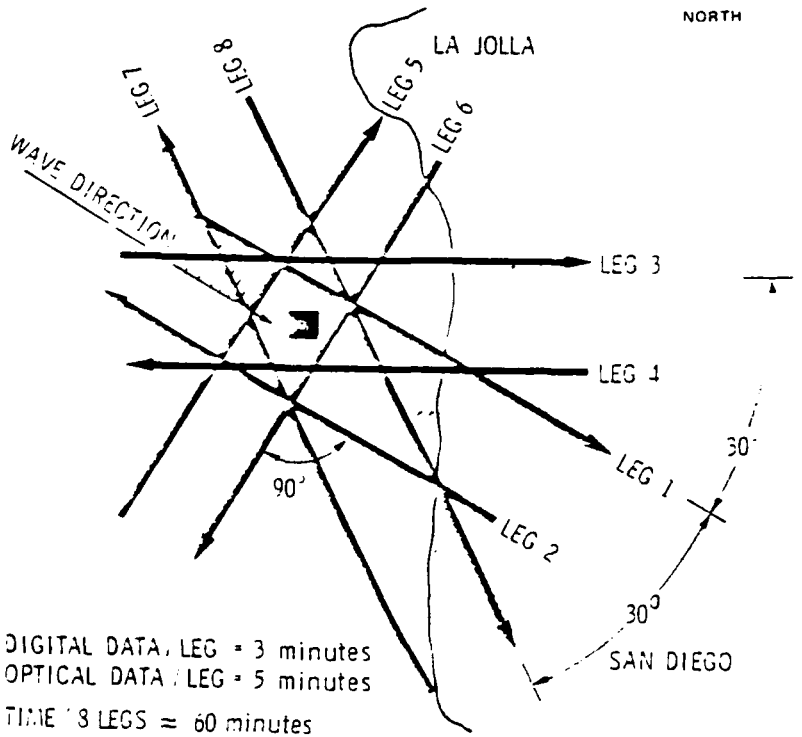

Figure 49. Typical OV-1(D) Flight Pattern Executed in Early Part of Phase-II.

was not achieved. This was one of the few attempted data sets that were not acquired satisfactorily. It was not a data set required for meeting a primary TOWARD objective, however. It was also not part of the original "Science Plan".

As indicated before, the L-Band SAR images were assigned highest priority relative to X-Band SAR and RAR images. Of the L-Band data sets collected, ten frames were selected for detailed focus processing, as indicated in Table 7. Each frame was processed fifteen times independently with the chirp rate set to correspond to a different ground speed. The range of velocities were varied (with respect to a rigid surface), from -2.33 to +2.33 times the phase-speed of the long waves. Hence, the processings specified in Table 7 amount to producing 150 images, or fifteen variations for each frame. The production of these 150 images has been completed recently.

B. Early Results from SAR

Of the ten frames specified for focus processing to date, only four have been analyzed to determine wave detectibility at different focus settings. The four frames correspond to Legs 1, 2, 4, and 7 of the 31 October 1984 flight, at aircraft elevation 11,585 m (38,000 feet). The analysis procedure for Leg 1 is described in detail by Tajirian, Volume II of this report. The available early results are described in the following.

1. Wave Number Spectra

The SAR image frame most extensively analyzed corresponds to Leg 1, where purely azimuthal waves are clearly seen. A sample image at zero focus setting (equivalent to stationary surface) is shown in Figure 50a. The same frame is shown in Figure 50b for focus setting -2.33C, where C is the dominant wave phase-speed. This focus setting corresponds to a surface moving in the same direction as the aircraft with a speed of 2.33C. In Figure 50c the same frame is presented at focus setting +2.33 which corresponds to a surface moving in the opposite direction of aircraft at speed 2.33C. In Figure 50c, the waves are hardly detectable. These observations confirm that SAR detects motion properties of the surface. The precise determination of this motion is described in detail in the next section.

The one-dimensional SAR spectrum is shown in Figure 51, for Leg 1 at optimum focus (highest wave detectability). Details of the computation are given by Tajirian in Volume II. The spectrum has a dominant peak at a wave length 133 ± 10 m. Considerable care has to be given to the determination of this spectrum. The degrees of freedom are 62. The wave number resolution is 0.002 rad/m; it is degraded to 0.006 rad/m and the spectral peak is normalized to 1.0 to facilitate comparison with in-situ measurements.

Guza (see Volume II) provided wave frequency spectra measured by pressure gages at the tower, as shown in Figure 15. The frequency spectrum. transformed to an equivalent deep water wave-number spectrum, is given in Figure 52. The spectrum has 88 degrees of freedom and a frequency resolution of 0.004 Hz which corresponds to a wave number resolution of 0.004 rad/m. The transformed spectrum shows a well defined peak at wave length 114 m ± 6 m. This peak is distinct from the one shown in Figure 51.

Figure 50a. SAR Image of 31 October 1984, Leg 1 (Heading 110°), Aircraft Altitude = 38,000 feet, Processed for Surface Speed 0.0 m/s.

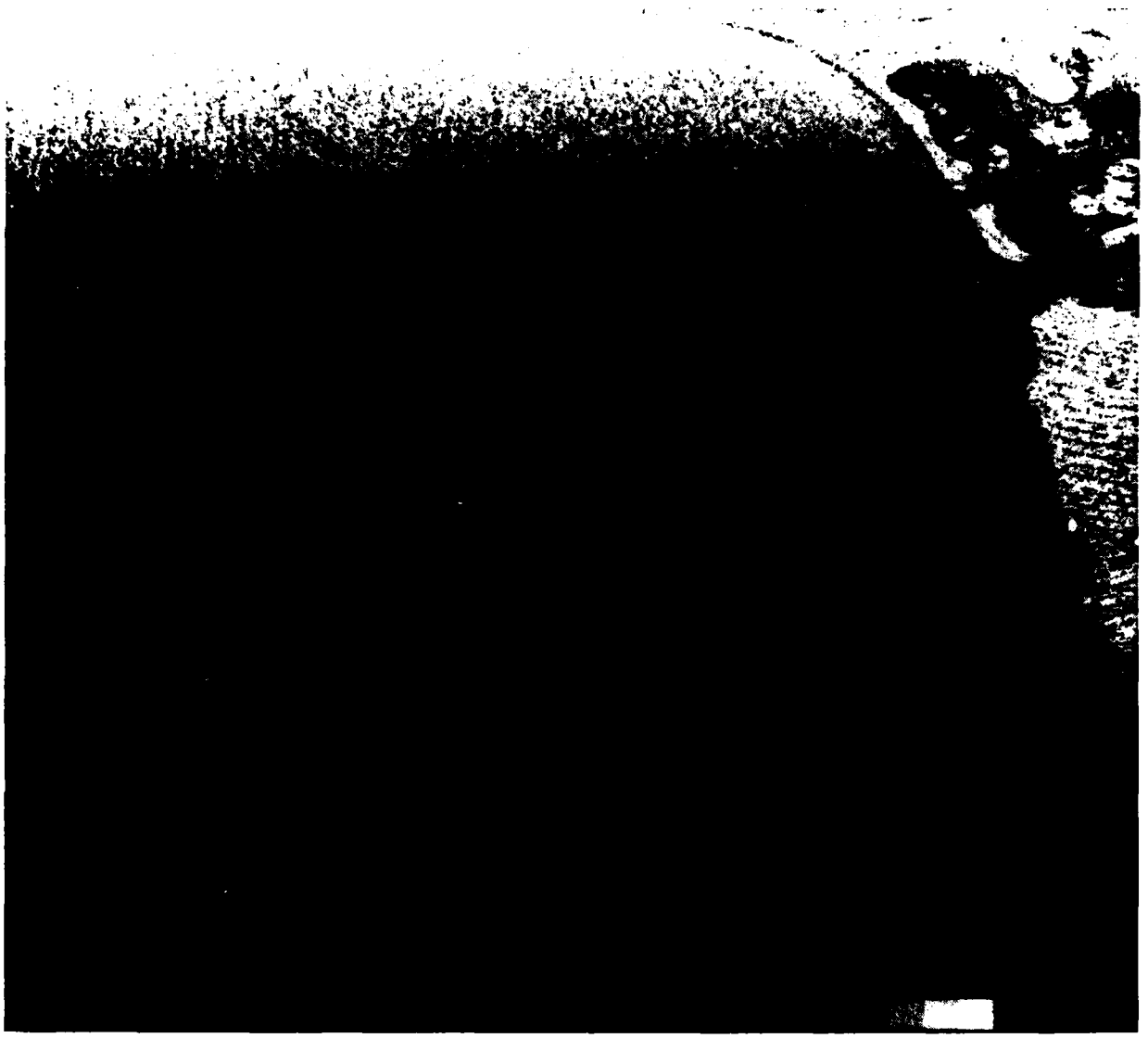

Figure 50b. SAR Image of 31 October 1984, Leg 1 (Heading 110^{o}), Aircraft Altitude = 38,000 feet, Processed for Surface Speed 25.6 m/s.

Figure 50c. SAR Image of 31 October 1984, Leg 1 (Heading 110°), Aircraft Altitude = 38,000 feet, Processed for Surface Speed -25.6 m/s.

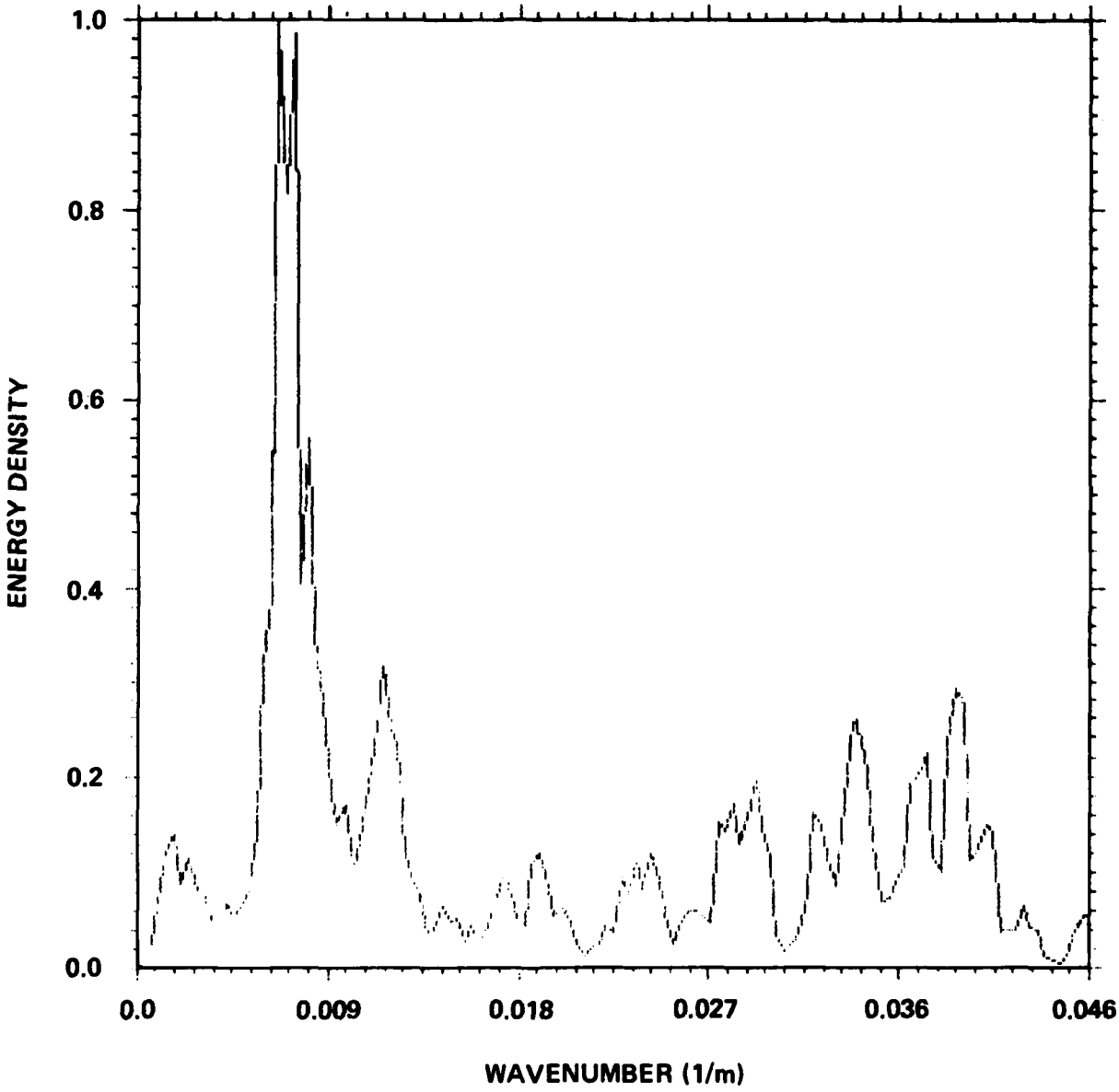

Figure 51. Wave Number Spectrum at Optimum Focus for Image of 31 October 1984, Leg 1. Peak Spectral Density (10.2 in Arbitrary Units) is Normalized to 1.0 to Facilitate Comparison with In-Situ Spectrum.

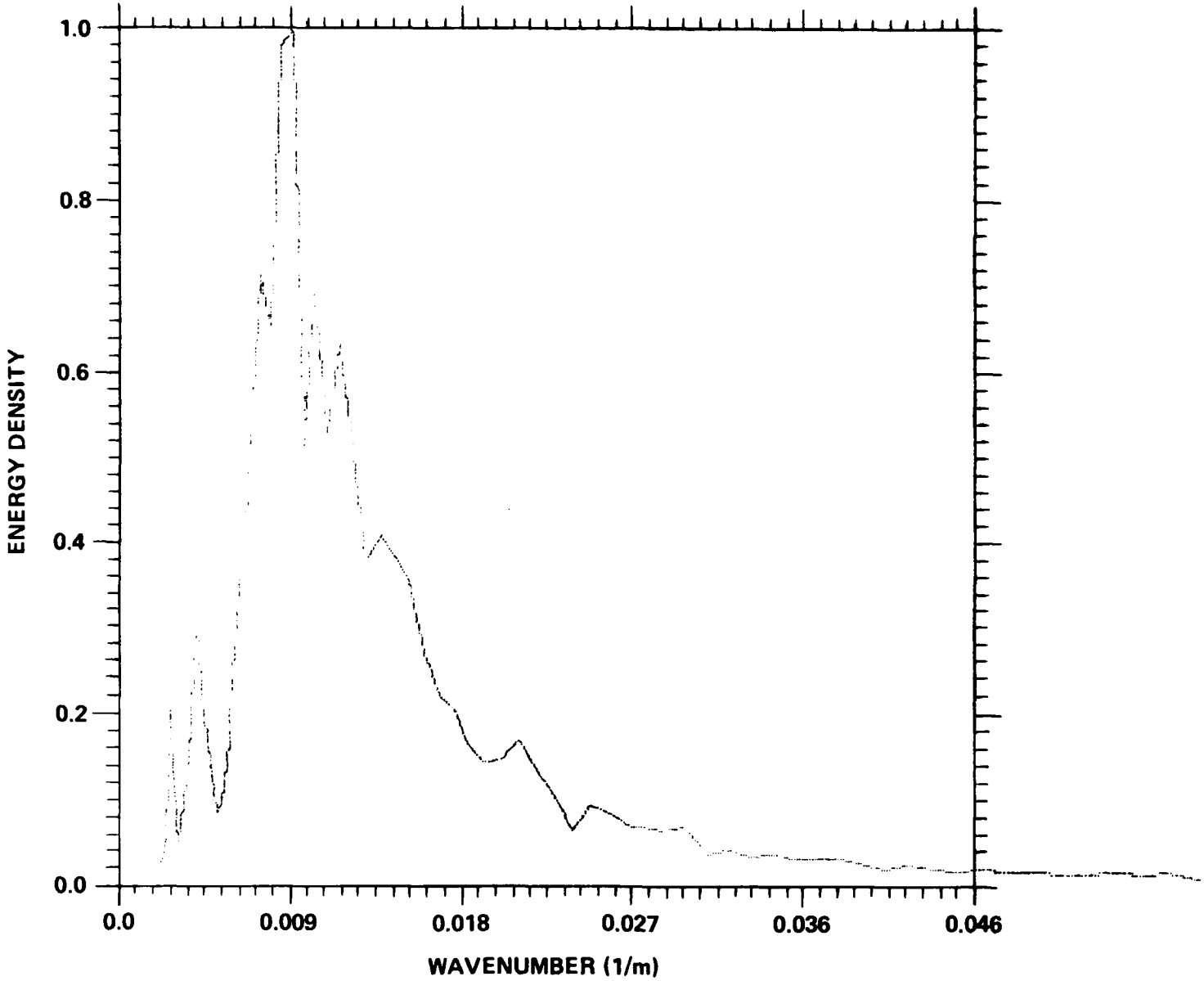

Figure 52. In-Situ Spectrum Transformed to Equivalent Deep Water Wave Number Spectrum. Peak Spectral Density (12.5 m^3) is Normalized to 1.0 to Facilitate Comparison with SAR Spectrum.

Comparisons of the SAR spectrum with the transformed wave height spectrum is given in Figure 53. The SAR spectrum emphasizes the 133m wave length which is a secondary peak in the wave height spectrum. The wave height spectrum, on the other hand, emphasizes the 108m wave length which is a secondary peak in the SAR spectrum. In a comparison between SAR spectra and other airborne-measured wave-height spectra (Beal et al, 1985), the inference has been drawn that the SAR spectrum is equivalent to a surface wave slope spectrum. There is evidence to suggest that this may be valid for range-traveling waves. The TOWARD results in Figure 53 contradict this possibility for azimuth-traveling waves. The latter suggests that the SAR spectrum is a low pass filter of the true wave height spectrum. The nature of this filter is related to the SAR imaging mechanisms under investigation. It is an objective in TOWARD to delineate this transfer function from a wave height spectrum to a SAR spectrum.

2. SAR Focusing Results

Significant attention has been devoted to analysis of wave detectability at various focus settings (see Tajirian in Volume II). The motivation is to determine the magnitude of surface motion that influences the formation of ocean wave images. The analysis consists of computing one dimensional wave number spectra with 62 degrees of freedom for each image. The wave spectral density at the dominant wave number is plotted as a function of focus. A focus setting that corresponds to the highest dominant density also corresponds to waves in the SAR image that are most detectable. The result for Leg 1, given in Figure 54a, represents a detectability distribution for azimuthal waves traveling in the same direction as the aircraft. The distribution is asymmetric with respect to zero focus, i.e. detectability is not maximum for zero surface motion. The waves are most detectable at focus setting 3, which corresponds to 11.0 m/s. Here, the waves are most detectable for a surface that propagates in the direction of aircraft with a speed of 11.0m/s.

In Figure 54b the detectability result for Leg 2 is shown. Here, the density values are low at all focus settings, which suggests that the waves are barely detectable in the SAR images processed at all focus settings. This result is substantiated by visual observation of the images. A clear explanation of this result is not in hand yet.

In Figure 54c the detectability result is given for Leg 4. It indicates that optimum detectability of waves is associated with a surface that translates in a direction opposite to the flight direction. The peak density shown is for a surface that translates with a speed of 14.6 m/s. The reversal in direction of asymmetry, when the flight direction is reversed with respect to the wave propagation direction, is an indication that the SAR image detects a surface wave pattern that propagates with a characteristic speed that is of the order of the wave phase speed (or one order of magnitude greater than the wave orbital velocity).

In Figure 54d the detectability result for Leg 7 is shown. The highest dominant wave densities confirm the previous results, i.e. peak detectability is in the direction opposite the flight direction and occurs at a speed that is of the order of the wave phase speed. The most detectable waves appear at 14.6 m/s.

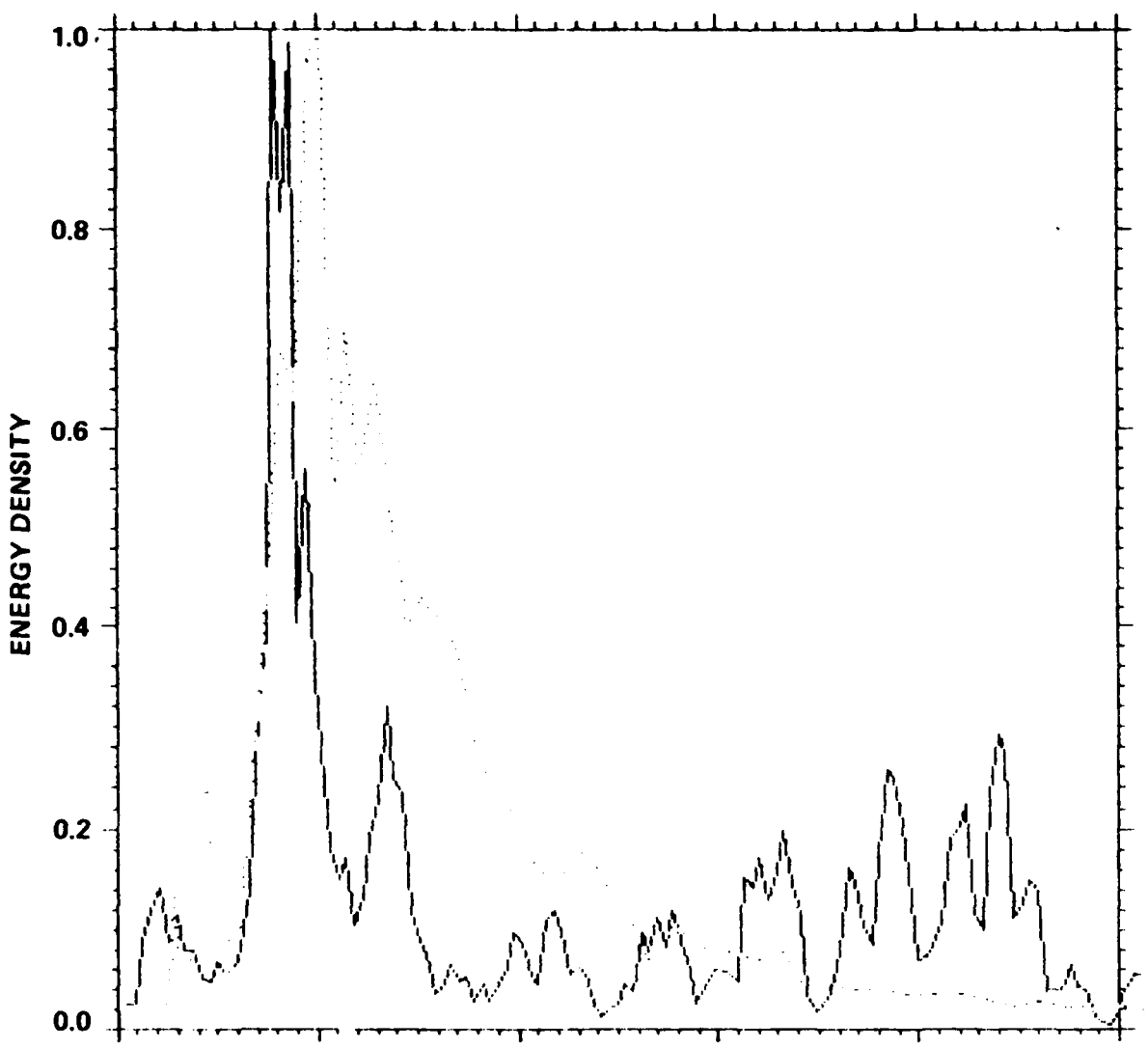

Figure 53. Comparison: SAR Image Spectrum, Solid Line, (Figure 51) with Wave Number Spectrum in Deep Water, Dotted Line, Transformed from Guza's Frequency Spectrum at the Tower (Figure 52).

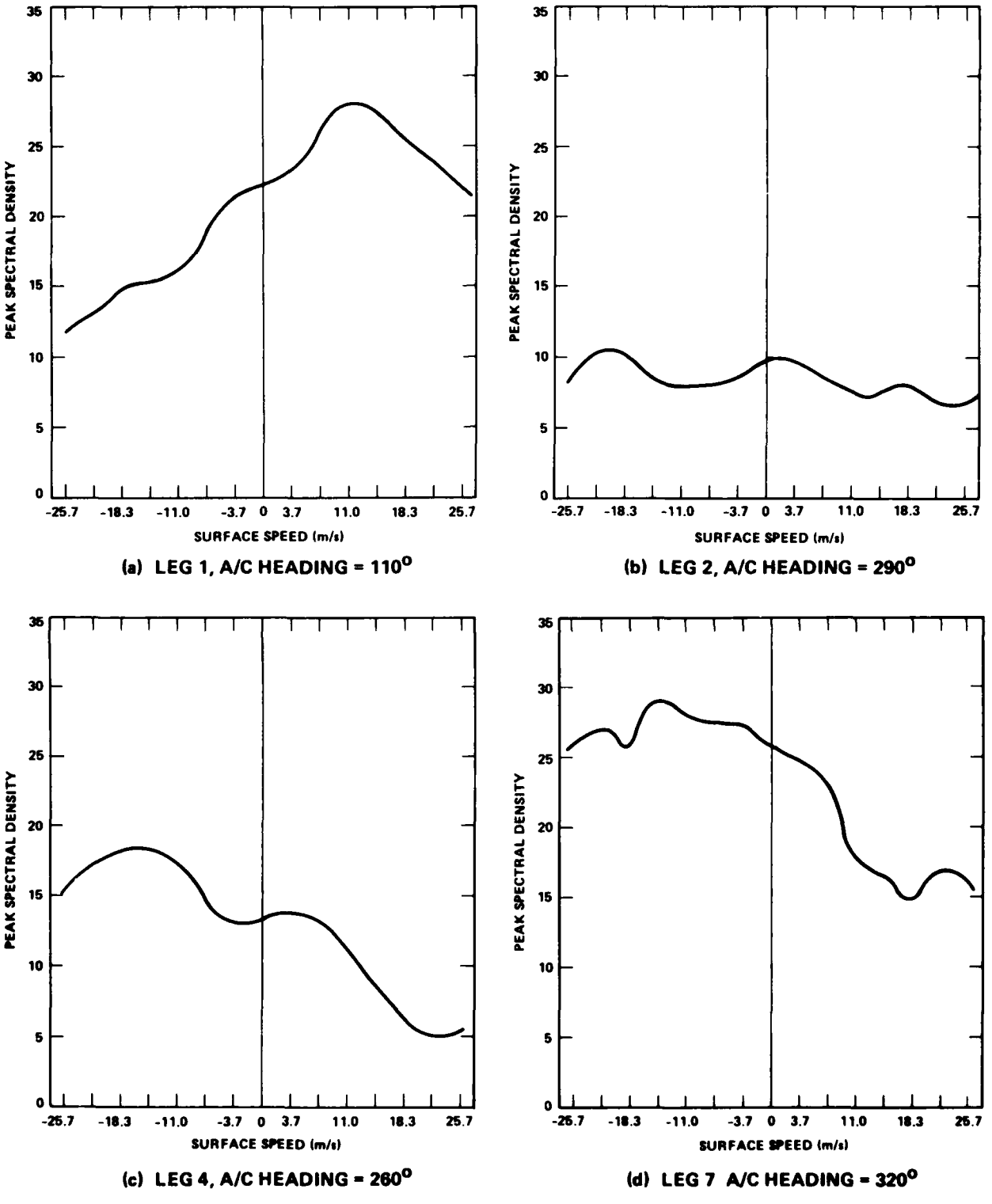

Figure 54. Peak SAR Wave Spectral Density vs. Surface Speed, Wave Direction is Toward 110°, Flight Day 31 October 1984.

3. SAR Simulations

Simulations using two distinct theoretical approaches have been executed for the SAR waves observed on 31 October 1986. The simulation by Plant (see Volume II), follows the assumptions stipulated by the "velocity bunching" or "orbiting patch" approach. Details of the simulated spectra are given by Plant in Volume II, for Legs 1, 2, 4 and 7.

Comparisons between wave spectra obtained from SAR images and simulated spectra are desirable, but cannot be achieved for TOWARD in absolute terms. The available L-Band SAR images are not calibrated. Calibration is potentially achievable but requires additional resources. Calibrated SAR images are not required to achieve the objectives stated for TOWARD. Comparisons between normalized spectra, where the spectral peaks are set equal to 1.0, are used, as shown in Figure 53.

Normalized spectra are compared here between those obtained with the Plant simulation and those computed from the SAR images. In Figure 55 such a comparison is shown, at optimum focus, for both simulated and actual spectra. Both spectra are computed for deep water conditions. Here the SAR wave-number resolution has been degraded to match Plant's spectrum. The Plant simulation shows the peak to occur at wave length = 106.6m, while the actual SAR Spectrum shows the peak at wave length = 127.0m. Another comparison is provided in Figure 56, where the simulated Plant Spectrum at optimum focus is compared with the transformed wave height spectrum (of Guza). Again, both spectra are compared for deep water conditions. Here, the Plant simulated spectral peak (wave length = 106.6m) agrees with the wave height peak (wave length = 107.4 m). The comparisons in Figures 55 and 56 indicate that the Plant simulated spectrum is related in some form to the in-situ spectrum, but that it is not a satisfactory simulation of the actual SAR spectrum.

Wave detectability dependence on focus setting (or surface motion) is useful as a criterion for testing SAR imaging theories. Comparisons based based on absolute numbers requires a calibrated SAR, which is unavailable. Useful detectability comparisons can be made based on a Peak-to-Baseline Ratio, PBR, as defined and used by Jain and Shemdin (1983); it is the ratio of the peak spectral density at each focus settting divided by the defocused spectral density at the same peak wave number. The Plant "Velocity Bunching" simulation (Volume II) is used to compute the simulated PBR values. Figure 54 is used to compute the actual SAR PBR values. A comparison between the simulated PBR dependence on focus (surface speed) and actual PBR dependence on focus is shown in Figure 57, for Leg 1. In this figure, zero focus corresponds to optimum SAR processing (highest resolution) for a stationary surface (e.g. land). This is verified by measuring the width of the Mission Beach pier in each of the SAR images that were processed. These results are shown in Figure 57 as the upper curve. They verify the correct selection of zero focus in processing of the SAR images. The Plant simulation in this figure shows optimum wave detectability at zero surface speed, while the SAR images show optimum detectability at 11.0 m/s. This implies that: (i) the true SAR imaging process of surface waves is sensitive to the dispersive property of surface waves, and (ii) the Plant simulation is not incorporating this aspect correctly in its procedure. Another difference, although less indicative, is in the magnitudes of the PBR values. The Plant simulation shows a maximum value of 3.3 vs. a TOWARD experi-

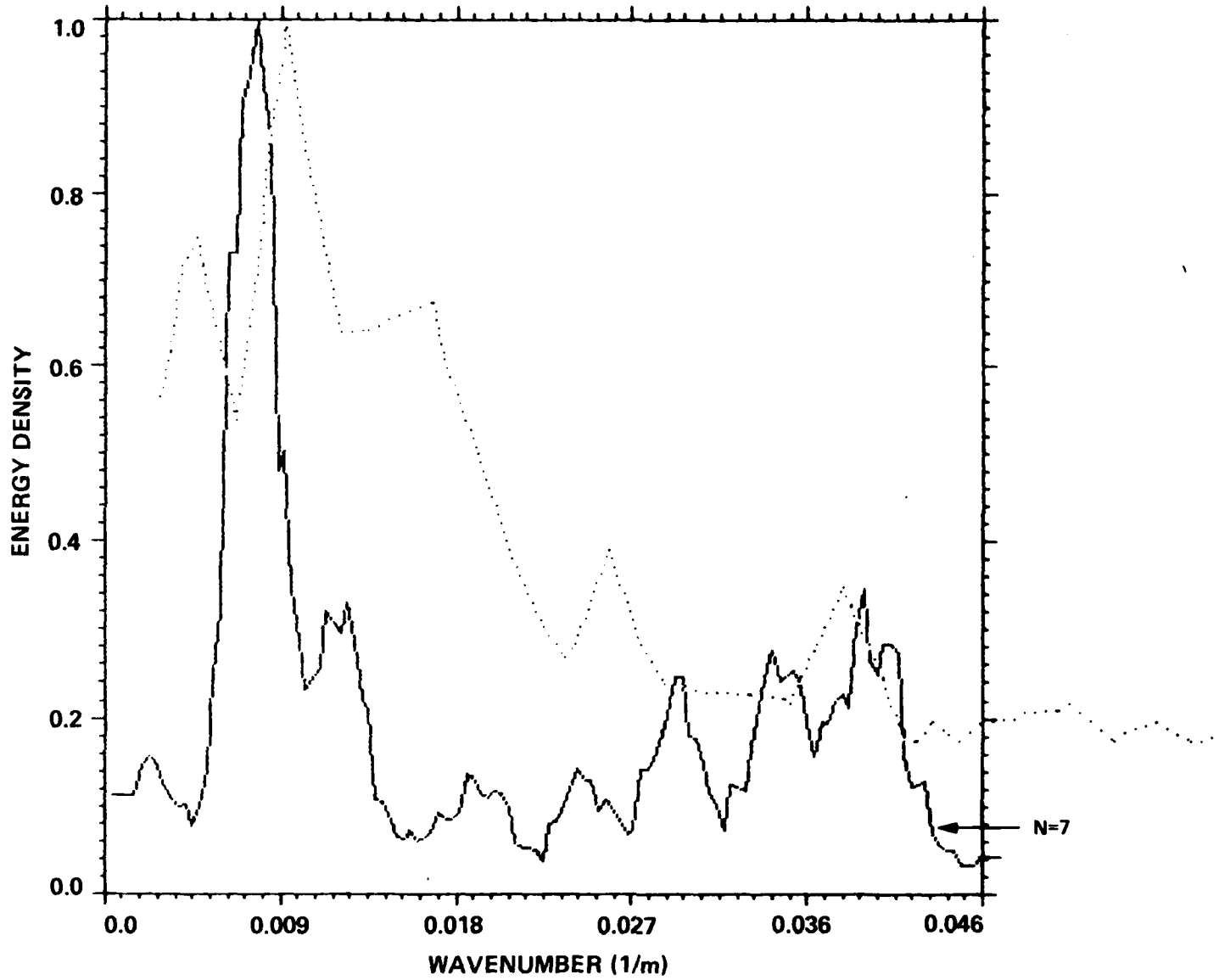

Figure 55. Comparison of SAR Spectrum at Optimum Focus, Solid Line, with Plant Simulated Spectrum, Dotted Line, at Optimum Focus. The SAR Spectrum Resolution is Degraded to 0.015 rad/m to Correspond Plant Spectral Resolution of 0.009 rad/m.

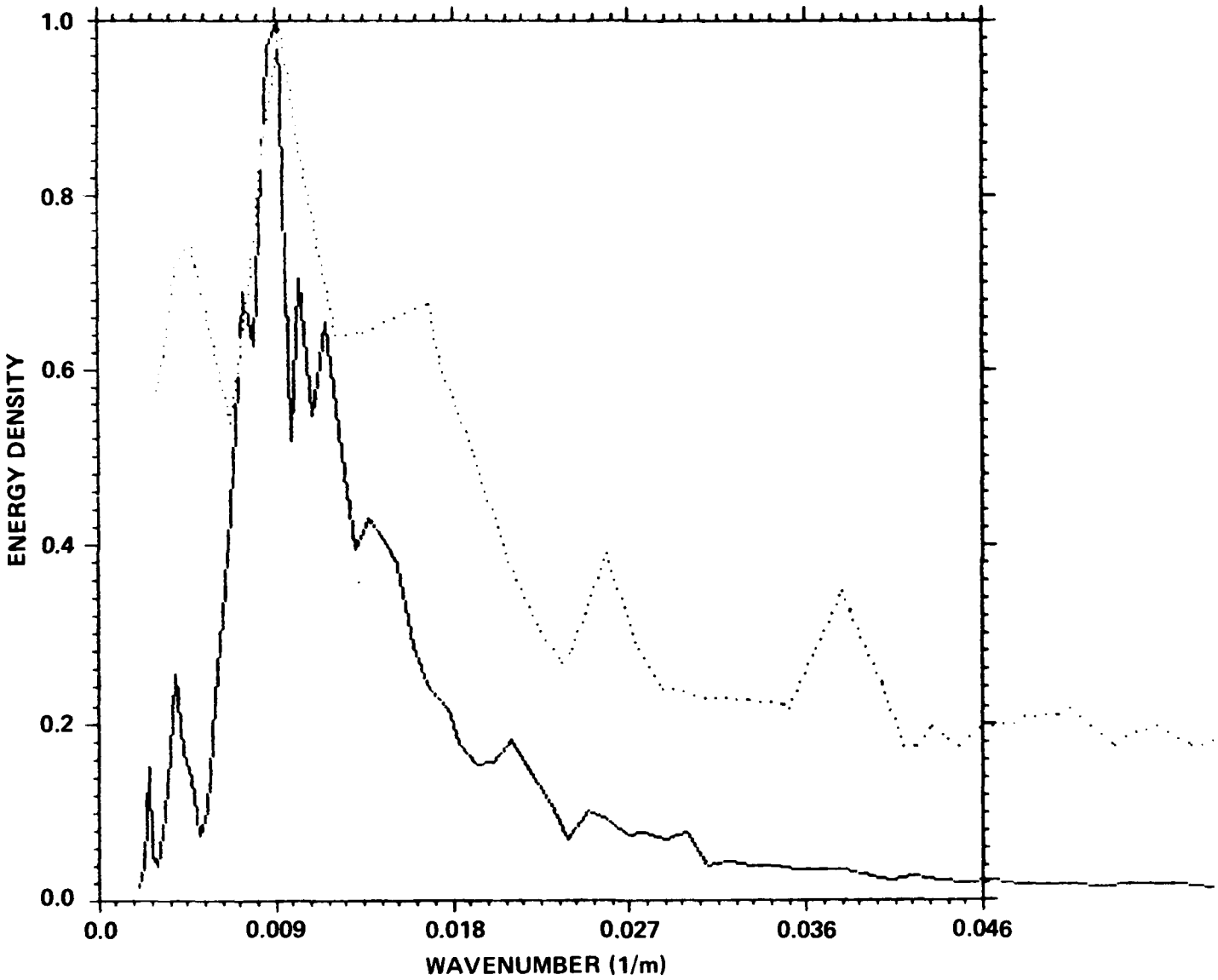

Figure 56. Comparison of Transformed In-Situ Spectrum, Solid Line, with Plant Simulated Spectrum, Dotted Line, at Optimum Focus.

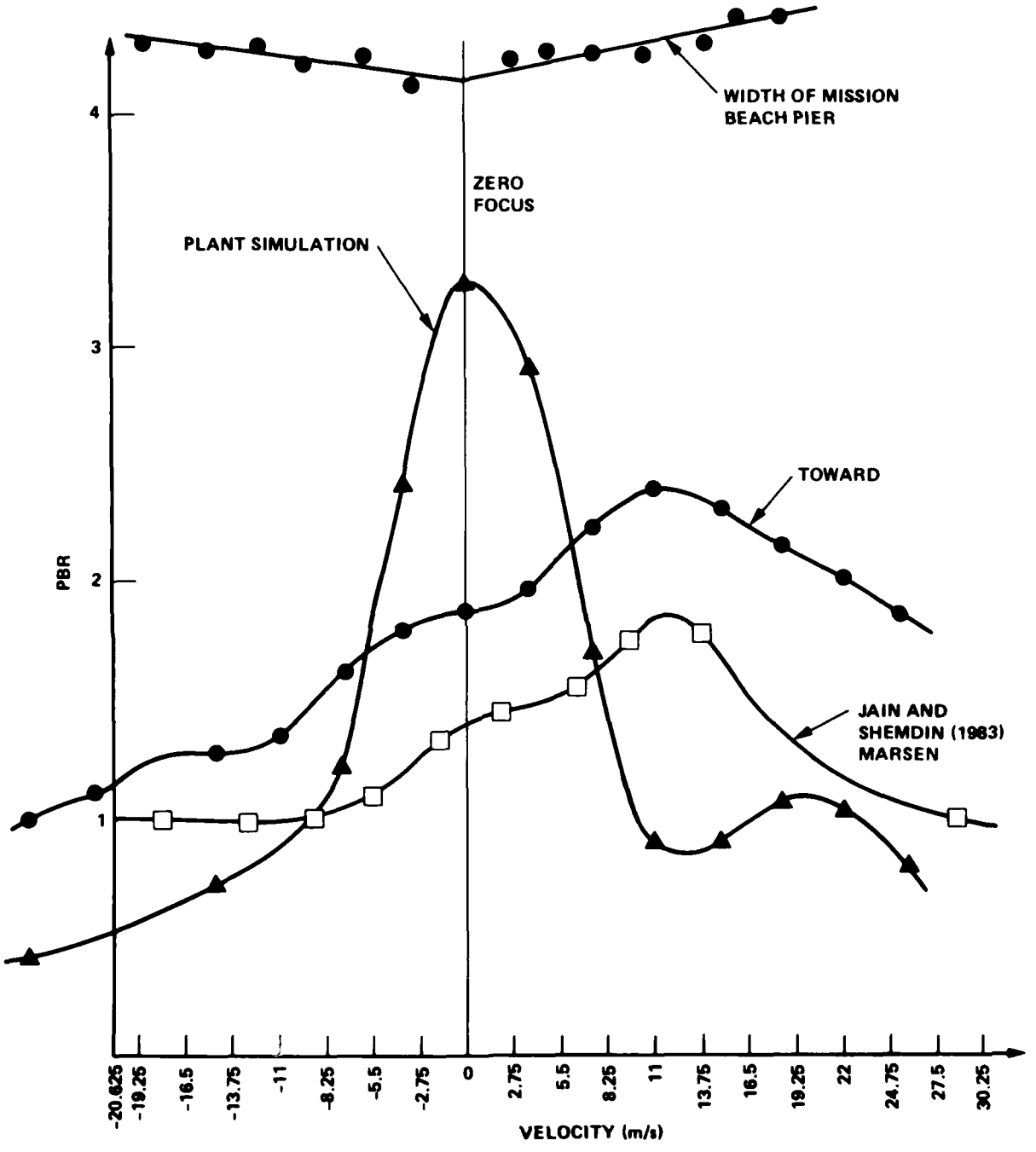

Figure 57. Comparisons of Peak-to-Baseline Ratio. ● - TOWARD Leg 1 (See Figure 54a), ▲ - Plant Simulation for Leg 1 (See Volume II), ■ - MARSEN Results for Azimuthal Waves (See Jain and Shemdin, 1981, Figure 5c).

mental maximum of 2.4. The latter difference is not clearly understood at present.

In Figure 57 a comparison of the TOWARD PBR results with those obtained in MARSEN (Jain and Shemdin, 1983) is shown, both for azimuthally traveling waves. The MARSEN results exhibit a maximum PBR value at 13.0 m/s. The TOWARD and MARSEN results both show optimum detectability at surface speed values of the order of the dominant wave phase-speeds. Hence, the TOWARD results confirm the MARSEN results which were obtained under a different set of environmental conditions. MARSEN was a wind-generated sea in the North Sea, and TOWARD was a swell filtered directionally by the Channel Islands of Southern California. The difference in PBR values between the two experiments is attributed to SAR processing, which was optical in MARSEN and digital in TOWARD.

Another simulation of the waves imaged on 31 October 1983 is given by Harger in Volume II. Harger stipulated that the wave phase-speed is a parameter in his simulation. However, his simulation so far does not demonstrate clearly the type of detectability results shown in Figures 54a-d. In principle, such simulations can be produced.

In summary, the results derived from the L-Band SAR images clearly demonstrate ocean surface motion that is one order of magnitude greater than orbital velocity of long waves. An asymmetry is shown in the direction of wave motion that has not been simulated satisfactorily by any of the available SAR models. The SAR data sets and in-situ measurements obtained in TOWARD provide a sufficient data base to derive and test theories that are consistent with observations. It is suggested that simulations based on available SAR models be matched to the TOWARD experimental results.

VIII. SUMMARY AND PRELIMINARY CONCLUSIONS

The field operations of TOWARD 84/86 were executed in accordance with the Science Plan, or exceeded it. The environmental conditions encountered were typical of Southern California with wind speeds ranging 0-40 knots (during intense fronts) and swell height ranging 0-2 meters. Unique data sets were acquired that are critical for understanding the dynamics of short waves and their interaction with long waves, internal waves and local ambient ocean features. Other data sets collected are useful for testing SAR backscatter models. The complementary hydrodynamic, radar backscatter and SAR data sets are of good quality and are adequate to resolve the critical issues in SAR imaging of the ocean surfce at L-Band.

The early results indicate that:

1. The probability density function of wave slope suggest Gaussian distribution for wave frequencies less than 2.5 Hz and non-Gaussian distribution for wave frequencies greater than 7.5 Hz. It is inferred that the longer ocean waves are weakly coupled, as expected, but that the very short waves are strongly coupled, i.e. experience possibly strong non-linear interaction. The transition from weakly to strongly coupled short waves is expected to be dependent on wind speed and sea state.

2. The measured wave slope spectra in TOWARD have significantly different intensity levels compared to predictions by Pierson and Stacy (1973) for equivalent wind speeds.

3. Radar backscatter results from multi-frequency radars suggest that sea spikes do not contribute significantly to the average backscattered power at L-Band, for the geometries implemented in TOWARD. Sea spike occurrence increases with radar frequency and wind speed.

4. Cross-wind radar backscatter results suggest that cross-wind or cross-wave modulation can occur, and may constitute the mechanism for SAR imaging of azimuthally traveling waves. We have also data indicating that the radar backscatter spectrum has a small peak near the dominant frequency of long waves. The resolution of this question is presently under debate.

5. SAR focusing results for azimuth traveling waves indicate that waves are most detectable at a focus setting that is of one order of magnitude larger than the wave orbital velocity.

6. Based on data analysis results to date, neither the "Velocity Bunching" model nor the "Distributed Surface" model has been demonstrated to explain the TOWARD observations, but the data sets obtained in TOWARD will allow significant progress toward resolution of the differences.

In conclusion, the available data sets and preliminary results strongly suggest that definitive conclusions, regarding the physics of SAR imaging of the ocean surface, will follow the data analysis effort that is in progress. Also, because the TOWARD data sets provide the most complete, surface-truth

measurements in support of SAR, it is anticipated that these data sets will be used for a number of specific scientific investigations related to SAR in the future. It is noted, however, that the TOWARD data sets were directed at solving the L-Band SAR problem. The available X-Band measurements are useful but incomplete. The solution of the X-Band SAR problem will require a separate follow-on experiment that will require theoretical investigations, laboratory studies and sea-testing of instruments. These are now being planned.

IX. ANALYSIS PLANS AND A PERSPECTIVE ON FUTURE RESEARCH

The discussions on available data sets and early results presented in this report do not reflect the effort that is now in progress, nor the analysis plans in force. These are discussed below in section A. Also, the insights gained to date allow formulation of a perspective on future SAR research. The latter is presented in section B.

A. Analysis Plans and Work in Progress

A substantial effort is now in progress in data analysis and simulation studies to achieve the scientific objectives set for TOWARD. The analysis plans and respective studies are discussed below for each objective.

1. SAR Imaging of Surface Waves - The results to date are based on analysis of SAR images obtained on 31 October 1984. SAR images obtained on other flight days have been processed at different focus settings; the follow-on analysis to determine detectability at each focus setting is in progress. It is important that the latter analysis be completed in order to establish the dependence of SAR-derived wave spectra on the ratio of range to platform velocity, azimuthal angle of waves and environmental conditions. For this purpose, SAR derived spectra will be compared with in-situ measurements to establish the differences between the true ocean surface and what SAR measures.

   The available SAR imaging theories for surface waves have not been demonstrated to explain the observation obtained to date (based on results from 31 October 1984). The "Velocity Bunching" theory is not able so far to explain why waves are most visible at a focus setting that is one order of magnitude greater than the wave orbital velocity. The "Distributed Surface" theory agrees in principle with such observations, but comparisons between SAR-derived spectra and simulated spectra have not been achieved yet.

   Vigorous effort, consisting of data analysis and SAR image simulations, is now in progress to determine whether the above theories can be modified to explain the TOWARD observations, or whether a new theory is needed. It is estimated that the present theoretical effort has reasonable promise to achieve the goal of explaining the SAR observations. The available TOWARD data sets are adequate for providing supporting information to test the SAR imaging hypotheses, and to determine the form of the SAR system transfer function.

2. Radar Backscatter Intercomparisons and Simulation - The radar backscatter data sets obtained by the Naval Research Laboratory, University of Kansas and Jet Propulsion Laboratory appear to be all of good quality. There is presently lack of agreement on the strength of radar backscatter modulation in the cross-wind or cross-wave direction. Intercomparisons of data sets obtained simultaneously will be pursued for different environmental conditions. The strength of such modulation is directly related to mechanisms of SAR imaging of surface waves. Hence, resolution of this matter is an integral part of achieving the objectives stated in item 1, above.

Stereo-photography gives a description of the ocean surface that is especially suited for radar backscatter simulation. Stereo-photography provides information on the mean slope of the surface, directional information on surface roughness in the range 3-100 cm, and information on wave breaking that occurs on the surface.

Radar backscatter models that are presently in wide use employ a two-scale ocean surface model. The assumptions involved in a two-scale model have been questioned. A "full-wave" solution approach has been proposed. With stereo-photography an opportunity exists for testing the radar backscatter models in present use. Here, the same patch of the ocean (depicted by stereo-photography) can be used as input in the different radar backscatter models, and the outputs compared with each other.

The above simulation effort is not intended to yield comparisons between radar backscatter measurements from the tower and in-situ observations. Such comparison is planned as another TOWARD study. Here, the surface slope measurements obtained with the wave follower will be used as input in simplified radar backscatter models (such as the two-scale model) to yield simulated backscatter results that can be compared with observations. Long time series for such a study are available, both for the input (wave slope records) and for comparison with output (radar backscatter measurements).

3. Hydrodynamic Data Intercomparison and Simulations - Complementary data sets are available with wave follower slope measurements and stereo-photography. The TOWARD Hydrodynamics Committee has emphasized the desirability of such intercomparisons. Work is now in progress to produce surface elevation maps from stereo-photographs. Forty (40) frames (stereo-pairs) have been specified and are being processed. Completion of stereo-processing is planned for the latter part of the summer. Follow-on analysis is required to transform surface elevation maps to wave number spectra. Additional analysis is required to convert wave-number spectra to wave-frequency spectra, to allow comparison with laser slope measurements. The inverse comparison is also possible. Laser-slope time series can be transformed to wave-number spectra, and compared with those obtained from stereo-analysis. Both types of comparisons will be made. Comparisons in the wave-number domain involve fewer assumptions, and will be executed first. This effort will remain in progress through December 1986. Early results are anticipated in September 1986.

Another type of hydrodynamic analysis that is pursued (also in accord with the recommendations of the Hydrodynamics Committee) is the characterization of the directional wave height spectra (and/or structure functions) of short waves relative to phase along the long waves. Initial work has been completed using the laser slope data from the wave follower, and modulated wave number spectra have been distributed to interested investigators. Similar modulated spectra of short waves can be obtained from stereo-data. A processed stereo data set for this purpose is expected to be available in September 1986.

The hydrodynamic analysis plans include a theoretical investigation of the modulation of short waves by long waves. Here, the action density equation along refracted ray paths will be used to investigate the relaxation rates under which the simulated modulation can be favorably compared with the measured modulation (obtained from laser-slope date and/or stereo-photography).

4. Modulation of Short Waves and Radar Backscatter by Internal Waves - A useful data set is available for investigating the modulation of short waves by internal waves. In Phase I of TOWARD, shallow water internal waves propagated through the tower site during periods when measurements of short waves and radar backscatter were being recorded. An effort to characterize the near-surface orbital velocities generated by these internal waves is presently in progress. Time series of modulated currents are being produced for use in cross-correlations with wave-slope and/or radar-backscatter time series.

   The modulation derived experimentally from the laser-slope measurements will be compared with those obtained independently from radar backscatter data. In addition, hydrodynamic modulation of short waves by internal waves will be simulated and compared with the measured modulations.

5. Surface Tension and Microlayer - Time series of surface tension provide an important data set for estimating the influence of the microlayer on radar backscatter. The modulation of short waves by long waves, and the intensity levels in wave slope spectra are, in principle, influenced by surface tension. The hydrodynamic simulations discussed in item 3, above, will be subjected to sensitivity analyses with regard to the influence of surface tension. Further progress in item 3 is prerequisite to appropriate use of the data set discussed here.

6. Decay of Short Waves Using "Bobbing Buoy" Data - This data set, obtained in "Mini-TOWARD", provides unique information on the decay of short waves in the open ocean, under various wind speeds (0-6 m/s). The "Bobbing Buoy" was operated so as to produce waves approximately 30 cm long. Stereo-photographs of the radially propagating waves were obtained and are being processed. Upon completion, additional analysis will be pursued to separate the influence of radial dispersion from the decay rate of waves. This analysis is projected for completion in December 1986.

B. A Perspective on Future SAR Research

The TOWARD experiment provides a data set that appears to be adequate for solving the most important issues related to SAR imaging of surface waves at L-Band. The data set is also useful for addressing problems related to SAR imaging of internal waves, imaging of the ocean surface with X-Band SAR and for investigating the influence of the microlayer.

The achievement derived from understanding SAR imaging of surface waves at L-Band has importance that transcends the immediate application of SAR detection of surface waves (although this application is important in itself). The most

significant outcome of understanding the SAR imaging processes is the development of a theory for imaging the ocean surface that is consistent with observations. Present discrepancies between SAR imaging models of surface waves impair our ability to understand imaging of other ocean signatures, as demonstrated in Chapter VI. Hence, understanding SAR imaging of surface waves at L-Band is a critical first step towards understanding SAR imaging of other ocean surface signatures. It is, therefore, a natural follow-on from present research to consider future experiments whereby present understanding of SAR at L-Band can be utilized for oceanographic research, and possibly for operational use.

The limitations of the TOWARD experiment stem from the fact that the Southern California Bight is located in an area where the environmental conditions are relatively quiescent. Follow-on experiments, conducted in more vigorous ocean environments, are desirable to test the limitations of the models developed based on the TOWARD data sets.

Other follow-on experiments may utilize TOWARD-derived models for detecting ship wakes, internal waves and ocean current features (i.e. eddies and current boundaries). For such experiments, sufficient understanding of SAR imaging exists only at L-Band.

The mechanisms involved in SAR imaging at X-Band are far less understood (C-Band is in near proximity of X-Band vs. L-Band). Here, an experiment similar in scope to TOWARD is required for understanding the hydrodynamics and radar backscatter processes associated with very short surface waves (1-5 cm in length). For this purpose a stable platform is mandatory to produce credible hydrodynamic data (directional wave height spectra) and useful radar backscatter data (fixed incidence angles). The insight gained at L-Band in determining the transfer function (from a radar backscatter map to a SAR scene) is useful at X-Band. That is, the SAR imaging model derived for L-Band can be extended in frequency to X-Band. The primary issues at X-Band relate to the hydrodynamics of the very short waves which appear to be strongly nonlinear and interconnected in wave numbers near X-Band, compared to L-Band. This is clearly indicated in the PDF results presented in Chapter IV. The radar backscatter measurements at X-Band and higher frequencies have different characteristics compared to L-Band, as shown in Chapter V. Hence, an experiment at X-Band, similar in scope to TOWARD, appears to be a natural follow-on.

In summary, the following perspective emerges from the TOWARD insights gained so far:

(a) A basic X-Band experiment, similar in scope to TOWARD, should be pursued as a follow-on to TOWARD. Here, extensive in-situ measurements from a stable platform are required to define the characteristics of both the short waves and the ambient environment.

(b) Application experiments should be pursued at L-Band to investigate: (i) SAR imaging of ocean waves in intense weather conditions (desirable small scale measurements will be difficult to obtain), (ii) imaging of current boundaries, (iii) imaging of internal waves and (iv) imaging of ship wakes. Such experiments at X-, C- and K_u-Bands will be useful only after the associated hydrodynamic and radar backscatter mechanisms are understood better.

REFERENCES

Alpers, W. R. and C. L. Rufenach (1979) "The Effect of Orbital Motions on Synthetic Aperture Radar Imagery of Ocean Waves," IEEE Trans. Ant. Prop., 27, 685-690.

Alpers, W. R., C. Bruening and K. Richter (1985a) "Comparison of Simulated and Measured SAR Image Spectra with Buoy-Derived Ocean Wave Spectra During the SIR-B Mission," IEEE Trans. Geosci. Remote Sensing, SIR-B Special Issue.

Alpers, W. R. and C. Bruening (1985b), "On the Non-Linearity of the Synthetic Aperture Radar Response to Moving Ocean Surface Waves," Private Communication.

Beal, R. C., D. G. Tilley and F. M. Monaldo (1983) "Large- and Small-Scale Spatial Evolution of Digitally Processed ocean Wave Spectra from SEASAT SAR," J. Geophys. Res., 88, 1761-1778.

Beal, R. C., F. M. Monaldo, D. G. Tilley, D. E. Irvine, E. J. Walsh, F. C. Jackson, D. W. Hancock III, D. E. Hines, R. N. Swift, F. I. Gonzales, D. R. Lyzenga and L. F. Zambresky (1985) "A Comparison of SIR-B Directional Ocean Spectra and Global Spectral Ocean Wave Model Predictions," Submitted to SIR-B Special Issue of Science.

Cote, L. F., J. O. Davis, W. Marks, R. F. McGough, E. Mehr, W. J. Pierson, Jr., J. F. Ropek, G. Stephenson and R. C. Vetter (1960) "The Directional Spectrum of a Wind Generated Sea as Determined from Data Obtained by the Stereo Wave Observation Project," Meteorological Papers Vol. 2, No. 6, New York University, 88 pgs.

Cox, C. and W. Munk (1954) "Statistics of Sea Surface Derived from Sun Glitter," J. Marine Research, 13, 198-227.

Garret, W. D. (1986) "Development and Utilization of a Surface Energy Measurement System in TOWARD 84/85," TOWARD Interim Report, Vol. II.

Geernaert, G. L. (1986) "TOWARD Meteorology Measurements," TOWARD Interim Report, Vol. II.

Beernaert, G. L., B. L. Byars, K. L. Davidson, S. E. Larsen and T. Mikkelsen (1986) "Meteorology Results from the Tower Ocean Wave and Radar Dependence Experiment," Technical Report, Naval Post Graduate School, Monterey, 114 pgs.

Guza, R. T. (1986) "Surface Gravity Wave Measurements," TOWARD Interim Report, Vol. II.

Harger, R. (1985) "The SAR Image of Short Gravity Waves on a Long Gravity Waves," Proc. IUCRM Symposium, Miami.

Harger, R. O. (1986) "Sample Predictions and Simulations of SAR Ocean Imagery," TOWARD Interim Report, Vol. II.

Hasselmann, K., R. K. Raney, W. F. Plant, W. R. Alpers, R. A. Shuchman, D. R. Lyzenga, C. L. Rufenach and M. F. Tucker (1985) "Theory of SAR Ocean Wave Imaging: A MARSEN View," J. Geophys. Res., 90, 4659-4686.

Hughes, B. A., H. L. Grant and R. W. Chappell (1977) "A Fast Response Surface-Wave Slope Meter and Measured Wind-Wave Moments," Deep-Sea Research, 24, 1211-1223.

Hwang, P. (1986) "Wave Follower Measurements During TOWARD 84/85," Tech. Report No. ORE 86-1, Ocean Research and Engineering, La Canada, 43 pgs. Also TOWARD Interim Report, Vol. II.

Ivanov, A. V. (1983) "On the Mechanism for Imaging Ocean Waves by SAR," IEEE Trans. Antennas Propagation, AP-31, 538-541.

Jain, A. (1981) "SAR Imaging of Ocean Waves: Theory," IEEE J. Ocean Eng., OE-6, 130-139.

Jain, A. and O. Shemdin (1983) "L-Band SAR Ocean Wave Observations During MARSEN," J. Geophys. Res., 88, 9792-9808.

Keller, W. C. and J. W. Wright (1975) "Microwave Scattering and the Straining of Wind-Generated Waves," Radio Sci., 10, 139-147.

Large, W. G. and S. Pond (1981) "Open Ocean Momentum Flux Measurements in Moderate to Strong Winds," J. Phys. Oceangr., 11, 324-336.

Larsen, T. R., L. I. Moskowitz and J. W. Wright (1976) "A Note on SAR Imagery of the Ocean," J. Geophys. Res., 81, 2655-2656.

Longuett-Higgins, M. S. (1986) "The Propagation of Short Surface Waves on Longer Gravity Waves," TOWARD Interim Report, Vol. II.

Lyzenga, D. and R. Shuchman (1983) "Analysis of Scatterer Motion Effects in MARSEN X-Band SAR Imagery," J. Geophys. Res., 88, 9769-9775.

Pierson, W. F., Jr. and R. A. Stacy (1973) "The Elevation, Slope, and Curvature Spectra of a Wind Roughened Sea Surface," Report No. NASA CR-2247, New York University, University Heights.

Pierson, W. J. and M. A. Donelan (1986) "Verification Results for a Two-Scale Model of Microwave Backscatter from the Sea Surface," Proc. IGARSS, 86.

Raney, R. K. (1971) "Synthetic Aperture Imaging Radar and Moving Targets," IEEE Trans. Aerosp. Electron. Syst., AES-7, 499-505.

Raney, R. K. and R. A. Shuchman (1978) "SAR Mechanisms for Imaging Ocean Waves," Proc. 5th Canadian Symposium on Remote Sensing, Victoria, BC, 495-505.

Plant, W. (1982) "SAR Simulation of Ocean Waves," Private Communication.

Plant, W. J. and W. C. Keller (1983) "The Two-Scale Radar Wave Probe and SAR Imaging of the Ocean," J. Geophys. Res., 88, 9776-8784.

Plant, W. J. (1986) "SAR Imagery Simulated from Two-Scale Radar Wave Probe Return," TOWARD Interim Report, Vol. II.

Shemdin, O. H. (1980) "Measurement of Wind and Surface Wave Slopes with a Wave Follower," Tech. Report No. 715-123, Jet Propulsion Laboratory, Pasadena.

Shemdin, O. H. (1984) "TOWARD 84/85 Science Plan," CIT-JPL Tech. Report, Pasadena.

Shemdin, O. H. and D. Hoff (1986) "A Wave Following Instrumentation System for Studying Process Near the Air-Water Interface," Tech. Report (in preparation) Jet Propulsion Laboratory, Pasadena.

Shuchman, R. and O. Shemdin (1983) "SAR Imaging of Ocean Waves During the Marineland Experiment," IEEE-J. Ocean Eng., OE-8, 83-90.

Shuchman, R. A., A. Klooster and A. L. Moffett (1979) "SAR Modeling of Surface Ocean Waves," Proc. 13th Int'l. Symp. Rem. Sens. of Environment, Ann Arbor, 603-627.

Smith, S. D. (1980) "Wind Stress and Heat Flux over the Ocean During Gale Force Winds," J. Phys. Oceanogr., 10, 709-726.

Tajirian, E. K. (1986) "Processing of JPL SAR Frame: Azimuthal Waves on 31 October 1984," TOWARD Interim Report, Vol. II.

Tang, S. and O. H. Shemdin (1983) "Measurement of High Frequency Waves Using a Wave Follower," J. Geophys. Res., 88, 9832-9840.

APPENDIX

DATA LOGS AND ENVIRONMENTAL DATA IN SUPPORT OF MATERIAL IN TEXT

APPENDIX

List of Figures

List of Tables

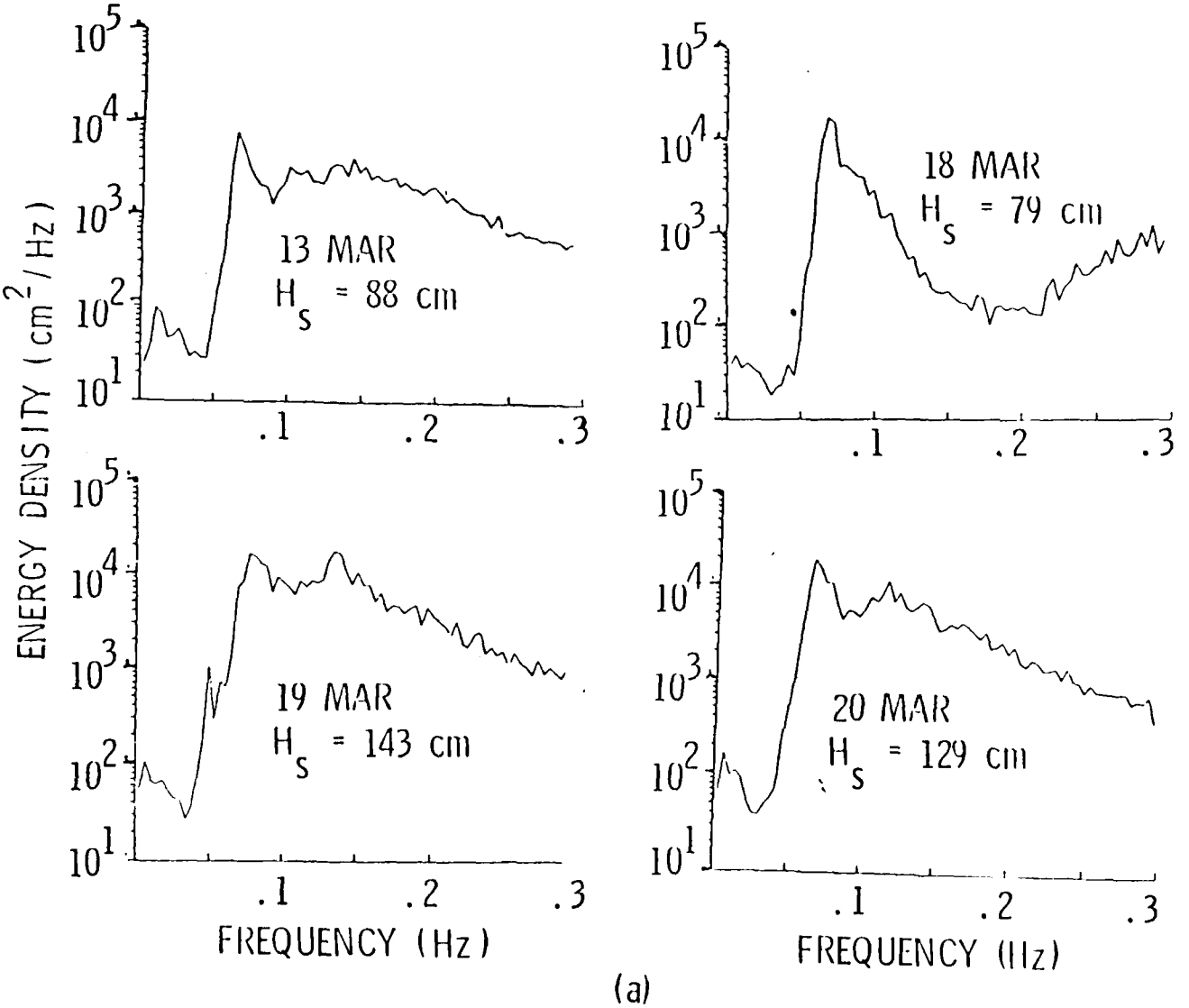

Figure A1. Wave Height Spectra for Eight Overflight Days in Phase-II.

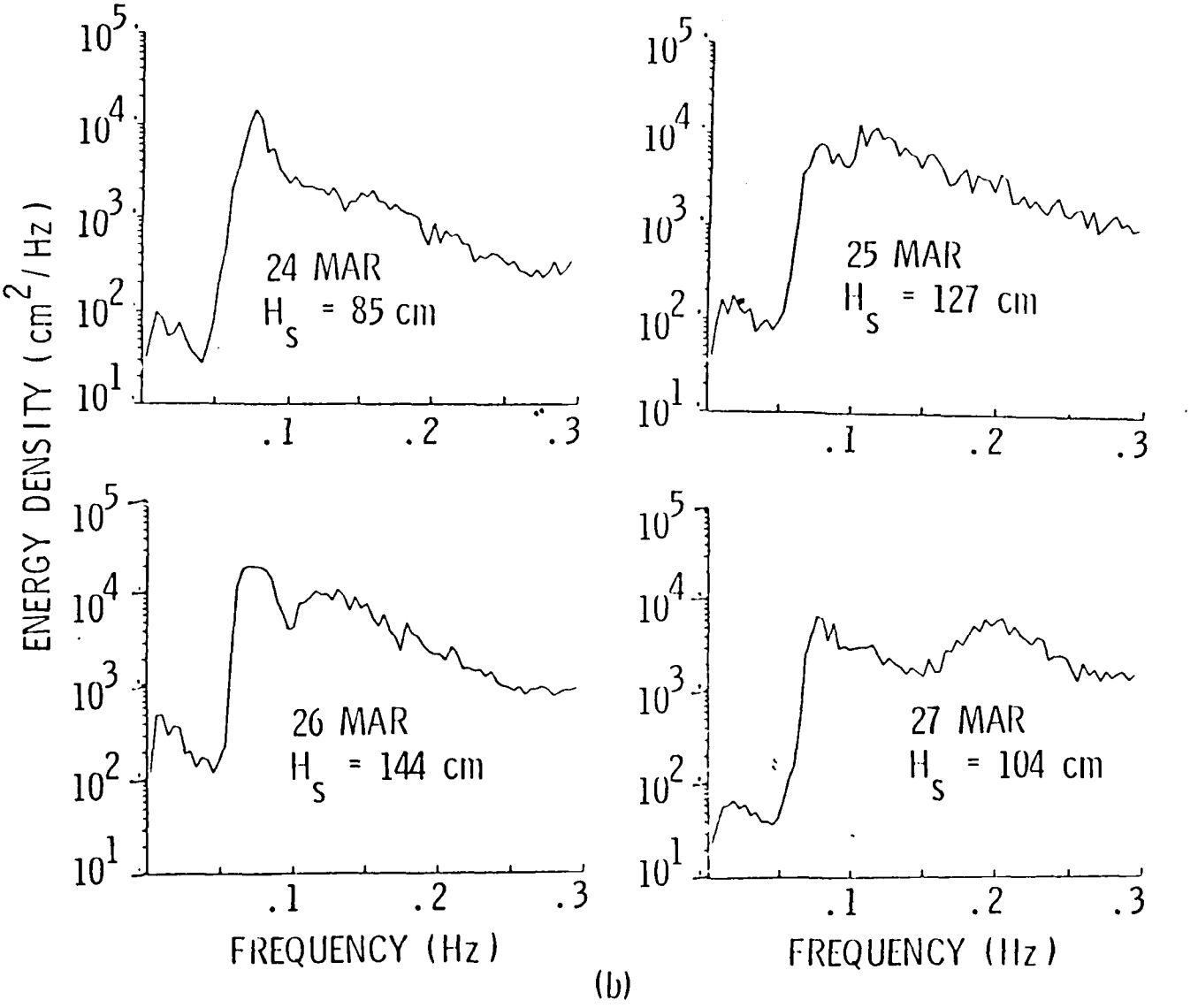

Figure A2. Wave Height Spectra for Eight Overflight Days in Phase-II. (Continued)

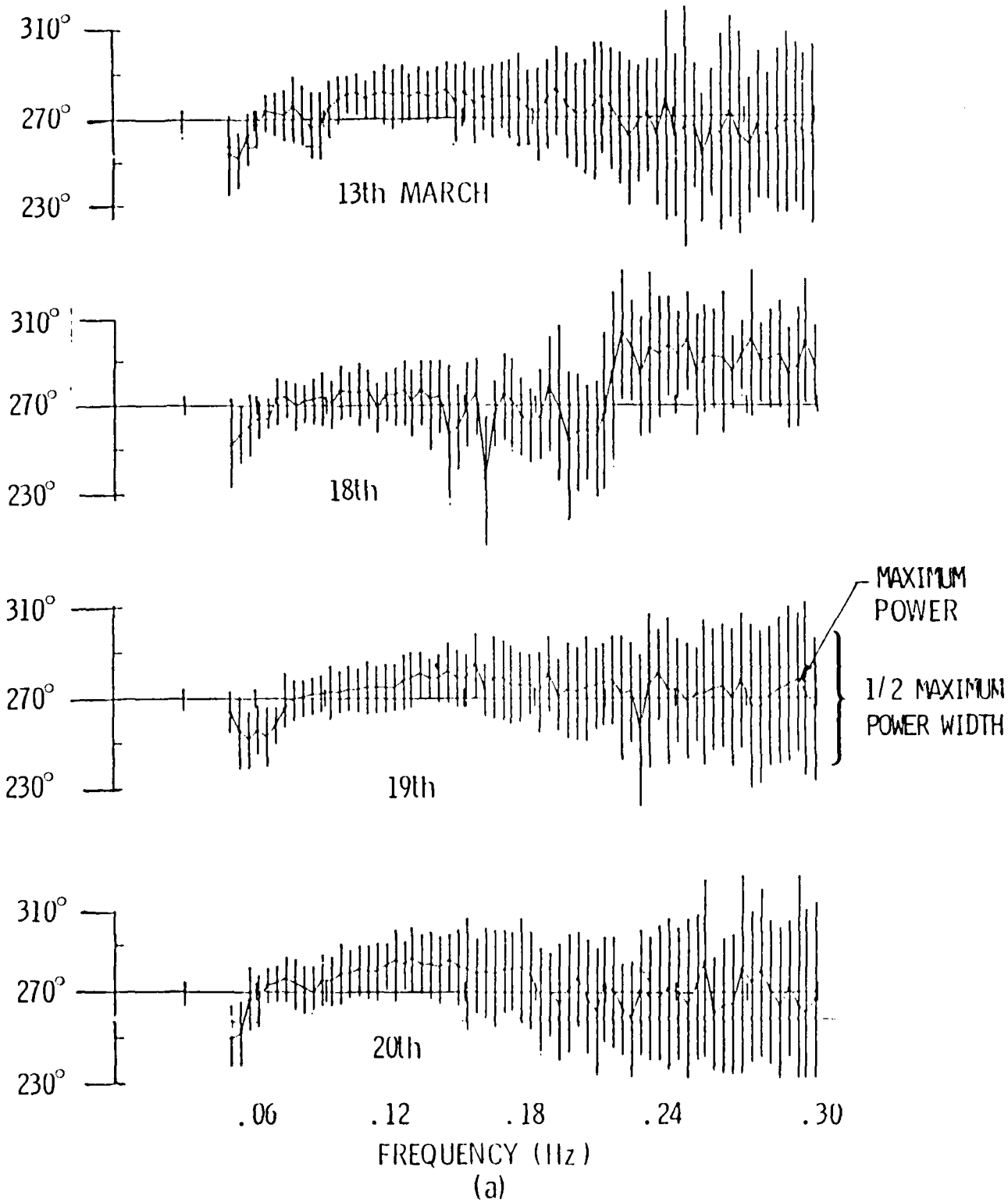

Figure A3. Wave Direction (at Maximum Power) and Angular Spread (at Half Maximum Power Vs. Frequency), in Phase-II.

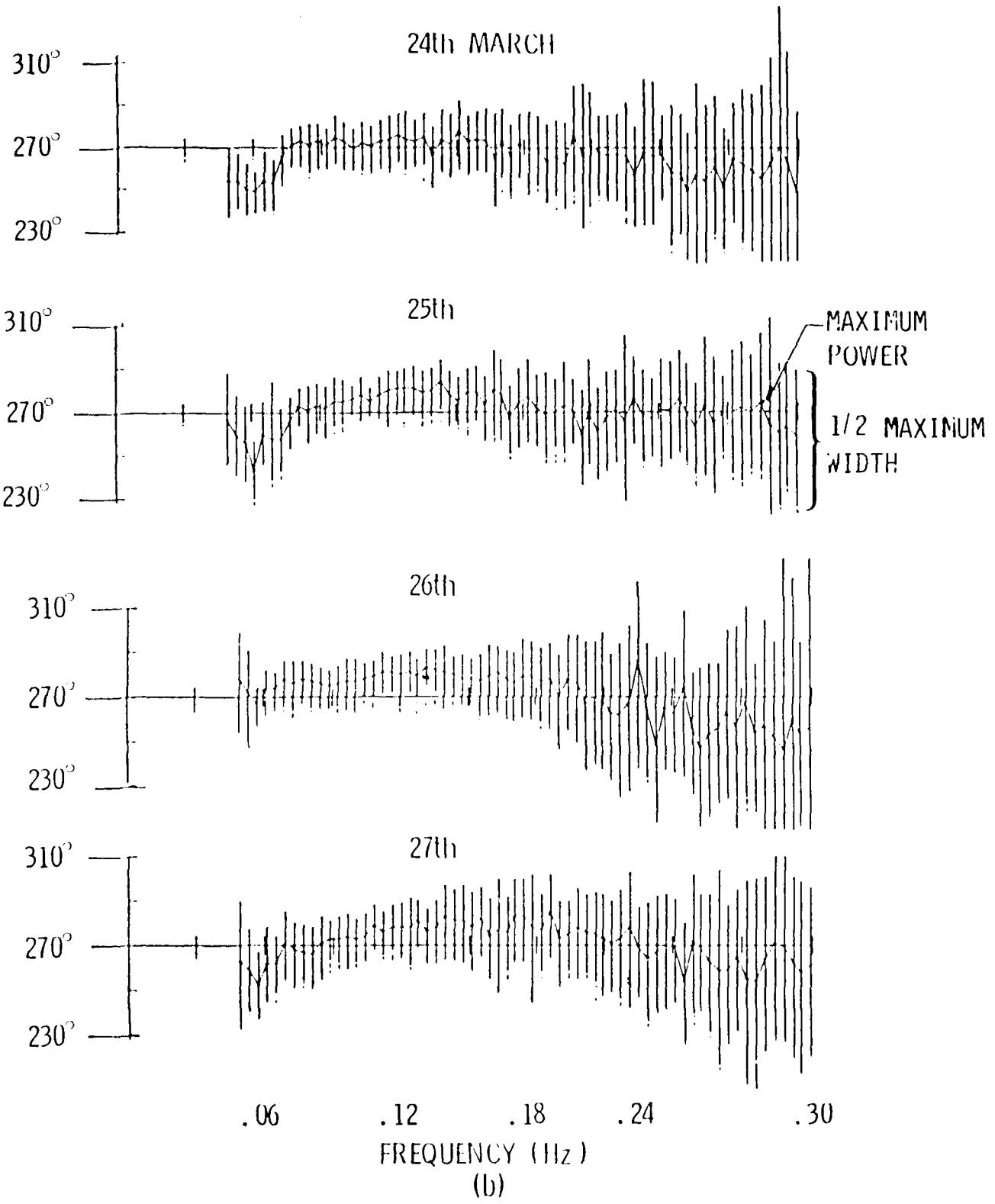

Figure A4. Wave Direction (at Maximum Power) and Angular Spread (at Half Maximum Power Vs. Frequency). (Continued)

Table A1. Stereo-Photograph Data Summary, Phase-I.

DATE	START TIME (PST)	INTERVAL	AZMUTH	REMARKS
10-31-84	13:17:46	2:00		
10-31-84	13:53:53	2:00		
10-31-84	14:17:25	2:00		
10-31-84	15:20:34	2:00		
10-31-84	15:48:07	1:00		
11-04-84	11:33:29	1.5	190	
11-04-84	11:50:30	1.5	190	
11-04-84	15:21:54	2:00	190	
11-04-84	15:53:12	1.5	200	
11-04-84	16:19:42	2:00	190	
11-04-84	16:57:20	2:00	280	
11-07-84	14:16:24	2:00	260	
11-07-84	14:30:23	2:00	330	
11-07-84	15:00:54	2:00	270	
11-07-84	15:17:50	1.5	330	
11-07-84	15:46:19	1.5	290	
11-07-84	16:02:24	1.5	270	
11-07-84	16:21:27	1.5	200	
11-07-84	16:36:42	1.5	200	
11-07-84	16:49:26	1.5	200	

Table A2. Stereo-Photograph Data Summary, Phase-II.

DATE	START TIME (PST)	INTERVAL	AZMUTH	REMARKS
3-28-85	09:51:00	1.5	270	
3-28-85	09:51:02	1.5	270	
3-28-85	09:51:03	1.5	270	
3-28-85	09:51:05	1.5	270	
3-28-85	09:51:06	1.5	270	
3-28-85	09:51:08	1.5	270	
3-28-85	09:51:09	1.5	270	
3-28-85	09:51:11	1.5	270	
3-28-85	09:51:12	1.5	270	No Flights
3-28-85	09:51:14	1.5	270	
3-28-85	09:51:15	1.5	270	
3-28-85	09:51:17	1.5	270	
3-28-85	09:51:19	1.5	270	
3-28-85	09:51:20	1.5	270	
3-28-85	09:51:21	1.5	270	Very Good Structure
3-28-85	09:51:23	1.5	270	
3-28-85	09:51:24	1.5	270	
3-28-85	09:51:26	1.5	270	
3-28-85	09:51:27	1.5	270	
3-28-85	09:51:29	1.5	270	
3-28-85	09:51:30	1.5	270	
3-28-85	09:51:32	1.5	270	
3-28-85	09:51:33	1.5	270	
3-28-85	09:51:35	1.5	270	
3-28-85	09:51:36	1.5	270	
3-28-85	09:51:38	1.5	270	
3-28-85	09:51:39	1.5	270	
3-28-85	09:51:41	1.5	270	
3-28-85	09:51:42	1.5	270	

Table A2. Stereo-Photograph Data Summary (Continued), Phase-II.

DATE	START TIME (PST)	INTERVAL	AZMUTH	REMARKS
3-21-85	15:00:13	2.001	270	
3-21-85	15:00:15	2.001	270	
3-21-85	15:00:17	2.001	270	
3-21-85	15:00:19	2.001	270	
3-21-85	15:00:21	2.001	270	
3-21-85	15:00:23	2.001	270	
3-21-85	15:00:25	2.001	270	
3-21-85	15:00:27	2.001	270	No Flights
3-21-85	15:00:29	2.001	270	
3-21-85	15:00:31	2.001	270	
3-21-85	15:00:33	2.001	270	
3-21-85	15:00:35	2.001	270	
3-21-85	15:00:37	2.001	270	
3-21-85	15:00:39	2.001	270	
3-21-85	15:00:41	2.001	270	
3-21-85	15:00:43	2.001	270	
3-21-85	15:00:45	2.001	270	
3-31-85	15:00:47	2.001	270	
3-21-85	15:00:49	2.001	270	
3-21-85	15:00:51	2.001	270	
3-21-85	15:00:53	2.001	270	
3-21-85	15:00:55	2.001	270	
3-21-85	15:00:57	2.001	270	
3-21-85	15:00:59	2.001	270	
3-21-85	15:50:43	2.00	270	Rough Patch
3-21-85	15:50:45	2.00	270	
3-21-85	15:50:47	2.00	270	
3-21-85	15:50:49	2.00	270	
3-21-85	15:50:51	2.00	270	
3-21-85	15:50:53	2.00	270	
3-21-85	15:50:55	2.00	270	
3-21-85	15:50:57	2.00	270	
3-21-85	15:50:59	2.00	270	
3-21-85	15:51:01	2.00	270	
3-21-85	15:51:03	2.00	270	
3-21-85	15:51:05	2.00	270	
3-21-85	15:51:07	2.00	270	
3-21-85	15:51:09	2.00	270	
3-21-85	15:51:11	2.00	270	
3-21-85	15:51:13	2.00	270	
3-21-85	15:51:15	2.00	270	
3-21-85	15:51:17	2.00	270	
3-21-85	15:51:19	2.00	270	
3-21-85	15:51:21	2.00	270	
3-21-85	15:51:23	2.00	270	
3-21-85	15:51:25	2.00	270	
3-21-85	15:51:27	2.00	270	
3-21-85	15:51:29	2.00	270	

Table A2. Stereo-Photograph Data Summary (Continued), Phase-II.

DATE	START TIME (PST)	INTERVAL	AZMUTH	REMARKS
3-22-85	11:50:43	1.5	270	
3-22-85	11:50:45	1.5	270	
3-22-85	11:50:46	1.5	270	
3-22-85	11:50:48	1.5	270	
3-22-85	11:50:49	1.5	270	Good Stereo Data
3-22-85	11:50:51	1.5	270	
3-22-85	11:50:52	1.5	270	
3-22-85	11:50:54	1.5	270	
3-22-85	11:50:55	1.5	270	
3-22-85	11:50:57	1.5	270	
3-22-85	11:50:58	1.5	270	Frequent Breaking
3-22-85	11:51:00	1.5	270	
3-22-85	11:51:01	1.5	270	
3-22-85	11:51:03	1.5	270	
3-22-85	11:51:04	1.5	270	
3-22-85	11:51:06	1.5	270	No Flights
3-22-85	11:51:07	1.5	270	
3-22-85	11:51:09	1.5	270	
3-22-85	11:51:10	1.5	270	
3-22-85	11:51:12	1.5	270	
3-22-85	11:51:13	1.5	270	
3-22-85	11:51:15	1.5	270	
3-22-85	11:51:16	1.5	270	
3-22-85	11:51:18	1.5	270	
3-22-85	12:10:15	1.5	270	
3-22-85	12:10:17	1.5	270	
3-22-85	12:10:18	1.5	270	
3-22-85	12:10:20	1.5	270	
3-22-85	12:10:21	1.5	270	Good Stereo Data
3-22-85	12:10:23	1.5	270	
3-22-85	12:10:24	1.5	270	
3-22-85	12:10:26	1.5	270	
3-22-85	12:10:27	1.5	270	
3-22-85	12:10:29	1.5	270	Frequent Breaking
3-22-85	12:10:30	1.5	270	
3-22-85	12:10:32	1.5	270	
3-22-85	12:10:33	1.5	270	
3-22-85	12:10:35	1.5	270	
3-22-85	12:10:36	1.5	270	
3-22-85	12:10:38	1.5	270	
3-22-85	12:10:39	1.5	270	
3-22-85	12:10:41	1.5	270	
3-22-85	12:10:42	1.5	270	
3-22-85	12:10:44	1.5	270	
3-22-85	12:10:45	1.5	270	
3-22-85	12:10:47	1.5	270	
3-22-85	12:10:48	1.5	270	
3-22-85	12:10:50	1.5	270	

Table A2. Stereo-Photograph Data Summary (Continued), Phase-II.

DATE	START TIME (PST)	INTERVAL	AZMUTH	REMARKS
3-26-85	10:11:51	1.5	540	
3-26-85	10:11:52	1.5	540	
3-26-85	10:11:54	1.5	540	
3-26-85	10:11:55	1.5	540	
3-26-85	10:11:57	1.5	540	
3-26-85	10:11:58	1.5	540	
3-26-85	10:12:00	1.5	540	Good Structure
3-26-85	10:12:01	1.5	540	
3-26-85	10:12:03	1.5	540	
3-26-85	10:12:04	1.5	540	Less Breaking
3-26-85	10:12:06	1.5	540	waves
3-26-85	10:12:07	1.5	540	
3-26-85	10:12:09	1.5	540	
3-26-85	10:12:10	1.5	540	
3-26-85	10:12:12	1.5	540	
3-26-85	10:12:13	1.5	540	
3-26-85	10:12:15	1.5	540	F-4 Flight
3-26-85	10:12:16	1.5	540	
3-26-85	10:12:18	1.5	540	
3-26-85	10:12:19	1.5	540	OV-10 Flight
3-26-85	10:12:21	1.5	540	
3-26-85	10:12:22	1.5	540	
3-26-85	10:12:24	1.5	540	
3-26-85	10:12:25	1.5	540	
3-26-85	10:12:27	1.5	540	
3-26-85	10:12:28	1.5	540	
3-26-85	10:12:30	1.5	540	
3-26-85	10:26:22	1.5	270	
3-26-85	10:26:23	1.5	270	
3-26-85	10:26:25	1.5	270	
3-26-85	10:26:26	1.5	270	
3-26-85	10:26:28	1.5	270	Good Structure
3-26-85	10:26:29	1.5	270	No Extensive
3-26-85	10:26:31	1.5	270	Breaking
3-26-85	10:26:32	1.5	270	
3-26-85	10:26:34	1.5	270	
3-26-85	10:26:35	1.5	270	
3-26-85	10:26:37	1.5	270	
3-26-85	10:26:38	1.5	270	No. 22 on Film
3-26-85	10:26:40	1.5	270	
3-26-85	10:26:41	1.5	270	
3-26-85	10:26:43	1.5	270	
3-26-85	10:26:44	1.5	270	
3-26-85	10:26:46	1.5	270	
3-26-85	10:26:47	1.5	270	
3-26-85	10:26:49	1.5	270	
3-26-85	10:26:50	1.5	270	
3-26-85	10:26:52	1.5	270	
3-26-85	10:26:53	1.5	270	
3-26-85	10:26:55	1.5	270	
3-26-85	10:26:56	1.5	270	

Table A2. Stereo-Photograph Data Summary (Continued), Phase-II.

DATE	START TIME (PST)	INTERVAL	AZMUTH	REMARKS
3-26-85	10:51:51	1.5	270	
3-26-85	10:51:52	1.5	270	
3-26-85	10:51:54	1.5	270	
3-26-85	10:51:55	1.5	270	
3-26-85	10:51:57	1.5	270	
3-26-85	10:51:58	1.5	270	
3-26-85	10:52:00	1.5	270	
3-26-85	10:52:01	1.5	270	
3-26-85	10:52:03	1.5	270	
3-26-85	10:52:04	1.5	270	
3-26-85	10:52:06	1.5	270	
3-26-85	10:52:07	1.5	270	
3-26-85	10:52:09	1.5	270	
3-26-85	10:52:10	1.5	270	
3-26-85	10:52:12	1.5	270	
3-26-85	10:52:13	1.5	270	
3-26-85	10:52:15	1.5	270	
3-26-85	10:52:16	1.5	270	
3-26-85	10:52:18	1.5	270	
3-26-85	10:52:19	1.5	270	
3-26-85	10:52:21	1.5	270	
3-26-85	10:52:22	1.5	270	
3-26-85	10:52:24	1.5	270	
3-25-85	10:52:25	1.5	270	
3-26-85	11:14:24	1.5	270	
3-26-85	11:14:25	1.5	270	
3-26-85	11:14:27	1.5	270	Very good Structure-Film #3
3-26-85	11:14:28	1.5	270	
3-26-85	11:14:30	1.5	270	
3-26-85	11:14:31	1.5	270	
3-26-85	11:14:33	1.5	270	
3-26-85	11:14:34	1.5	270	
3-26-85	11:14:36	1.5	270	
3-26-85	11:14:37	1.5	270	
3-26-85	11:14:39	1.5	270	
3-26-85	11:14:40	1.5	270	
3-26-85	11:14:42	1.5	270	
3-26-85	11:14:43	1.5	270	
3-26-85	11:14:45	1.5	270	
3-26-85	11:14:46	1.5	270	
3-26-85	11:14:48	1.5	270	
3-26-85	11:14:49	1.5	270	
3-26-85	11:14:51	1.5	270	
3-26-85	11:14:52	1.5	270	
3-26-85	11:14:54	1.5	270	
3-26-85	11:14:55	1.5	270	
3-26-85	11:14:57	1.5	270	
3-26-85	11:14:58	1.5	270	

Table A2. Stereo-Photograph Data Summary (Continued), Phase-II.

DATE	START TIME (PST)	INTERVAL	AZMUTH	REMARKS
3-27-85	10:48:01	1.5	270	
3-27-85	10:48:03	1.5	270	
3-27-85	10:48:04	1.5	270	
3-27-85	10:48:06	1.5	270	
3-27-85	10:48:07	1.5	270	
3-27-85	10:48:09	1.5	270	CV-990 Flight
3-27-85	10:48:10	1.5	270	
3-27-85	10:48:12	1.5	270	
3-27-85	10:48:13	1.5	270	
3-27-85	10:48:15	1.5	270	
3-27-85	10:48:16	1.5	270	
3-27-85	10:48:18	1.5	270	
3-27-85	10:48:19	1.5	270	
3-27-85	10:48:21	1.5	270	
3-27-85	10:48:22	1.5	270	Breaking Patch and Good Structure Wind Waves 12m/s
3-27-85	10:48:24	1.5	270	
3-27-85	10:48:25	1.5	270	
3-27-85	10:48:27	1.5	270	
3-27-85	10:48:28	1.5	270	
3-27-85	10:48:30	1.5	270	
3-27-85	10:48:31	1.5	270	
3-27-85	10:48:33	1.5	270	
3-27-85	10:48:34	1.5	270	
3-27-85	10:48:36	1.5	270	Breaking Patch

Table A2. Stereo-Photograph Data Summary (Continued), Phase-II.

DATE	START TIME (PST)	INTERVAL	AZMUTH	REMARKS
3-28-85	10:04:52	1.5	270	
3-28-85	10:04:53	1.5	270	
3-28-85	10:04:55	1.5	270	
3-28-85	10:04:56	1.5	270	Very Good
3-28-85	10:04:58	1.5	270	Structure
3-28-85	10:04:59	1.5	270	
3-28-85	10:05:01	1.5	270	
3-28-85	10:05:02	1.5	270	
3-28-85	10:05:04	1.5	270	
3-28-85	10:05:05	1.5	270	
3-28-85	10:05:07	1.5	270	
3-28-85	10:05:08	1.5	270	
3-28-85	10:05:10	1.5	270	
3-28-85	10:05:11	1.5	270	
3-28-85	10:05:13	1.5	270	
3-28-85	10:05:14	1.5	270	
3-28-85	10:05:16	1.5	270	
3-28-85	10:05:17	1.5	270	
3-28-85	10:05:19	1.5	270	
3-28-85	10:05:20	1.5	270	
3-28-85	10:05:22	1.5	270	
3-28-85	10:05:23	1.5	270	
3-28-85	10:05:25	1.5	270	
3-28-85	10:05:06	1.5	270	

Table A3. JPL: Multi. - Frequency Radar Data Summary, Phase I.

DATE	START TIME (1)	STOP TIME	FREQ. (GHz)	POL.	RADAR LOOK DIRECTION	INCIDENCE ANGLE	WIND SPEED	REMARKS
10-06-84	15:18	15:26	7	HH	270	45		
10-06-84	15:29	15:38	7	"	"	"		
10-06-84	15:40	15:49	2	"	"	"		
10-06-84	15:50	15:58	3	"	"	"		
10-07-84	5:56	6:05	5	"	"	"		
10-07-84	6:06	6:15	3	"	"	"		
10-07-84	6:51	6:59	V	"	"	"		2
10-07-84	7:05	7:14	V	"	"	"		2
10-20-84	21:03	21:13	5	"	"	"		
10-20-84	21:16	21:25	"	"	"	"		
10-21-84	8:40	8:49	"	"	"	"		
10-21-84	8:57	9:06	"	"	"	"		
10-23-84	15:30	15:38	"	"	"	"		
10-23-84	15:43	15:51	"	"	"	"		
10-24-84	15:30	15:38	"	"	"	"		
10-24-84	16:37	16:45	"	"	"	"		
10-25-84	9:18	9:26	"	"	"	"		
10-25-84	10:09	10:18	"	"	"	"		
10-27-84	16:09	16:19	"	"	"	"		5
10-27-84	16:34	16:42	"	"	"	"		5,6
10-31-84	10:37	10:46	"	"	"	"		
10-31-84	16:19	16:28	"	"	"	"		
11-03-84	13:05	13:14	"	"	"	"		
11-03-84	13:57	14:05	"	"	"	"		
11-03-84	14:18	14:27	"	"	"	"		
11-03-84	14:30	14:39	"	"	"	"		
11-03-84	16:43	16:52	"	"	"	"		
11-03-84	16:58	17:06	3	"	"	"		
11-03-84	19:49	19:58	"	"	"	"		
11-03-84	20:01	20:11	"	"	"	"		
11-03-84	20:14	20:24	"	"	"	"		
11-03-84	20:36	20:45	"	"	"	"		
11-03-84	15:39	16:25	"	"	"	"		
11-03-84	17:13	17:54	"	"	"	"		
11-03-84	18:05	18:07	1.5	"	"	"		
11-03-84	18:10	18:12	2	"	"	"		
11-03-84	18:15	18:20	3	"	"	"		

(1) PDT before 28 October 1984 and PST after 28 October 1984.

Table A3. (Continued) JPL: Multi. - Frequency Radar Data Summary, Phase I.

DATE	START TIME (PST)	STOP TIME	FREQ. (GHz)	POL.	RADAR LOOK DIRECTION	INCIDENCE ANGLE	WIND SPEED	REMARKS
11-03-84	18:24	18:28	5	HH	270	45		
11-03-84	18:30	18:32	7	"	"	"		
11-03-84	18:34	18:37	10	"	"	"		
11-03-84	18:39	18:41	13	"	"	"		
11-03-84	18:43	18:46	3	"	"	"		
11-03-84	18:47	18:50	1	"	"	"		
11-03-84	18:52	18:55	1.5	"	"	"		
11-03-84	18:57	19:00	1.75	"	"	"		
11-03-84	19:02	19:04	1.25	"	"	"		
11-03-84	19:06	19:09	3	"	"	"		
11-04-84	2:43	9:05	"	"	"	"		
11-04-84	17:46	00:13	"	"	"	"		
11-04-84	12:30	12:39	"	"	"	"		
11-04-84	15:02	15:12	"	"	"	"		
11-04-84	17:32	17:41	"	"	"	"		
11-05-84	16:11	16:13	"	"	"	"		7
11-05-84	8:22	8:25	"	"	"	"		
11-05-84	8:46	9:04	"	"	"	"		
11-05-84	9:06	9:28	"	"	"	"		
11-06-84	8:43	8:51	1-3	"	"	"		
11-06-84	8:52	9:18	3	"	"	"		
11-06-84	9:19	9:21	2	"	"	"		
11-06-84	9:22	9:25	1.5	"	"	"		
11-06-84	9:35	9:39	1.25-2	"	"	"		
11-06-84	10:03	10:06	1.5-4	"	"	"		8
11-06-84	10:07	10:10	1.5-3	"	"	"		8
11-06-84	10:11	11:22	2-8	"	"	"		8
11-06-84	11:34	12:19	2-10	"	"	"		8
11-07-84	12:43	12:52	3	"	"	"		
11-07-84	12:58	13:07	"	"	"	"		
11-07-84	13:09	13:18	"	"	"	"		

Table A3. (Continued) JPL: Multi. - Frequency Radar Data Summary, Phase I.

DATE	START TIME (PST)	STOP TIME	FREQ. (GHz)	POL.	RADAR LOOK DIRECTION	INCIDENCE ANGLE	WIND SPEED	REMARKS
11-07-84	17:17	17:25	3	HH	270	45		
11-07-84	17:31	17:39	"	"	"	"		
11-08-84	9:06	9:14	"	"	"	"		
11-08-84	9:37	9:46	"	"	"	"		

Remarks

1. Run without 30 Hz modulation for 'noise' reference only
2. Uses 'Fhop4' frequency hopping program; 1.5, 2, 3, 5, 7, 10, 13, 18GHz
3. Time code will read 21 Hrs 45 Min less....clock error
4. Print-out of SA718 screen to document frequency/amplitude spectrum
5. 10 d3 pad in series with SA711 input. (w/o 50 ohm termination)
6. SA711 gain changed from BS10 to BS09
7. Uses 'Tda' time varrying data gathering program
8. Graph normalized for transmitter power output

Table A4. JPL: Multi. - Frequency Radar Data Summary , Phase II.

DATE	START TIME (PST)	STOP TIME	FREQ. (GHz)	POL.	RADAR LOOK DIRECTION	INCIDENCE ANGLE	WIND SPEED	REMARKS
03-13-85	12:32	14:35	2,4,8,12	HH	270	45		
03-14-85	9:43	16:00	"	"	"	"		
03-18-85	....	....	"	"	"	"		
03-19-85	10:50	17:03	"	"	"	"		
03-20-85	8:17	15:58	"	"	"	"		
03-21-85	3:21		"	"	"	"		
03-22-85		10:25	"	"	"	"		
	12:48	13:17	"	"	"	"		
03-24-85	13:11	15:40	"	"	"	"		
03-25-85	9:01	10:26	"	"	"	"		
	11:09	12:58	"	"	"	"		
	13:02		"	"	"	"		
03-26-85		8:00	"	"	"	"		
	11:15	16:05	"	"	"	"		
	16:33	18:47	"	"	"	"		
03-27-85	8:00	10:40	"	"	"	"		
	10:54	17:20	"	"	"	"		
	17:31		"	"	"	"		
03-28-85		6:35	"	"	"	"		
	8:53	9:23	"	"	"	"		
	9:33	9:47	"	"	"	"		

Table A5. NRL L-Band Tower Scatterometer Data Summary, Phase-I.

Date (1984)	Start Time[1]	Tape #	Remarks
9-26	10:52	1,2	F-4
9-28	10:40	3	F-4
10-2	10:45	4,5	F-4
10-3	10:40	6,7	
10-6	11:20	8,9	F-4
10-7	06:00	10	F-4
10-15	10:00	11	
10-16	10:00	12,13, 14,15	
10-17	00:00	16,17,18	CV-990
10-18	10:00	19,20	
10-20	10:00	21,22, 23,24	
10-21	00:00	25	
10-23	11:45	26,27,28	
10-24	10:00	29,30	
10-27	10:00	31	
10-28	12:00	32	
10-29	09:30	34,35	
10-31	11:00	36	CV-990 and F-4
11-2	11:00	37,38	
11-3	13:00	39	
11-4	00:00	40,41,42 43,44	CV-990
11-5	00:00	45,46	
11-6	10:00	47	
11-8	11:00	48	CV-990

(1) PDT and PST before and after 28 October 1984, repectively. In most cases data runs continued until the tower shut down, except when there were problems with the 110 VAC power.

Table A6. NRL L-Band and KU-Band Scatterometer Data Summary, Phase-II.

Date (1985)	Start Time (PST)	Tape #	Remarks
3-8	11:00	49,50	CV-990
3-12	13:00	51	
3-13	08:00	52,53	F-4; Mohawks
3-14	09:00	54	
3-15	11:00	55	
3-16	10:00	55	
3-18	11:00	56	Mohawks
3-19	12:00	57	CV-990; F-4
3-20	11:00	58,59	F-4
3-21	07:00	60,61, 62,63	
3-22	00:00	64,65,66.	
3-24	11:00	67	
3-25	08:00	68,69 70,71	
3-26	00:00	72,73,74, 75,76	
3-27	00:00	77,78,79, 80,81,82	CV-990

Table A7. University of Kansas Multi-Frequency Radar Data Summary, Phase I.

DATE	START TIME (PDT)	STOP TIME	FREQ. (GH_z)	POL.	RADAR LOOK DIRECTION	INCIDENCE ANGLE	WIND SPEED	REMARKS
10-06-84	3:06	3:09	9.6	HH	290°N	50°		Run #1
10-06-84	3:10	3:12	9.6	HH	200°N	50°		Run #2
10-06-84	3:14	3:17	9.6	HH	350°N	50°		Run #3
10-06-84	3:25		9,6	HH	235°N	50°		Run #4
10-06-84	3:32		9.6	HH	200°N	50°		Run #5
10-06-84	3:37	3:41	9.6	HH	350°N	50°		Run #6
10-06-84	3:44	3:48	9.6	HH	235°N	50°		Run #7
10-06-84	3:50	3:59	9.6	HH	290°N	50°		Run #8
10-06-84	3:54	4:00	9.6	HH	200°N	50°		Run #9
09-28-84			9.6	HH	UP	55°		
09-28-84	2:46	2:54	9.6	HH	UP	55°		
09-28-84			9.6	HH	UP	55°		A/CRun#1
09-28-84	10:47		9.6	HH	UP			Run #2
09-28-84	10:57		9.6	HH	UP	55°		Run #3
09-28-84	11:04		9.6	HH	UP	55°		Run #4
09-28-84			9.6	HH	UP	55°		Run #5
09-28-84	11:21		9.6	HH	UP	55°		Run #6
09-28-84	11:29		9.6	HH	UP	55°		Run #7
09-28-84	11:35		9.6	HH		55°		Run #7A
09-28-84			9.6	HH		55°		Bad Run #5 Repeat
09-28-84	11:46		9.6	HH				Run #7 Repeat
09-28-84			9.6	HH		55°		Run #7 Repeat
10-02-84	10:46	10:50	9.6	HH	290°N	55°		Run #1
10-02-84	10:55	11:02	9.6	HH	200°N	55°		Run #2
10-02-84	11:03	11:09	9.6	HH	333°N	55°		Run #3
10-02-84	11:10	11:16	9.6	HH	235°N	55°		Run #4
10-02-84	11:17	11:23	9.6	HH	200°N	55°		Run #5

Table A7. University of Kansas Multi-Frequency Radar Data Summary, Phase I. (Continued)

DATE	START TIME (PDT)	STOP TIME	FREQ. (GH_z)	POL.	RADAR LOOK DIRECTION	INCIDENCE ANGLE	WIND SPEED	REMARKS
10-02-84	11:25	11:30	9.6	HH	330°N	55°		Run #6
10-02-84	11:32	11:36	9.6	HH	235°N	55°		Run #7
10-02-84	11:37	11:48	9.6	HH	290°N	55°		Run #8
10-02-84	11:50	11:52	9.6	HH	200°N	55°		Run #9
10-02-84	1:16		9.6	HH	UP	55°		
10-02-84	1:39		9.6	HH	UP	55°		
10-06-84	12:23	12:57	9.6	HH	UP	55°	5	
10-06-84	2:15	2:23	9.6	HH	CROSS	55°	4	
10-06084	2:31	2:43	9.6	HH	CROSS	55°	4	Sine Tracker was not tracking so set Fm=233
09-27-84	2:01	2:27	14.6	HH	UP	44°		
09-27-84	3:11	3:18	14.6	HH	UP	44°		
10-15-84	16:06	16:07	14.6	HH	UP	45°	3	
10-15-84	16:08	16:43	14.6	HH	UP	45°	3	
10-23-84	15:35	15:55	14.6	HH	CROSS	45°	10	
09-28-84	2:55	3:54	14.6	HH	UP	55°		
10-06-84	1:30	1:41	14.6	HH	UP	55°	5	
10-06-84	3:01		14.6	HH	CROSS	55°		
09-27-84	3:22	3:37	5.2	VV	UP	44°		
10-15-84	14:47	14:57	5.2	VV	UP	44°	3	
10-16-84	11:37	12:07	5.2	VV	UP	45°		
10-16-84	20:35	21:10	5.2	VV	CROSS	45°		
10-20-84	12:08	12:40	5.2	VV	UP	45°	7	
10-20-84	21:38	21:43	5.2	VV	Looing into waves	45°	2	
10-23-84	12:01	13:03	5.2	VV	CROSS	45°	5	

Table A7. University of Kansas Multi-Frequency Radar Data Summary, Phase I. (Continued)

DATE	START TIME (PDT)	STOP TIME	FREQ. (GHz)	POL.	RADAR LOOK DIRECTION	INCIDENCE ANGLE	WIND SPEED	REMARKS
10-20-84	11:52	12:02	5.2	HH	UP	45°	7	
09-28-84	1:20	1:30	5.2	HH	UP	55°		
10-06-84	12:54	13:03	5.2	HH	UP	55°	Not tracked thru run	
10-06-84	1:06	1:27	5.2	HH	UP	55°	5	
10-06-84	2:45	2:56	5.2	HH	CROSS	55°		
10-29-84	13:49	13:59	5.2	HH	CROSS	55°	5	
10-29-84	14:08	14:24	5.2	HH	CROSS	55°	5	
09-26-84	3:05	3:14	9.6	HH	UP	46°		
09-27-84	1:54	1:58	9.6	HH	UP	44°		
09-27-84	3:01	3:08	9.6	HH	UP	44°		
10-06-84	4:06		9.6	HH	UP	45°		
10-07-84	9:04		9.6	HH	290°N	45°	2	A/C Run #1
10-07-84	9:08	maybe	9.6	HH	200°N	45°	2	A/C Run #2
10-07-84	9:15	stop	9.6	HH	360°N	45	2	A/C Run #3
10-07-84	9:23	times	9.6	HH	235°N	45°	2	A/C Run #4
10-07-84	9:31		9.6	HH	200°N	45°	2	A/C Run #5
10-07-84	9:37		9.6	HH	350°N	45°	2	A/C Run #6
10-07-84	9:43		9.6	HH	235°N	45°	3	A/C Run #7
10-07-84	9:48		9.6	HH	290°N	45°	3	A/C Run #8
10-07-84	9:53		9.6	HH	200°N	45°	3	A/C Run #9
10-07-84	10:03		9.6	HH	UP	45°		
10-15-84	15:33	15:43	9.6	HH	UP	45°	3	
10-15-84	16:50	17:11	9.6	HH	UP	45°	4	Noted: not a Continuous run
10-20-84	9:16	9:20	9.6	HH	UP	45°	4	Tracking problem
10-20-84	11:37	11:47	9.6	HH	UP	45°	6	
10-23-84	14:41	15:00	9.6	HH	CROSS	45°	10	
10-23-84	15:01	15:33	9.6	HH	CROSS	45°		Last few minutes out of track

Table A7. University of Kansas Multi-Frequency Radar Data Summary, Phase I. (Continued)

DATE	START TIME (1)	STOP TIME	FREQ. (GH_z)	POL.	RADAR LOOK DIRECTION	INCIDENCE ANGLE	WIND SPEED	REMARKS
10-16-84	19:28	20:05	9.6	VV	CROSS	45°		
10-17-84	15:56	16:03	9.6	VV		45°		
10-17-84	16:20	16:31	9.6	VV	UP	45°		
10-20-84	12:44	12:45	9.6	VV	UP	45°	7	
10-20-84	21:46	22:48	9.6	VV	Looking into wave	45°	2	Tracker didn't track
10-23-84	10:57	11:28	9.6	VV	CROSS	45°	4	
10-23-84	13:42		9.6	VV	CROSS	45°	10	
11-05-84	13:20	13:28	9.6	VV	UP	45°	3	
11_05-84	13:54	14:15	9.6	VV	UP	45°	3	Last couple of min. out of tract
11-05-84	14:40	15:07	9.6	VV	CROSS	45°	3	
11-07-84	10:10	10:11	9.6	VV	UP	45°	3	TEAC stuck on these 2 runs
11-07-84	10:26		9.6	VV	UP	45°	3	
11-07-84	11:15	11:30	9.6	VV	UP	45°	3	
09-27-84	4:59	5:08	9.6	VV	UP	55°		
09-28-84	10:35		9.6	VV	UP	55°		
10-20-84	13:57	14:59	9.6	VV	UP	55°	6	
10-20-84	16:06	17:45	9.6	VV	UP	55°	5	
10-25-84	11:26	11:32	9.6	VV	UP	55°	3	
10-25-84	11:35	11:49	9.6	VV	UP	55°	5	
10-25-84	14:43	14:53	9.6	VV	UP	55°	4	
10-25-84	15:54	15:57	9.6	VV	UP	55°	5	
10-25-84	16:46	17:16	9.6	VV	CROSS	55°	5	
10-27-84	9:41	10:08	9.6	VV	UP	55°	7	
10-27-84	13:04	13:59	9.6	VV	UP	55°	6	
10-29-84	12:32	13:00	9.6	VV	CROSS	55°	4	
10-29-84	13:12	13:39	9.6	VV	CROSS	55°	5	
10-30-84	13:03	13:27	9.6	VV	UP	55°	3	
10-30-84	14:36	14:53	9.6	VV	UP	55°	3	TEAC?

(1) PDT and PST before and after 28 October 1984.

Table A7. University of Kansas Multi-Frequency Radar Data Summary, Phase I. (Concluded).

DATE	START TIME (1)	STOP TIME	FREQ. (GH_z)	POL.	RADAR LOOK DIRECTION	INCIDENCE ANGLE	WIND SPEED	REMARKS
11-04-84	11:40		9.6	VV	340°N	55°		A/C Run #3 Leg #4
11-04-84	11:49		9.6	VV	235°N	55°		Run #4 Leg #8
11-04-84	11:56		9.6	VV	205°N	55°		Run #5 Leg #1
11-04-84	12:03		9.6	VV	340°N	55°		Run #6 Leg #3
11-04-84	12:11		9.6	VV	235°N	55°		Run #7 Leg #7
11-04-84	12:18		9.6	VV	290°N	55°		Run #8 Leg #5
10-15-84	14:59	15:21	14.6	VV	UP	45°	3	
10-20-84	18:07	18:50	14.6	VV	UP	45°	3	
10-23-84	13:07	13:40	14.6	VV	CROSS	45°	6	
11-05-84	14:21	14:35	14.6	VV	UP	45°	3	
11-07-84	12:00	12:21	14.6	VV	UP	45°	4	
11-07-84	12:41	13:28	14.6	VV	UP	45°	5	
09-27-84	5:12		14.6	VV	UP	55°		
10-25-84	15:30	15:51	14.6	VV	UP	55°	5	
10-27-84	10:10	11:38	14.6	VV	UP	55°	7	
10-30-84	16:22	16:38	14.6	VV	UP	55°	5	
10-31-84	10:47	11:07	14.6	VV	UP	55°	2.5	
11-02-84	15:01	15:43	14.6	VV	UP	55°	5	
11-03-84	21:54	22:16	14.6	VV	UP	55°	5	

(1) PDT and PST before and after 28 October 1984.

Table A7. University of Kansas Multi-Frequency Radar Data Summary, Phase I. (Continued)

DATE	START TIME (PST)	STOP TIME	FREQ. (GH_z)	POL.	RADAR LOOK DIRECTION	INCIDENCE ANGLE	WIND SPEED	REMARKS
10-28-84	12:16	12:43	1.5	HH	CROSS	45°	2	
10-28-84	12:52	13:20	1.5	HH	CROSS	45°	3	
10-28-84	13:36	14:16	1.5	HH	CROSS	45°	4	
10-28-84	14:20	14:21	1.5	HH	CROSS	45°	5	
10-28-84	15:01	15:12	1.5	HH	CROSS	45°	5	
10-28-84	15:14	15:16	1.5	HH	CROSS	45°	5	something
10-28-84	15:16	15:16	1.5	HH	CROSS	45°	5	wrong with tapedeck on these 2 runs
10-28-84	16:09	17:25	1.5	HH	CROSS	45°	5	
10-29-84	14:44	15:35	1.5	HH	CROSS	45°	5	
10-29-84	15:43	15:44	1.5	HH	CROSS	45°	6	TEAC Messed up
10-29-84	16:00	16:30	1.5	HH	UP	45°	5	
10-31-84	12:28	12:47	1.5	HH	CROSS	45°	3-4	
10-31-84	12:50	12:57	1.5	HH	30°N	45°		
10-31-84	12:58	13:02	1.5	HH	320°N	45°		A/C CWFlight Leg #7
10-31-84	13:06	13:10	1.5	HH	20°N	45°		Leg #1
10-31-84	13:12	13:23	1.5	HH	350°N	45°		Leg #4
10-31-84	13:25	13:35	1.5	HH	20°N	45°		Leg #2
10-31-84	13:37	13:44	1.5	HH	290°N	45°		Leg #6
10-31-84	13:45		1.5	HH	50°N	45°		Leg #7
10-31-84	13:52		1.5	HH	20°N	45°	3	Leg #1
10-31-84	14:00		1.5	HH	350°N	45°		Leg #4
10-31-84	14:05		1.5	HH	20°N	45°		Leg #2
10-31-84	14:22		1.5	HH	290°N	45°		Leg #6
11-02-84	15:54	15:54	1.5	HH	CROSS	45°	5	L-Band won't track

Table A7. University of Kansas Multi-Frequency Radar Data Summary, Phase-I. (Continued)

DATE	START TIME (PDT)	STOP TIME	FREQ. (GH_z)	POL.	RADAR LOOK DIRECTION	INCIDENCE ANGLE	WIND SPEED	REMARKS
10-17-84	12:34	13:27	1.5	HH	30°N	38°		
10-17-84	13:29		1.5	HH	30°N	38°		
10-17-84	13:30	13:40	1.5	HH	50°N	38°		
10-17-84	13:41	13:46	1.5	HH	30°N	38°		
10-17-84	13:47	13:54	1.5	HH	360°N	38°		
10-17-84	13:55	14:10	1.5	HH	30°N	38°		
10-17-84	14:13	14:20	1.5	HH	300°N	38°		
10-17-84	14:24	14:45	1.5	HH	360°N	38°		
10-17-84	14:46	14:51	1.5	HH	50°N	38°		
10-17-84	14:53		1.5	HH	30°N	38°		
10-17-84	15:02	15:06	1.5	HH	30°N	38°		
10-17-84	15:07	15:13	1.5	HH	360°N	38°		
10-17-84	15:15	15:28	1.5	HH	30°N	38°		
10-17-84	15:30	15:45	1.5	HH	300°N	38°		
09-29-84	12:20	12:32	1.5	HH	UP	40°		
09-29-84	12:34	12:40	1.5	HH	UP	40°		
09-29-84			1.5	HH	UP	40°		
09-29-84	12:13		1.5	HH	UP	40°		
10-07-84	5:59		1.5	HH	295°N	40°		
10-17-84	9:01	9:11	1.5	HH	UP	40°		
10-17-84	9:14	9:32	1.5	HH	UP	40°		
10-17-84	9:37	10:36	1.5	HH	CROSS	40°		

Table A7. University of Kansas Multi-Frequency Radar Data Summary, Phase I. (Continued)

DATE	START TIME (PST)	STOP TIME	FREQ. (GH_z)	POL.	RADAR LOOK DIRECTION	INCIDENCE ANGLE	WIND SPEED	REMARKS
11-04-84	13:37	14:01	1.5	HH	CROSS	45°	2.5	
11-04-84	15:20		1.5	HH	20°N	45°	2	A/C Run 2, Leg #1
11-04-84	15:30		1.5	HH	350°N	45°		Run 3 Leg #4
11-04-84	15:40		1.5	HH	20°N	45°		Run 4 Leg #2
11-04-84	15:56		1.5	HH	35°N	45°		Run 6 Leg #7
11-04-84	16:17		1.5	HH	20°N	45°		Run 7 Leg #1
11-04-84	16:25		1.5	HH	350°N	45°		Run 8 Leg #4
11-04-84	16:36		1.5	HH		45°		Run 9 Leg #2
11-04-84			1.5	HH		45°		Run 9 Leg #2
11-04-84	16:50		1.5	HH	CROSS	45°	3	Low wind speed at end of run
11-05-84	10:56	10:57	1.5	HH	UP	45°	2	Boats passed
11-05-84	10:58		1.5	HH	UP	45°	2	thru antenna beam
11-07-84	14:04		1.5	HH	40°N	45°	5	A/C Run 1 Leg #7
11-07-84	14:18		1.5	HH	20°N	45°		Run 2 Leg #1
11-07-84	14:26		1.5	HH	350°N	45°		Run 3 Leg #4
11-07-84	14:34		1.5	HH	20°N	45°		Run 4 Leg #2
11-07-84	14:51		1.5	HH	40°N	45°		Run 6 Leg #7
11-07-84	15:05		1.5	HH	20°N	45°		Run 7 Leg #1
11-07-84	15:13		1.5	HH	350°N	45°		Run 8 Leg #4
11-07-84	15:24		1.5	HH	20°N	45°		Run 9 Leg #2
11-07-84	15:38		1.5	HH	290°N	45°		Run 10 Leg #6
11-07-84	15:51		1.5	HH	35°N	45°		Teac stuck Run 11 Leg #7
11-07-84	15:57		1.5	HH	35°N	45°		Run 11 Leg #7
11-07-84	16:07		1.5	HH	20°N	45°		Run 12 Leg #1
11-07-84	16:16		1.5	HH	350°N	45°		Run 13 Leg #4
11-07-84	16:27		1.5	HH		45°		Run 14 Leg #2

Table A7. University of Kansas Multi-Frequency Radar Data Summary, Phase I. (Continued)

DATE	START TIME (PST)	STOP TIME	FREQ. (GH_z)	POL.	RADAR LOOK DIRECTION	INCIDENCE ANGLE	WIND SPEED	REMARKS
11-05-84	11:24	11:30	5.2	VV	UP	45°	2	
11-05-84	12:56	13:19	5.2	VV	UP	45°	3	
11-05-84	15:08	15:15	5.2	VV	UP	45°	3	
11-05-84	15:28		5.2	VV	UP	45°		TEAC stuck
09-27-84	4:47	4:58	5.2	VV	UP	55°		
10-20-84	15:04	15:37	5.2	VV	UP	55°	6	
10-25-84	14:55	15:25	5.2	VV	UP	55°	4	
10-27-84	11:41	12:59	5.2	VV	UP	55°	8	Tracker out of track last few seconds
10-29-84	11:26	12:28	5.2	VV	CROSS	55°	4	
10-30-84	15:42	16:20	5.2	VV	UP	55°	3	
10-31-84	10:40	10:45	5.2	VV	UP	55°	2.5	
10-31-84	11:47	11:54	5.2	VV	UP	55°	3	
11-02-84	11:21	12:03	5.2	VV	CROSS	55°	3	
11-03-84	12:59	14:04	5.2	VV	UP	55°	3	
11-03-84	16:42	17:24	5.2	VV	UP	55°	3	
11-04-84	9:00	9:06	5.2	VV	UP	55°	2	Reject first 3 min. of data
11-04-84	10:50	11:22	5.2	VV	UP	55°	1	
09-27-84	3:39	3:56	9.6	VV	UP	44°		
10-15-84	14:22	14:42	9.6	VV	UP	45°		
10-16-84	12:30	12:46	9.6	VV	UP	45°		
10-16-84	12:50	13:13	9.6	VV	UP	45°	5	
10-16-84	13:19	14:04	9.6	VV	CROSS	45°	5	
10-16-84	14:06	14:41	9.6	VV	CROSS	45°		
10-16-84	19:06	19:17	9.6	VV	CROSS	45°		

Table A7. University of Kansas Multi-Frequency Radar Data Summary, Phase I. (Continued)

DATE	START TIME (PST)	STOP TIME	FREQ. (GH_z)	POL.	RADAR LOOK DIRECTION	INCIDENCE ANGLE	WIND SPEED	REMARKS
11-07-84	16:42		1.5	HH		45°		Run 14 Leg6
10-20-84	9:35	10:03	1.5	HH	CROSS	55°	5	
10-20-84	10:08	11:09	1.5	HH	CROSS	55°	6	
10-20-84	11:21	11:22	1.5	HH	UP	55°	6	
10-20-84	11:23	11:30	1.5	HH	UP	55°	6	
10-20-84	19:00	19:12	1.5	HH	UP	55°	2	
10-21-84	9:41	10:19	1.5	HH	CROSS	55°	3.5	
10-23-84	16:01	16:21	1.5	HH	CROSS	55°	10	
10-23-84	16:24	16:33	1.5	HH	CROSS	55°	8	
10-23-84	16:39	16:51	1.5	HH	CROSS	55°		
10-25-84	10:52	10:57	1.5	HH	UP	55°	4	
10-25-84	16:15	16:35	1.5	HH	CROSS	55°	5	lost tract several times
10-27-84	8:48	9:11	1.5	HH	CROSS	55°	5	
10-27-84	9:12	9:22	1.5	HH	CROSS	55°	7	
10-27-84	14:40	14:41	1.5	HH	CROSS	55°	4	Problem with TEAC
10-27-84	15:48	16:34	1.5	HH	CROSS	55°	4	Problem with TEAC
10-28-84	11:31	11:56	1.5	HH	CROSS	55°	3	
10-17-84	10:55	11:26	1.5	HH	CROSS	58°	6	
10-17-84	11:39	11:46	1.5	HH	CROSS	58°	6	
09-26-84	3:20	3:24	5.2	HH	UP	46°		
09-27-84	2:39	2:43	5.2	HH	UP	44°		
09-27-84	2:48	2:56	5.2	HH	UP	44°		
10-15-84	15:45		5.2	HH	UP	45°		
10-20-84	11:~~53~~	11:49	5.2	HH	UP	45°	7	Noted: Bad Run
10-20-84	11:50	11:51	5.2	HH	UP	45°	7	Noted Bad Run

Table A7. University of Kansas Multi-Frequency Radar Data Summary, Phase I. (Continued)

DATE	START TIME (PST)	STOP TIME	FREQ. (GH_z)	POL.	RADAR LOOK DIRECTION	INCIDENCE ANGLE	WIND SPEED	REMARKS
10-31-84	9:34	10:06	9.6	VV	UP	55°	2.5	
10-31-84	10:09	10:11	9.6	VV	UP	55°	2	Not tracking
10-31-84	10:15	10:32	9.6	VV	UP	55°	2	
10-31-84	11:08	11:44	9.6	VV	UP	55°	3	Last few seconds out of track
10-31-84	14:57		9.6	VV	290°N	55°		Leg #6
10-31-84	15:06		9.6	VV	205°N	55°		Leg #2
10-31-84	15:12		9.6	VV	340°N	55°		Leg #4
10-31-84	15:22		9.6	VV	235°N	55°		Leg #8
10-31-84	15:28		9.6	VV	205°N	55°		Leg #1
10-31-84	15:37		9.6	VV	340°N	55°		Leg #3
10-31-84	15:49		9.6	VV	235°N	55°		Leg #7
10-31-84	15:56		9.6	VV	290°N	55°	3-4	Leg #5
10-31-84	16:06	16:36	9.6	VV	205°N	55°	5	Leg #1
11-02-84	12:04	12:13	9.6	VV	CROSS	55°	5	
11-02-84	12"14	12:48	9.6	VV	CROSS	55°	5	
11-02-84	13:21	14:?	9.6	VV	UP	55°	3	
11-02-84	16:19		9.6	VV	CROSS	55°	5	Something about
11-02-84	16:57		9.6	VV	UP	55°	5	about navy ships passing
11-03-84	14:06	14:18	9.6	VV	UP	55°	5	
11-03-84	20:27		9.6	VV	UP	55°	5	
11-03-84	22:17		9.6	VV	UP	55°	5	
11-04-84	11:27		9.6	VV	290°N	55°	3	Run #1 Leg #6
11-04-84	11:35		9.6	VV	?	55°		Run #2 Leg #2